SANDIA REPORT

SAND2005-5085
Unlimited Release
Printed August 2005

Characterization of Fuego for Laminar and Turbulent Natural Convection Heat Transfer

Nicholas D. Francis, Jr.

Prepared by Sandia National Laboratories
Albuquerque, New Mexico 87185 and Livermore, California 94550

Sandia is a multiprogram laboratory operated by Sandia Corporation,
a Lockheed Martin Company, for the United States Department of Energy's
National Nuclear Security Administration under Contract DE-AC04-94AL85000.

Approved for public release; further dissemination unlimited.

Issued by Sandia National Laboratories, operated for the United States Department of Energy by Sandia Corporation.

NOTICE: This report was prepared as an account of work sponsored by an agency of the United States Government. Neither the United States Government, nor any agency thereof, nor any of their employees, nor any of their contractors, subcontractors, or their employees, make any warranty, express or implied, or assume any legal liability or responsibility for the accuracy, completeness, or usefulness of any information, apparatus, product, or process disclosed, or represent that its use would not infringe privately owned rights. Reference herein to any specific commercial product, process, or service by trade name, trademark, manufacturer, or otherwise, does not necessarily constitute or imply its endorsement, recommendation, or favoring by the United States Government, any agency thereof, or any of their contractors or subcontractors. The views and opinions expressed herein do not necessarily state or reflect those of the United States Government, any agency thereof, or any of their contractors.

Printed in the United States of America. This report has been reproduced directly from the best available copy.

Available to DOE and DOE contractors from
U.S. Department of Energy
Office of Scientific and Technical Information
P.O. Box 62
Oak Ridge, TN 37831

Telephone: (865)576-8401
Facsimile: (865)576-5728
E-Mail: reports@adonis.osti.gov
Online ordering: http://www.osti.gov/bridge

Available to the public from
U.S. Department of Commerce
National Technical Information Service
5285 Port Royal Rd
Springfield, VA 22161

Telephone: (800)553-6847
Facsimile: (703)605-6900
E-Mail: orders@ntis.fedworld.gov
Online order: http://www.ntis.gov/help/ordermethods.asp?loc=7-4-0#online

SAND2005-5085
Unlimited Release
Printed August 2005

Characterization of Fuego for Laminar and Turbulent Natural Convection Heat Transfer

Nicholas D. Francis, Jr.
Thermal and Reactive Processes Department 1516

Sandia National Laboratories
P. O. Box 5800
Albuquerque, NM 87185

Abstract

A computational fluid dynamics (CFD) analysis is conducted for internal natural convection heat transfer using the low Mach number code Fuego. The flow conditions under investigation are primarily laminar, transitional, or low-intensity level turbulent flows. In the case of turbulent boundary layers at low-level turbulence or transitional Reynolds numbers, the use of standard wall functions no longer applies, in general, for wall-bounded flows. One must integrate all the way to the wall in order to account for gradients in the dependent variables in the viscous sublayer. Fuego provides two turbulence models in which resolution of the near-wall region is appropriate. These models are the v2-f turbulence model and a Launder-Sharma, low-Reynolds number turbulence model. Two standard geometries are considered: the annulus formed between horizontal concentric cylinders and a square enclosure. Each geometry emphasizes wall shear flow and complexities associated with turbulent or near turbulent boundary layers in contact with a motionless core fluid. Overall, the Fuego simulations for both laminar and turbulent flows compared well to measured data, for both geometries under investigation, and to a widely accepted commercial CFD code (FLUENT). However, in an effort to further improve predictions, recommendations for modifications have been made for both Fuego turbulence models.

Acknowledgements

Review comments from Darryl L. James, Department of Mechanical Engineering at Texas Tech University and Sandia National Laboratories consultant, Stefan P. Domino, staff member of the Thermal/Fluids Computational Engineering Department, and, E. S. Hertel, Department Manager of the Thermal and Reactive Processes Department, are greatly appreciated. Their insightful comments have made this a much better document.

Contents

Figures

Tables

Introduction

Thermal environment verification and validation (V&V) activities typically include very detailed formulations for conduction and enclosure thermal radiation heat transfer. Convection heat transfer is included in an analysis by assuming a correlation based heat transfer coefficient obtained from traditional geometries and steady-state fluid conditions (i.e., a constant temperature infinite vertical wall). This approach may in fact be adequate for many applications; however, it has yet to be shown in any detail that this is the case. Indeed, in some instances, it may be highly desirable to include a field of heat transfer coefficients that vary, both in time and space, with respect to specific heating conditions of the actual geometry of interest. The ASC program is emphasizing coupled physics that accurately reflects the actual physical environment. To support the move from single to coupled physics, there exists a need to validate the coupling approach and key physical processes.

This particular project focuses on coupling between Calore and Fuego and the convective heat transfer processes associated with the more general problem of conjugate heat transfer, with or without thermal radiation. Specifically, this report focuses solely on the aspects of fluid and heat flow in simple geometries traditionally considered in the literature. Conjugate heat transfer is not yet included. This incremental approach to model validation is one that lends confidence in complex coupling between a code with the capabilities of computational fluid dynamics (Fuego) to a computational heat transfer code including enclosure radiation (Calore). This report is the first step in this process and is analogous to a walk before you run approach. The final outcome of this project will be a validated approach for including explicit convection (both internal and/or external) heat transfer in future weapons systems analysis, or any other application that requires both fluid flow with conjugate heat transfer and thermal radiation (with either a participating or non-participating medium).

This report focuses on internal natural convection. The geometries analyzed in this document include square enclosures and horizontal concentric cylinders. The low Mach number code, Fuego, is employed to determine both fluid flow and heat transfer characteristics associated with these standard geometries and flow conditions. These particular geometries are selected because they have been investigated both experimentally and numerically in the literature for various fluid flow conditions. This fact allows for detailed code comparisons of fluid temperature and velocity, heat transfer characteristics such as Nusselt number and effective thermal conductivity, and various turbulence quantities such as the turbulence kinetic energy. With this information compiled for simple geometries, one can better assess the ability of Fuego to predict heat

transfer and fluid flow conditions encountered in weapons systems analysis. Although the geometries and flow conditions considered in this report are relatively simple, they are fundamentally representative of those encountered in more complex heat transfer analyses performed in the V&V program. It is emphasized up front that Fuego is being used in this project *strictly* as a computational fluid dynamics (CFD) code. Fire and related combustion and species transport processes are not required.

As implied by the title, both laminar and turbulent flow equations are solved by Fuego to determine the characteristics of the flow fields and heat transfer processes. Fuego solves laminar flow equations including mass continuity, momentum, and energy transport to determine temperature and velocity fields in the fluid encompassed by the geometries of interest. For turbulent flows, the laminar flow equations are time-averaged over an interval which is long compared to the characteristic time scale of turbulence. The Reynolds averaged Navier-Stokes (RANS) equations used in this CFD analysis apply turbulence closure models to all scales of turbulence. Subsequently, a RANS formulation provides time-averaged values of the dependent variables (e.g., fluid velocity, temperature, and pressure). Transient terms for time-averaged quantities may be necessary if variations of the mean values occur over time intervals longer than the averaging interval.

The analysis of internal flows focuses on wall-bounded shear flows. In the case of turbulent flows, the traditional approach to solving high-Reynolds number wall-bounded shear flows is to apply standard wall-functions in the thin viscous sublayer that resides in the near-wall region, thereby obviating the need to numerically resolve the near-wall region. Wall functions assume a priory knowledge of the temperature and velocity profiles in the near-wall region while relating conditions at the wall to the core turbulent flow. This is in fact precisely what the level-1 turbulence model in Fuego does and is indeed a typical and well-accepted approach for solving high-Reynolds number flows. However, in the case of turbulent boundary layers at low or transitional Reynolds numbers, the use of standard wall functions no longer applies in general. One must then integrate all the way to the wall in order to take into account gradients of the dependent variables in the viscous sublayer.

Therefore, an alternative turbulence model is required for this analysis. Fuego provides two turbulence models in which resolution of the near-wall region is appropriate. These models are the v2-f turbulence model and a Launder-Sharma, low-Reynolds number turbulence model. Both turbulence models have their basis in a standard two-equation k-ε turbulence model. The v2-f model formulation provides two-additional transport equations that account for kinematic blocking represented by walls. The suppression of eddy viscosity at

the wall is the desired result. The low-Reynolds number k-ε (LRKE) turbulence model modifies standard equation constants through the use of "damping functions." Again, suppression of the eddy viscosity at the wall is the desired result. Both Fuego turbulence models are compared to each other and to measured data obtained from the literature. Additionally, the Fuego turbulence flow models are also compared to CFD results obtained from various RANS turbulence models found in the commercial CFD code, FLUENT. The next section provides a brief overview of the v2-f and low-Reynolds number turbulence flow models found in Fuego.

Fuego Turbulence Models

v2-f Turbulence Model

The mathematical details of the v2-f turbulence model can be found in various sources in the literature [1] or in the Fuego users manual [2]. The v2-f turbulence model accounts for the non-homogenous near-wall region *without* the use of wall-functions or damping functions. It attempts to include the effects of kinematic wall-blocking by introducing turbulent velocity scaling as $\overline{v^2}$ (instead of k) and an elliptical partial differential equation that includes non-local effects in non-homogeneous turbulent flows. The v2-f turbulence model requires numerical resolution of the near-wall, viscosity affected region. This dictates that the placement of the first mesh point, specified by the normal distance from the wall nondimensionlized by a viscous length scale, is approximately one. This mesh requirement allocates appropriate discretization in the inner layer. Mathematically, this requirement is written as the following:

$$y^+ = \frac{y}{\nu}\sqrt{\frac{\tau_w}{\rho}} \approx 1 \qquad \text{(Eqn. 1)}$$

where y is the normal distance from the wall, ν is the kinematic viscosity of the fluid, τ_w is the wall shear stress, and ρ is the density of the fluid.

The v2-f turbulence model provides four transport equations for closure of the Reynolds stress terms in the RANS momentum equations. The transport equation for turbulence kinetic energy (the k-equation) is identical to that applied in the level-1 turbulence model. The dissipation rate of turbulence kinetic energy (the ε-equation) uses a slightly modified model constant and time-scale for the evolution of dissipation when compared to the dissipation equation in the level-1 turbulence model. A new transport equation (the v2-equation) is written for the appropriate turbulent velocity scale, $\overline{v^2}$. It represents the turbulent velocity component normal to the wall which must be

inviscidly brought to zero by the wall. It is noted that kinematic wall blocking occurs further away from the wall than viscous damping does. The fourth and final transport equation (the f-equation) is an elliptic partial differential equation that accounts for non-homogenous and anisotropic wall blocking effects in the $\overline{v^2}$ transport equation. Finally, the turbulent viscosity is written for the v2-f turbulence model as the following:

$$\frac{\mu_t}{\rho} = \nu_t = C_\mu \overline{v^2} T_t \qquad \text{(Eqn. 2)}$$

where C_μ is a constant (=0.22), and T_t is defined as the time-scale of turbulence and is the larger of k/ε, or, the Kolmogorov time-scale, $\left(\sqrt{\frac{\nu}{\varepsilon}}\right)$. The turbulent viscosity is written in terms of the normal Reynolds stress component which is naturally damped in the near-wall region.

Low-Reynolds Number k-ε Turbulence Model (LRKE)

The mathematical details of the LRKE turbulence model can be found in various sources in the literature [3] and [4] or in the Fuego user's manual. Standard model constants are applied; however, the LRKE turbulence model accounts for the near-wall region with the use of damping functions that modify the standard model constants. Damping functions are designed to reduce the eddy viscosity when y^+ is small. That is, in the near-wall region where viscosity effects are important. Like the v2-f model, this turbulence model also requires numerical resolution of the near-wall, viscosity affected region. The restriction on the non-dimensional distance is the same as in the v2-f model. That is, y^+ is required to be about one. Many different low-Reynolds number k-ε turbulence models exist in the literature. The Launder-Sharma version of the low-Reynolds number turbulence model is applied in Fuego.

The LRKE turbulence model includes two transport equations for closure of the Reynolds stress terms in the RANS momentum equations. The turbulent kinetic energy equation (k-equation) includes an additional source term introduced by the dissipation variable (refer to Equation 3 for the definition of the dissipation variable). A dissipation variable is introduced in the model to allow for convenient implementation of a zero wall boundary condition in the modified ε-equation. The dissipation rate of turbulent kinetic energy (the modified ε-equation) also includes a source term (typically denoted by E = $2\nu\nu_t\left(\frac{\partial^2 U_i}{\partial x_j \partial x_k}\right)^2$) and a modification to a model constant ($C_{\varepsilon 2}$). The modification to the constant is an exponential written as a function of the turbulence Reynolds

number. Finally, the turbulent viscosity is written in terms of the dissipation variable ($\tilde{\varepsilon} = \varepsilon - D$) for the LRKE turbulence model as the following:

$$\frac{\mu_t}{\rho} = \nu_t = C_\mu f_\mu \frac{k^2}{\tilde{\varepsilon}} \qquad \text{(Eqn. 3)}$$

where C_μ is a constant (=0.09), k is the turbulence kinetic energy, ε is the dissipation of turbulence kinetic energy, D is equal to $2\nu\left(\frac{\partial\sqrt{k}}{\partial y}\right)^2$, and f_μ $\left(= \exp\left[\frac{-3.4}{\left(1+R_T/50\right)^2}\right]\right)$ is a required damping function written in terms of the turbulence Reynolds number. Both of the additional source terms and the modifications to model constants are included to better represent the reduction in Reynolds stress associated with near-wall behavior.

Fuego turbulence models are compared to each other and to measured data from the natural convection literature. Additionally, in some instances, Fuego results will be compared directly to RANS turbulence models available in the commercial CFD code, FLUENT. In particular, comparisons will be made to the standard k-ε, realizable k-ε, RNG k-ε, and k-ω [5]. In each of these cases as well, integration is performed all the way to the wall. Application of the v2-f and LRKE turbulence models to two standard geometries is the topic of the next two sections. A number of sensitivity studies and grid independence studies are executed to determine the performance of the models and to determine under which conditions the models are or are not applicable.

Horizontal Concentric Cylinders

Natural convection heat transfer in the annulus between horizontal concentric cylinders has been studied previously in the literature [6] – [9]. Both laminar and turbulent flow conditions are analyzed. The boundary conditions applied in the fluids models are simple constant temperature surfaces. The inner cylinder is specified as the high temperature surface, the outer cylinder, the low temperature surface. The mesh applied in Fuego is pseudo two-dimensional. That is, the mesh is one element thick in the z-direction (third dimension). Figure 1 illustrates a mesh of the annulus formed by horizontal concentric cylinders.

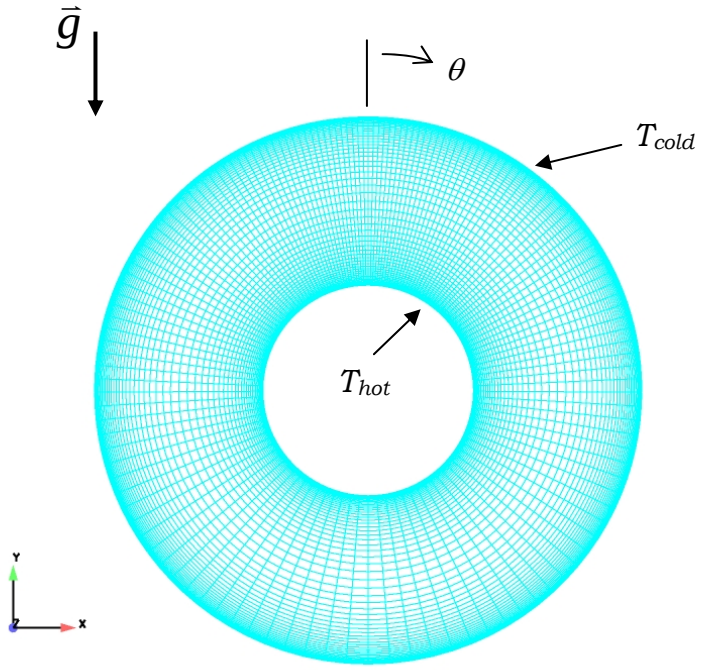

Figure 1. Fuego Mesh for the Annulus Between Horizontal Concentric Cylinders

It is noted from Figure 1 that cell-clustering occurs in the boundary layers adjacent to both inner and outer walls and in the plume region known to exist above the inner (hot) cylinder. The bottom of the annulus adjacent to the outer cylinder is most coarsely discretized due to the near lack of fluid motion in this region of the annulus (i.e., a region of essentially zero heat flux). Annulus symmetry conditions are not applied so as not to presume a non-oscillating fluids solution. That is, because both halves of the annulus are included in the analysis, a naturally occurring oscillatory motion of the upward moving plume is a possible flow solution. (Note, for the solution of laminar flow equations at transitional Rayleigh numbers, this is in fact the case. This flow feature will be shown in detail later in this section). Both the v2-f and the LRKE turbulence models will be applied to this geometry. In order to get a sense of the grid independent nature of the CFD solutions presented in this report, two additional fluids meshes are also considered. The numerical details of each mesh are given in Table 1. This mesh and that described in the next section were both created in Cubit.

Table 1. Three Horizontal Concentric Cylinder Meshes Applied in Fuego

Case	r	θ	Description
Coarse Mesh	52	144	—
Mid Mesh	70	192	33% more than coarse
Fine Mesh	78	216	50% more than coarse

Note that the z-direction is one element thick.

It is noted in Figure 1 and Table 1 that r represents discretization across the gap-width between cylinders and θ represents angular discretization around the circumference of the cylinders. Simulation data will be extracted from the mesh at various radial and angular locations. Local results are shown at angular locations of 0, 30, 60, 90, 120, 150, and 180°.

Both average and local heat transfer results are compared to measured data taken at various Rayleigh numbers. In some cases, just the average heat transfer data will be compared. Of particular importance in the analysis of horizontal concentric cylinders is the computation of an average equivalent thermal conductivity, k_{eq}. The average equivalent thermal conductivity is defined simply as the ratio of heat transfer by convection and conduction to that of conduction only through the annular fluid space. When the average equivalent thermal conductivity is approximately equal to one, the heat transfer through the fluid is essentially pure conduction. The expressions necessary to compute an average thermal conductivity are presented next.

A conduction Nusselt number, derived from the heat transfer expression for cylindrical systems, is written in terms of the diameters of the cylinders:

$$Nu_{cond} = \frac{2}{\ln \frac{D_o}{D_i}}, \text{ applies to concentric cylinders only} \qquad \text{(Eqn. 4)}$$

where D_i and D_o are the inner and outer diameters, respectively. An average heat transfer coefficient is computed from the simulation as follows:

$$\bar{h}_i = \frac{\overline{Q}}{\pi D_i l \Delta T} \qquad \text{(Eqn. 5)}$$

where $\overline{Q}$ is the average wall heat transfer rate, l is the thickness of the CFD model in the z-direction, and ΔT (= T_{hot} – T_{cold}) is the temperature difference between surfaces. The average, steady-state heat transfer rate is computed as a surface integral and is substituted directly into Equation (5) to compute an average heat transfer coefficient. To ensure the model has reached (an approximate) steady-state solution, the simulated energy balance between surfaces is required to approach zero. Additionally, the fluids solution (based on temperature isotherms) is observed to be essentially unchanging, either in a mean or periodic sense.

The average Nusselt number is then computed in terms of the average heat transfer coefficient as the following:

$$\overline{Nu}_{D_i} = \frac{\overline{h}_i D_i}{k} \qquad \text{(Eqn. 6)}$$

where k is the average fluid thermal conductivity evaluated at the average fluid temperature. The average equivalent thermal conductivity for natural convection in the annulus formed by horizontal concentric cylinders is given as the following:

$$k_{eq} = \frac{\overline{Nu}_{D_i}}{Nu_{cond}} = \frac{\overline{Q}}{Q_{cond}} \qquad \text{(Eqn. 7)}$$

where Q_{cond} is the conduction heat transfer rate, the average Nusselt number is given by Equation (6), and the conduction Nusselt number (Nu_{cond}) is given by Equation (4). Equation (7) can be evaluated for any geometry. For complex geometries, computation of the average equivalent thermal conductivity in terms of heat transfer rates may be much more straightforward than using Nusselt numbers due to the potential complexity in determining a relationship for the conduction Nusselt number. In the case of horizontal concentric cylinders, either form of the equation is straightforward. In fact, both were applied to ensure consistency of the calculations.

The local equivalent thermal conductivity, k_{eq_i}, is computed as the following:

$$k_{eq_i} = \frac{q_i}{q_{cond_i}} \qquad \text{(Eqn. 8)}$$

where q_i is a local heat flux and q_{cond_i} is the conduction heat flux for concentric cylinders. On any given surface (inner or outer), the local heat flux varies with respect to θ; the conduction heat flux does not.

Air as the Working Fluid, Ra_L = 4.85x10^4

The first flow simulation performed with Fuego is a laminar natural convection problem in which air is the working fluid in the annulus (refer to [6]). The Rayleigh number, based on annulus gap-width, L, is defined as

$$Ra_L = \frac{g\beta\Delta T L^3}{\nu\alpha} \qquad \text{(Eqn. 9)}$$

where the gap-width is defined in terms of the inner and outer radii as, $R_o - R_i$, α is the fluid thermal diffusivity ($k/\rho c_p$), ν is the fluid kinematic viscosity (μ/ρ), and, β is the volumetric thermal expansion coefficient ($1/T$, for ideal gases).

CFD Boundary Condition and Thermal Property Specifications

Boundary conditions for the laminar flow case are fixed inner and outer cylinder temperatures.

- T_{hot} = 321.53 K (48.38°C)
- T_{cold} = 295.23 K (22.08°C)
- ΔT = 26.3 K

The thermal properties, except for the fluid density, are evaluated at the film temperature. The density varies with temperature in a piecewise linear fashion (effectively an incompressible ideal gas assumption) in order to drive fluid motion.

Table 2 provides average thermal properties and Table 3 provides air density as a function of temperature.

Table 2. Average Thermal Properties for Air, Ra_L = 4.85x10^4

CFD Simulation	k (W/m-K)	c_p (J/kg-K)	μ (kg/m-s)
Air, Laminar	$26.92x10^{-3}$	1007.34	$1.8856x10^{-5}$

Note: each property is evaluated at a film temperature of 308.38 K

Table 3. Air Density, $Ra_L = 4.85x10^4$

Temperature (K)	Density (kg/m^3)
250	1.3947
300	1.1614
350	0.9950

CFD Simulation Specifications

To attain steady-state conditions for this laminar flow problem, the Courant-Friedrichs-Lewy (CFL) limit is specified as 25. The specification of a CFL limit dictates just how aggressively Fuego alters the time step when using an automatic time-stepping approach while marching to steady state. During the early transient, the time step is on the order of 10^{-3} to 10^{-2}s. Later in the simulation, the CFL limit resulted in a time step of about 0.2s. Under relaxation of pressure or momentum is not necessary when fourth order smoothing with time-step scaling is specified as the projection method. A projection method for pressure-velocity coupling is used to ensure an appropriate computation of a pressure field which is consistent with a velocity field that satisfies the continuity equation locally. Two nonlinear iterations are specified; however, marching towards steady-state probably only requires a single non-linear iteration. This will be investigated later in the report. Overall, (nonlinear) equation residuals were reduced by 3 to 4 orders of magnitude.

The interpolation method for convection uses a higher-order upwinding MUSCL (Monotonic Upwind Schemes for Conservation Laws) [2] approach with Fuego default values specified for the upwind limiter (Superbee), first-order upwind factor (0.01), and the hybrid upwind factor (1.0). The fluids solve method for continuity and all other scalar equations is Aztec GMRES (nonsymmetric, generalized minimum residual). The preconditioning method is DD-ILUT (domain decomposition with a sparse LU factorization) for continuity and Symmetric-Gauss-Seidel for all other scalars.

For a $Ra_L = 4.85x10^4$, the Fuego predicted steady-state temperature contours are shown in Figure 2, streamlines are shown in Figure 3. Streamlines are shown with temperature contours in the background.

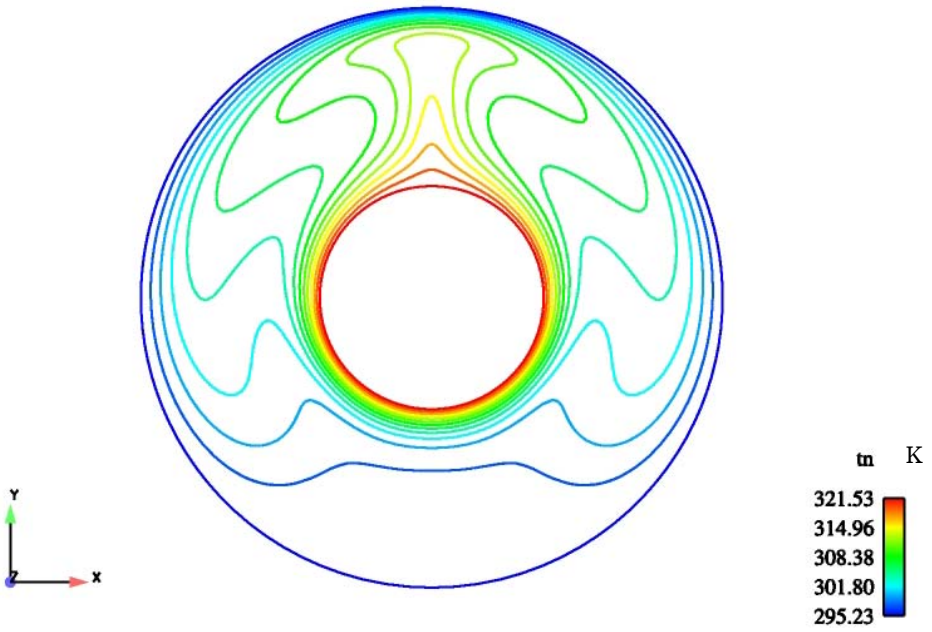

Figure 2. Predicted Temperature Contours for Laminar Natural Convection in the Annulus between Horizontal Concentric Cylinders $Ra_L \approx 5x10^4$

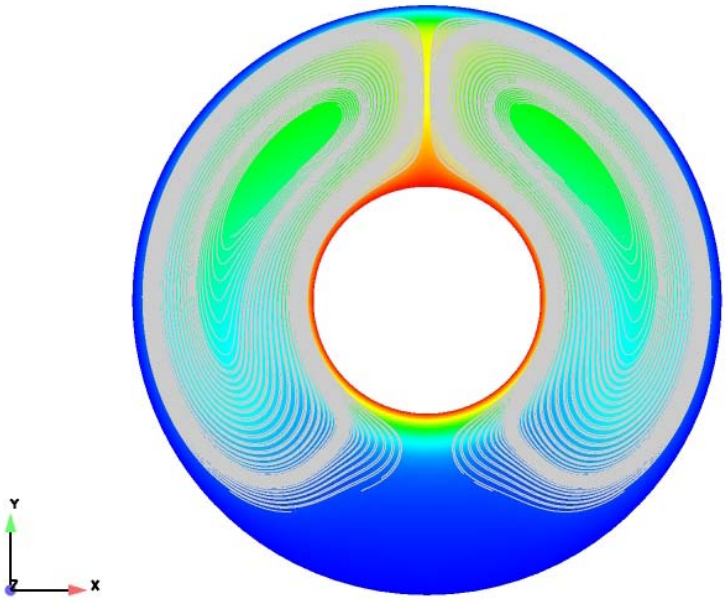

Figure 3. Predicted Streamlines for Laminar Natural Convection in the Annulus between Horizontal Concentric Cylinders $Ra_L \approx 5x10^4$

The Fuego predicted temperature contours and streamlines compare qualitatively to the temperature contours and streamlines shown in [6] (in reference [6]: refer to figure 10 for numerical results and figure 14 for measured data). No oscillations of the upward moving plume are noted at this low Rayleigh number. None are expected because this is a purely laminar Rayleigh number for these conditions. The predicted average equivalent thermal conductivity is computed using Equation (7). The predicted result is compared to measured data (from [6], table 1) in Table 4.

Table 4. Average Equivalent Thermal Conductivity, $Ra_L \approx 5x10^4$

CFD Simulation	k_{eq} Predicted	k_{eq} Measured
Air, Laminar	2.9	3.0

Overall, the Fuego predicted CFD results for this laminar natural convection analysis compare very well with both the measured data and numerical results presented in [6].

Pressurized Nitrogen as the Working Fluid, $Ra_L = 2.51x10^6$

The second flow simulation performed with Fuego is a transitional flow natural convection problem in which pressurized nitrogen (34.6 atm) is the working fluid within the annulus [7] – [9]. The Rayleigh number is at or near transition between laminar and turbulent flows. For Rayleigh numbers above approximately $2x10^5$, oscillations in the heated plume rising above the inner cylinder begin to appear. Above 10^6, the oscillations become more irregular and fluctuations in the outer cylinder boundary layer begin to increase. This is a difficult Rayleigh number to analyze numerically as both flow conditions (laminar and turbulent) are present within the same flow field. Subsequently, both laminar flow equations and the v2-f and LRKE turbulence models will each be assessed individually for these transitional flow conditions.

CFD Boundary Condition and Thermal Property Specifications

The boundary conditions for this flow problem are fixed inner and outer cylinder temperatures.

- T_{hot} = 301.305 K (28.155°C)
- T_{cold} = 300.395 K (27.245°C)
- ΔT = 0.91 K

The thermal properties, except for the fluid density, are evaluated at the film temperature. The density is allowed to vary in a piecewise linear fashion as a function of temperature in order to drive fluid motion. Table 5 provides average thermal properties and Table 6 provides the density as a function of temperature. The density is assumed an ideal gas at these temperatures and pressure (i.e., the compressibility factor is approximately equal to one at this state).

Table 5. Average Thermal Properties for Nitrogen, $Ra_L = 2.51x10^6$

CFD Simulation	k (W/m-K)	c_p (J/kg-K)	μ (kg/m-s)
N_2, Laminar and Turbulent	$2.735x10^{-2}$	1141.4	$1.754x10^{-5}$

Notes: Each average thermal property is evaluated at a film temperature of 300.85 K, a pressure of 3505.845 kPa and a Prandtl number (Pr) of 0.731.

The Fuego turbulence model requires an enthalpy function to compute temperature. This fluid property is treated as a temperature dependent quantity using the average specific heat. At T = 300 K, h = $342.42x10^3$ J/kg; at 302 K, h = $344.70x10^3$ J/kg.

Table 6. Nitrogen Density, $Ra_L = 2.51x10^6$

Temperature (K)	Density (kg/m^3)
300	39.347
300.1	39.334
300.2	39.321
300.3	39.308
300.4	39.295
300.5	39.282
300.6	39.269
300.7	39.256
300.8	39.243
300.9	39.230
301	39.217
301.1	39.204
301.2	39.191
301.3	39.178
301.4	39.165
301.5	39.152
301.6	39.139
301.7	39.126
301.8	39.113
301.9	39.100
302	39.087

Note that the N_2 pressure is 3505.845 kPa (34.6 atm)

CFD Simulation Specifications for Laminar Flow Conditions

To attain a steady-state condition (if one is achievable) for the laminar flow problem, the CFL limit is specified as 1.0. During the early transient, the time step is on the order of 10^{-3} to 10^{-2}s. Later in the simulation, the CFL limit resulted in a time step of about $3x10^{-2}$s. Under relaxation of pressure or momentum is not necessary because fourth order smoothing with time-step scaling is specified as the projection method. Two nonlinear iterations are specified in the event of obtaining an oscillatory fluids response. Overall, non-linear equation residuals were reduced by 3 to 4 orders of magnitude.

The interpolation method for convection is a higher-order upwinding MUSCL approach with Fuego default values for the upwind limiter (Superbee), first order upwind factor (0.01), and the hybrid upwind factor (1.0). The solution method for continuity and all scalar equations is Aztec GMRES. The preconditioning method is DD-ILUT for continuity and Symmetric-Gauss-Seidel for all other scalars.

For a Ra_L = $2.51x10^6$, the laminar flow temperature contours are shown in Figure 4 at a delta time of about 10 s. It is noted that the plume is indeed oscillating about the vertical centerline of the annulus. This plume oscillation results in a Strouhal number $\left(\frac{\tau L}{V_0}\right)$, based on annulus gap-width and a characteristic velocity $\{V_0 = \sqrt{g\beta L(T_{hot} - T_{cold})}\}$, of approximately 0.047. As expected, the laminar flow solution at this transitional Rayleigh number indicates an oscillating upward moving plume originating from the hot inner cylinder and impinging on the outer cylinder. That is, the laminar flow solution for these thermal conditions is inherently unsteady. The heat transfer results extracted from this simulation are for a vertically aligned upward moving plume. Time averaged heat transfer results are not considered in the comparison with the measured data, but are not expected to be that different from the single location vertical plume result.

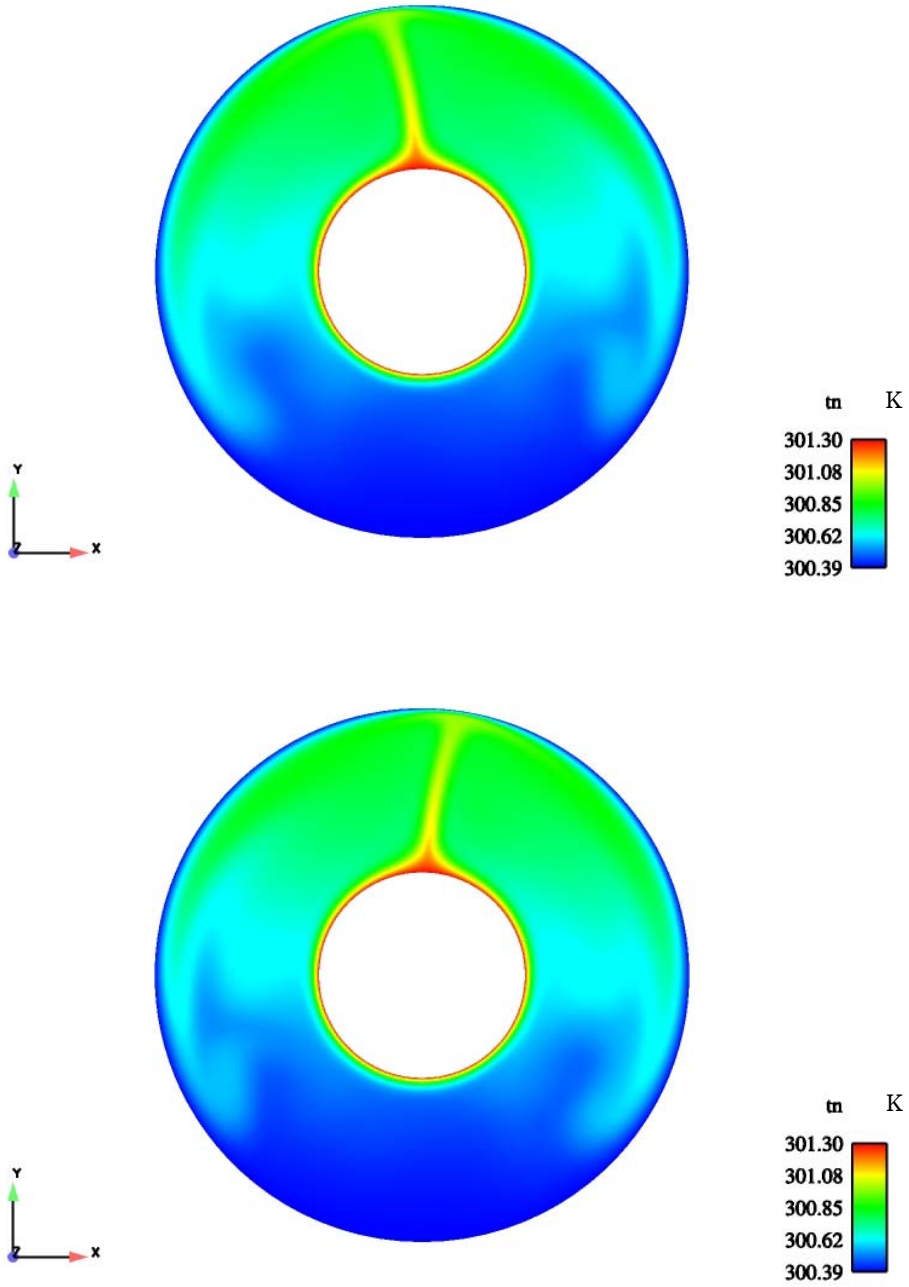

Figure 4. Predicted Temperature Contours for Laminar Natural Convection in the Annulus between Horizontal Concentric Cylinders, $Ra_L = 2.51x10^6$

CFD Simulation Specifications for Turbulent Flow Conditions: v2-f turbulence model

To attain a steady-state condition (if one is achievable) for the same problem, in this instance solving v2-f turbulent flow equations, a CFL limit of 1.0 is specified for time-stepping control. This resulted in a time step on the order of 10^{-3} to 10^{-2}s during the early transient and about $4x10^{-2}$s later in the simulation. Under relaxation of pressure or momentum is not necessary because fourth order smoothing with time-step scaling is specified as the projection method. However, under relaxation is performed to various degrees for the other scalar equations and turbulence properties. The under relaxation parameters are given in Table 7. Typically, under relaxation parameters are specified so that runtime modifications are not required. A single nonlinear iteration is specified in the analysis. Overall, nonlinear equation residuals were reduced by between 3 to 5 orders of magnitude. It is noted that the equation residuals from the f-equation had a tendency to wander; however, this equation too had low residuals, in the range of 10^{-4} to 10^{-9}.

The interpolation method for convection uses a higher-order upwinding MUSCL approach with Fuego default values used for the upwind limiter (Superbee) and the hybrid upwind factor (1.0). However, it was found that the v2-f turbulence model *required an increase* in the first-order upwind factor from the default value of 0.01. Subsequently, in order to compute a stable solution with the v2-f turbulence model, one must allow for a portion of the convection operator to contain some pure first-order upwind convection, thereby adding some artificial damping to the solution. An in-depth study was not performed on this particular parameter to determine an optimal numerical result. The first-order upwind factor was chosen to be 0.5. Therefore, 50% of the convection operator is composed of pure first-order upwind convection. The remaining 50% is higher-order upwind convection with default values/specifications for the upwind limiter (to prevent numerical oscillations) and hybrid upwind factor (to specify the relative amount of higher-order upwinding and central differencing). The solution method for continuity and all scalar equations is Aztec GMRES. The preconditioning method is DD-ILUT for continuity and Symmetric-Gauss-Seidel for all other scalars. A single preconditioning step is applied.

Simulation initial conditions are the following:

- Pressure = 0 Pa
- Velocity (U, V, W) = 0 m/s
- Temperature = 300.85 K
- k = 10^{-4} m^2/s^2

- $\overline{v^2} = 10^{-4}$ m^2/s^2
- $\varepsilon = 10^{-5}$ m^2/s^3
- f = 0

The velocity condition is specified everywhere as zero initially because much of the fluid domain is at or near no flow. That is, most of the flow occurs at the walls with the core fluid region essentially motionless.

Table 7. Under Relaxation Parameters for v2-f Turbulence Model, Ra_L = $2.51x10^6$

Quantity	Value
Enthalpy	0.9
Turbulent viscosity	0.6
Turbulent kinetic energy	0.4
Turbulence dissipation	0.4
Turbulence Helmholtz f-function	0.4
Turbulent v2	0.4

The predicted annulus temperatures are compared directly to the temperatures illustrated in [8] for a $Ra_L = 2.51x10^6$ (refer to [8]: figures 7 – 8 and table 1). Essentially no oscillations of the upward moving plume are noted at this transitional Rayleigh number when using the v2-f turbulence equations. This is expected because of the additional viscosity added when including the turbulent Reynolds stress terms in a RANS formulation.

As before, the average equivalent thermal conductivity is computed with Equation (7). Fuego predictions of an average equivalent thermal conductivity for both laminar and turbulent flows are compared to measured data in Table 8. Additionally, a local equivalent thermal conductivity for both laminar and turbulent flows as a function of θ is acquired with Equation (8). Figure 5 and Figure 6 compare predicted results to measured data for all three computational meshes described in Table 1, using the v2-f turbulence model. They provide a direct assessment of Fuego against measured data in the literature. An additional assessment of Fuego compares the low-Mach number code to a widely used commercial CFD code. Figure 7 and Figure 8 illustrate

Fuego results obtained from the coarse mesh, for both laminar and v2-f turbulence equations, compared to the results of the commercial CFD code, FLUENT. The turbulence model used in FLUENT is a RANS formulation known as the Renormalized Group (RNG) k-ε turbulence model with a differential viscosity model used for low Reynolds number effects [9]. It also includes production and dissipation of turbulent kinetic energy due to buoyancy in the k-equation and ε-equation. The FLUENT mesh described in [9] is slightly more coarse than the coarse mesh in Table 1.

Table 8. Fuego Predicted Average Equivalent Thermal Conductivity, Ra_L = $2.51x10^6$

Parameter	Laminar	v2–f Turbulent*	Data
k_{eq}	7.37	7.56[a], 7.64[b], 7.65[c]	7.88

a – 52x144

b – 70x192

c – 78x216

* - FLUENT average result is 7.29 (refer to [9])

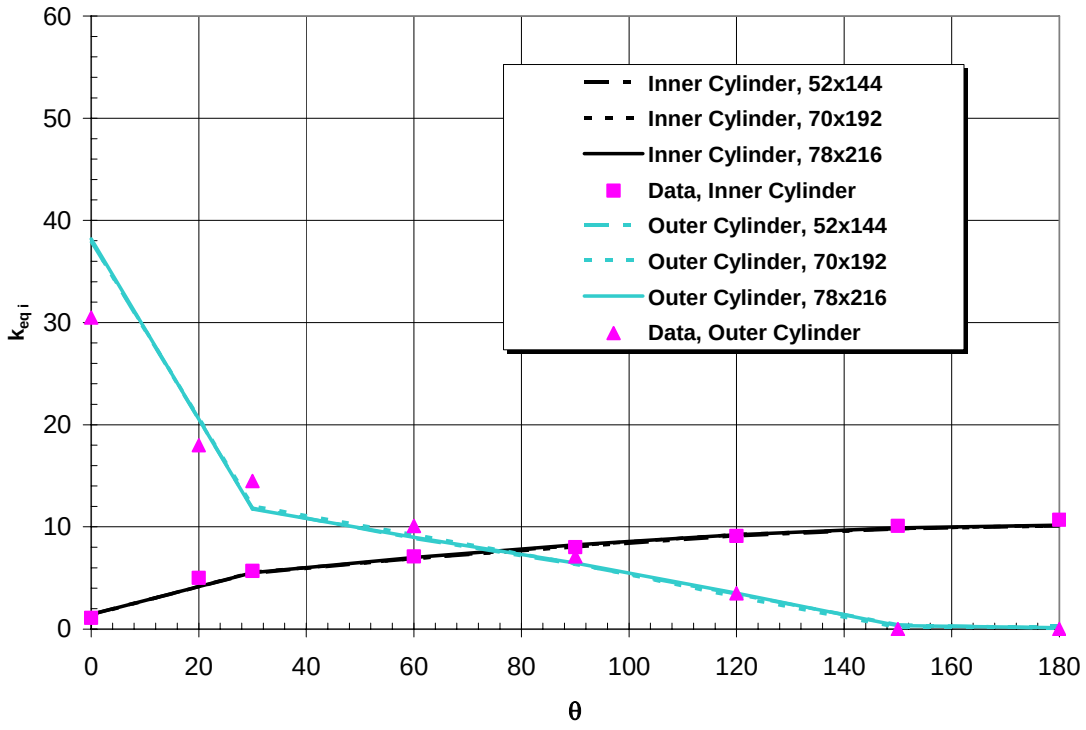

Figure 5. Local Equivalent Thermal Conductivity from Three Meshes as a Function of θ using the v2-f Turbulence Model (measured data in symbols)

The results given in Table 8 and in Figure 5 and Figure 6 illustrate that the fluids meshes are essentially grid independent. Additional discussion related to the quality of the fluids mesh, in particular, the resultant influence of cell aspect ratio (AR) on the sensitivity of the v2-f turbulence model predictions, is given later in this section.

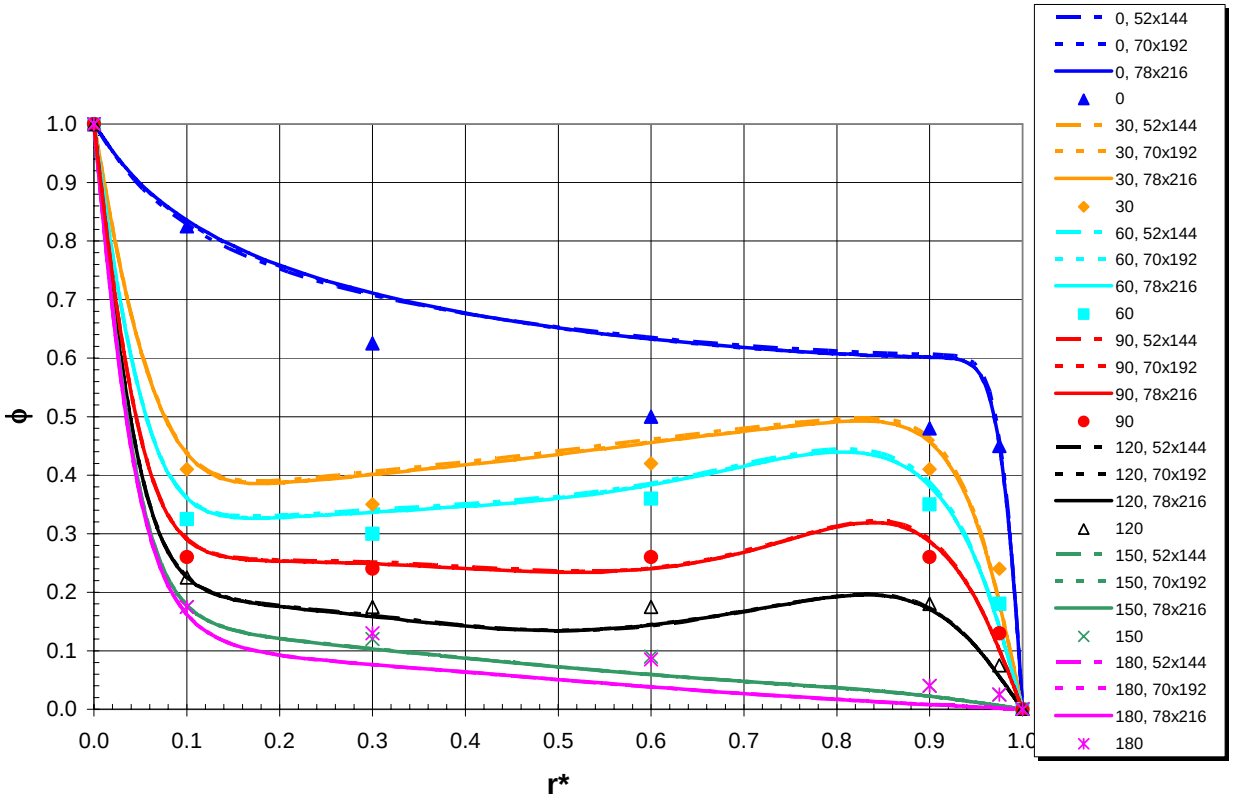

Figure 6. Dimensionless Annulus Temperature from Three Meshes as a Function of $r*$ and θ using the v2-f Turbulence Model (measured data in symbols)

In Figure 6 the dimensionless distance is defined as $r^* = \frac{R - R_i}{L}$ and the dimensionless temperature is defined as $\phi = \frac{T - T_{cold}}{T_{hot} - T_{cold}}$. Referring to Figure 5 and Figure 6, predicted results are reasonably close to the measured data. Most of the discrepancy occurs near the outer cylinder, in particular, within the region of the upward moving plume (at about $\theta = 0^o$, $r^* > 0.2$). The turbulence model over predicts the amount of heat transported by the fluid that separates from the top of the inner cylinder and impinges on the outer cylinder. If indeed the RANS formulation contains too much isotropic turbulent viscosity, the region in which turbulence primarily occurs, that is, in the upward moving plume, may result in too much heat diffusion thus elevating the temperature of the fluid near the outer cylinder. That is, the coefficient $\left(\frac{\mu}{\mathrm{Pr}} + \frac{\mu_t}{\mathrm{Pr}_t}\right)$ in the energy transport equation may allow for too much energy

transport by diffusion. The turbulent Prandtl number, $\mathrm{Pr}_t = (\nu_t/\alpha_t)$ is typically assumed to be about 1.0.

The wall heat flux is computed from a known wall temperature and adjacent fluid properties by performing a conduction energy balance between the prescribed wall and the first fluid node. Subsequently, the wall energy balance is a function of the molecular thermal diffusivity only. Alternatively, one can base the wall heat flux on an apparent heat flux. Consequently, the heat flux at the wall is written in terms of the molecular thermal diffusivity and a turbulent thermal diffusivity as the following:

$$q_w = \rho C_p (\alpha + \alpha_t) \left[\frac{T_w - T_p}{y_p} \right] \qquad \text{(Eqn. 10)}$$

where T_w and T_p are the temperature at the wall and at the first fluid node, respectively, and y_p is the normal distance from the wall to the node in the fluid. The turbulent thermal diffusivity can be implemented as a second-order closure in terms of a temperature variance and the dissipation rate of temperature variance. Consequently, one can model the turbulent thermal diffusivity in a manner analogous to Equation (2) using both the turbulence time-scale and a thermal field time scale written in terms of the temperature variance and its dissipation rate [10]. Furthermore, one can then compute (instead of assume) a turbulent Prandtl number in terms of the modeled turbulent viscosity and turbulent thermal diffusivity.

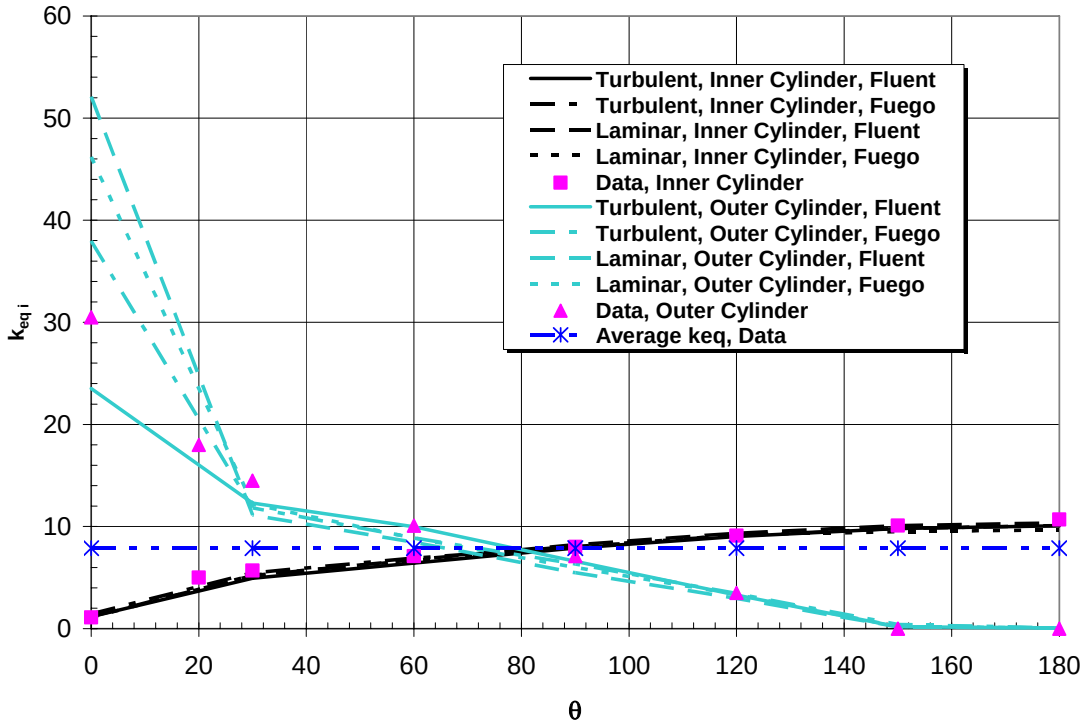

Figure 7. Local Equivalent Thermal Conductivity from Fuego (coarse mesh) and FLUENT as a Function of θ (measured data in symbols)

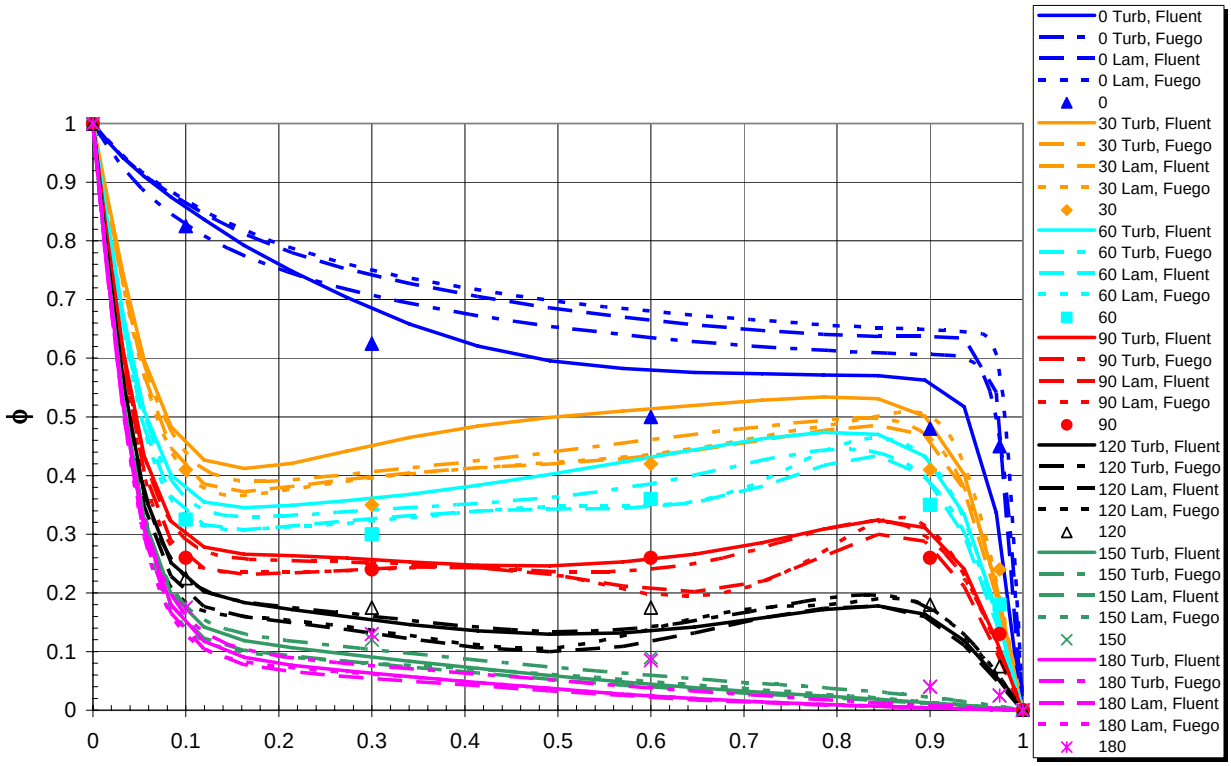

Figure 8. Dimensionless Annulus Temperature from Fuego (coarse mesh) and FLUENT as a Function of $r*$ and θ (measured data in symbols)

Reference to Figure 7 and Figure 8 indicate that the Fuego predictions are very similar to those from FLUENT. In fact, other than in the upward moving plume (at $\theta = 0^o$), the v2-f turbulence model somewhat outperforms the RNG k-ε turbulence model. As expected, the laminar predictions between CFD codes are essentially the same. Based on this comparison, the performance of Fuego is comparable to or slightly better than a widely accepted industrial CFD code. The comparison is largely a physics comparison only.

It is necessary to identify the y^+ values (refer to Equation 1) on both cylinder walls. As indicated by Equation (1), the near-wall region should be resolved such that inner region phenomenon are completely captured by the numerical grid. Typically, this requires that the first grid point be located from the wall a dimensionless normal distance of one or less, with several mesh elements located within the inner layer in order to calculate the higher order differencing schemes accurately. Figure 9 illustrates y^+ for each mesh in Table 1. The distance in Figure 9 represents the circumferential position along either cylinder.

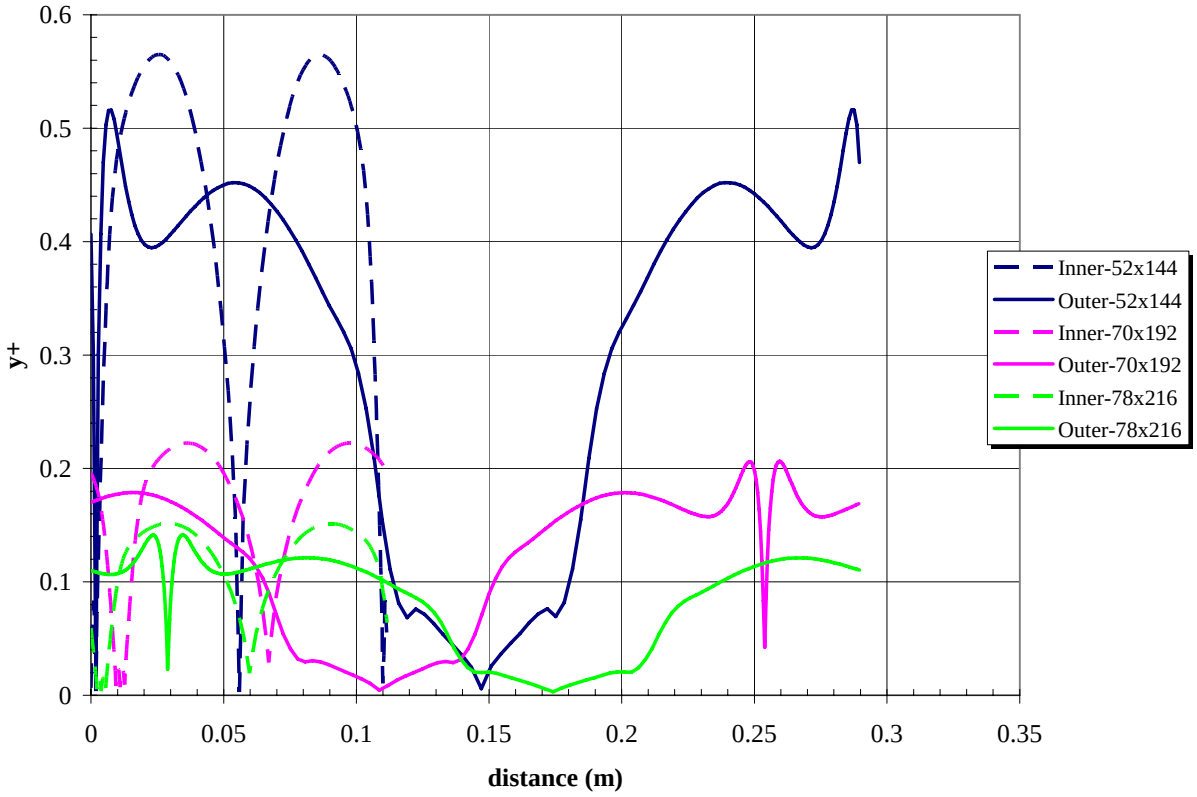

Figure 9. Dimensionless Normal Distance Computed from the v2-f Turbulence Model for each Mesh in Table 1

From Figure 9, it is evident that the near-wall regions are adequately resolved. The maximum y^+ value on any surface is approximately 0.6, all others are less. The near-wall mesh resolution is considered adequate enough to capture the peak turbulence kinetic energy and the peak in production of turbulence, both occurring within the inner region. This is essential in capturing the effects of turbulence in wall-bounded shear flows. Figure 9 illustrates that each mesh satisfies Equation (1). That is, the non-dimensional normal distance is approximately one.

It may be additionally instructive to determine the sensitivity of the v2-f turbulence model to cell aspect ratio. When resolving a very thin boundary layer adjacent to a wall, one can generate cell aspect ratios somewhat greater than 10 to 1. This is normally not a significant problem when the fluid flow direction is essentially aligned with the grid. In a boundary layer, the direction of flow is almost always aligned with the grid. However, other features of the v2-f turbulence model may require more stringent restrictions on just how "bad" cell aspect ratios can be in the boundary layer.

Using the same incremental specifications as the Fuego mid mesh given in Table 1, the cell-clustering factor at the walls is modified to ensure that all cell aspect ratios are approximately 10:1 everywhere in the fluids domain, including within the thin boundary layers adjacent to the cylinder walls. It is expected that mean fluid properties such as temperature and velocity should largely be unaffected by this change; however, the effect on turbulence properties will also be investigated. In particular, the effects on these quantities in the near-wall region are investigated, because the normal wall fluctuating velocity is important in predicting the turbulent viscosity. Figure 10 – Figure 12 illustrate the annulus equivalent thermal conductivity, temperature distribution, and vertical velocity, respectively. In Figure 12, the vertical velocity is presented at an angle of $\theta = 90^{o}$. From the figures, it is evident that the cell aspect ratio in the boundary layer does not drastically affect the local mean quantities (heat flux, temperature, and velocity). Additionally, the average equivalent thermal conductivity is 7.64 and 7.45 for the mid mesh and modified AR, respectively. So, as expected, the mean flow quantities are not overly affected by "bad" aspect ratios in the boundary layers because the flow is very well aligned with the grid.

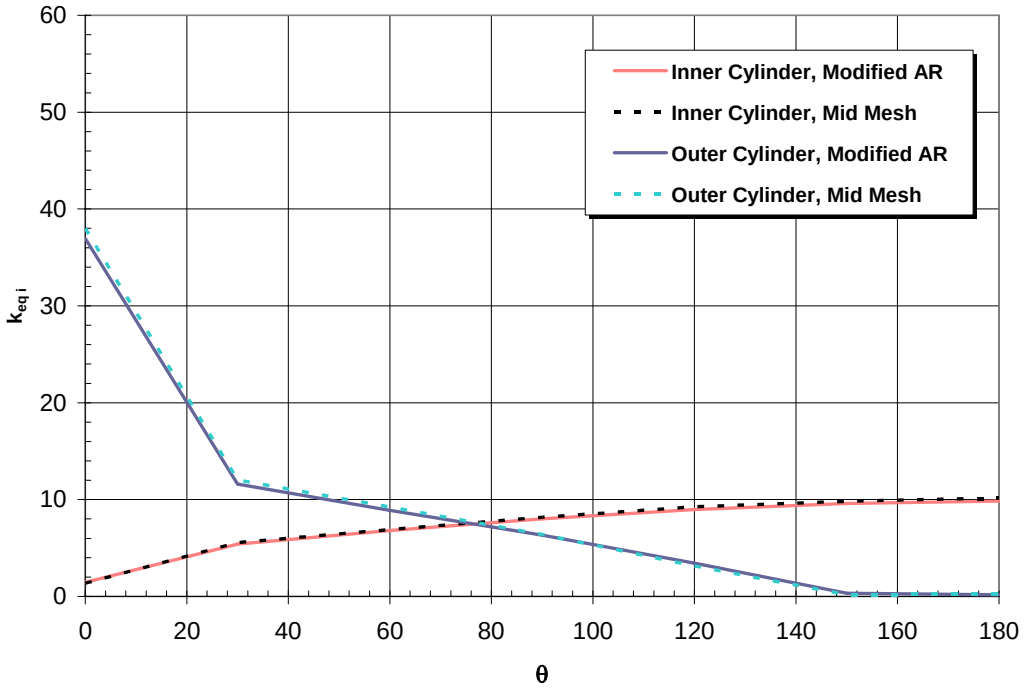

Figure 10. Heat Flux Comparison from the Mid Mesh (Table 1) to the Mid Mesh with Modified Aspect Ratio (AR)

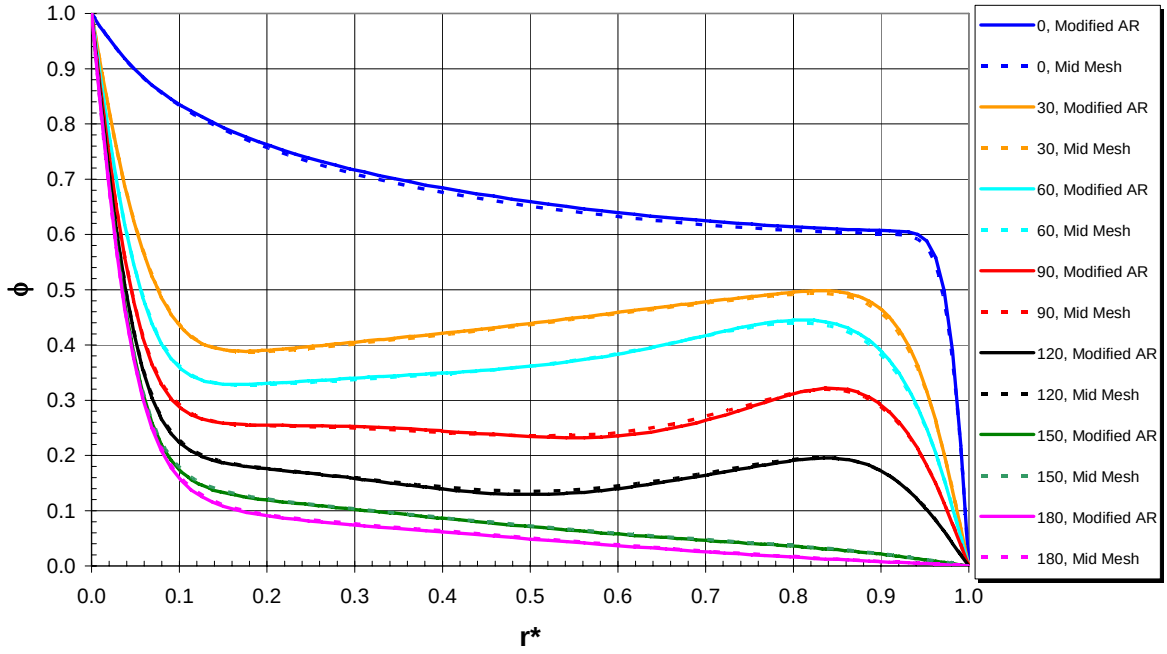

Figure 11. Annulus Temperature Comparison from the Mid Mesh (Table 1) to the Mid Mesh with Modified Aspect Ratio (AR)

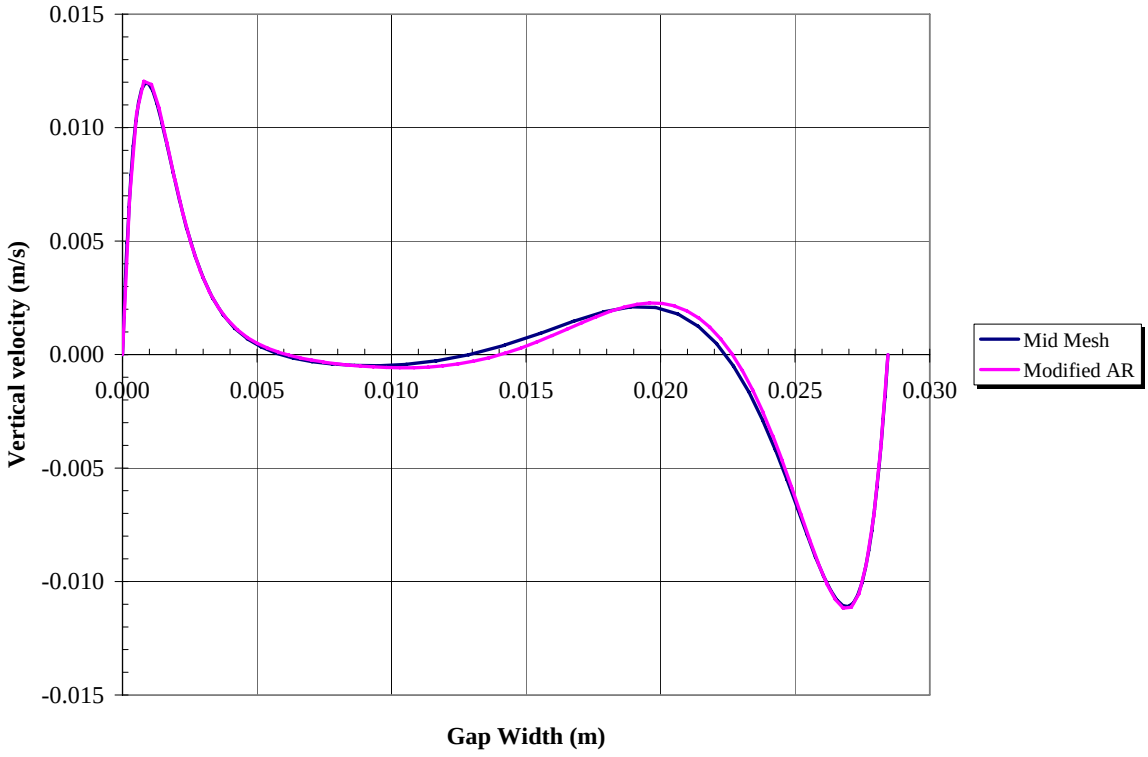

Figure 12. Vertical Velocity Comparison from the Mid Mesh (Table 1) to the Mid Mesh with Modified Aspect Ratio (AR)

It is important to verify that the first mesh point in the near-wall region of the modified AR mesh is still valid. A plot of non-dimensional normal distance, y^+, in Figure 13 indicates that the modified AR mesh satisfies the criterion given by Equation (1).

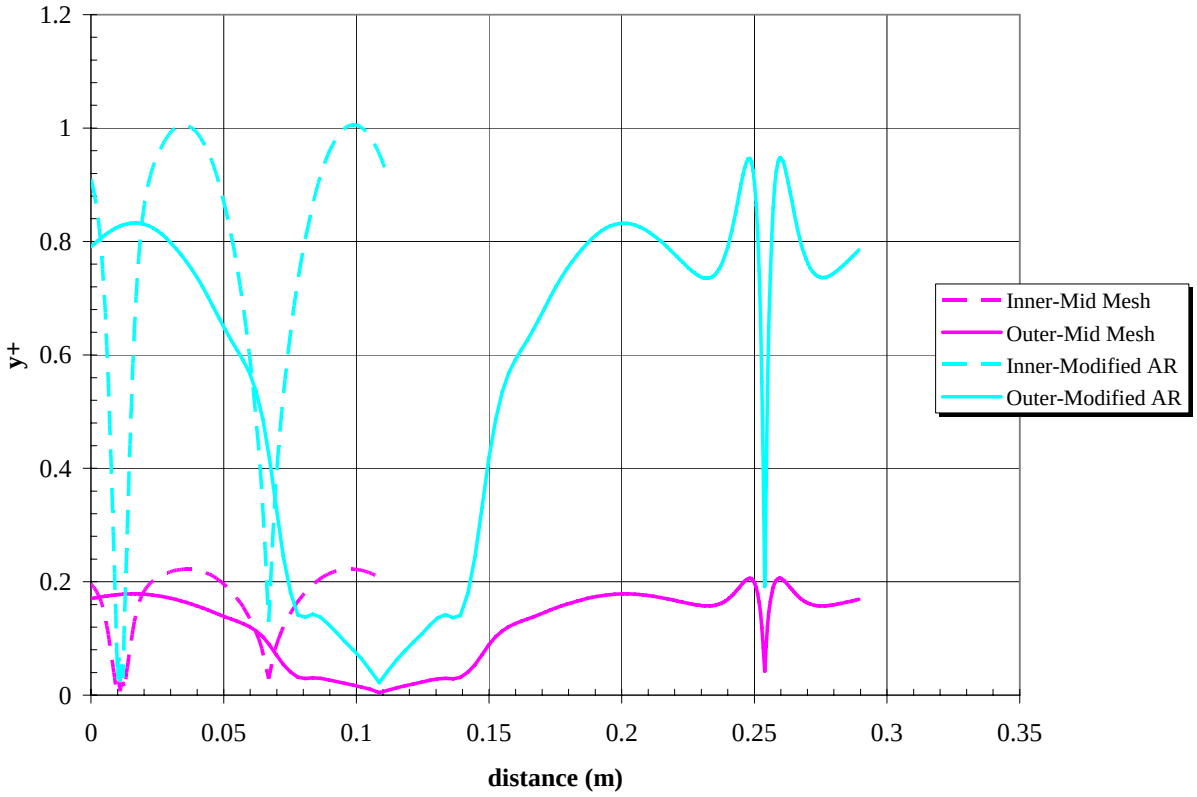

Figure 13. Dimensionless Normal Distance Computed from the v2-f Turbulence Model for the Mid Mesh and Modified AR Mesh

A final check is performed on a turbulence quantity. The turbulent kinetic energy in the annulus is investigated to determine the influence of cell aspect ratio on turbulence quantity. Figure 14 compares the turbulent kinetic energy from each fluids mesh at an angle of $\theta = 90^o$.

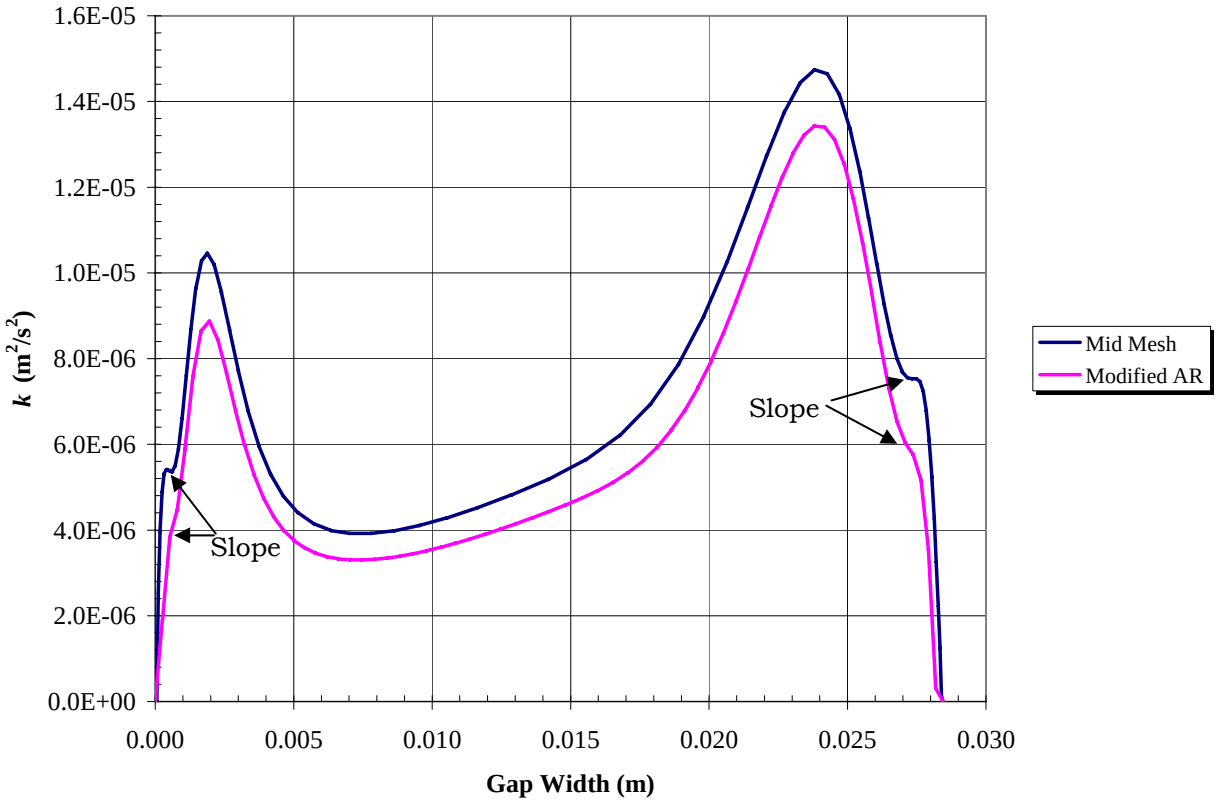

Figure 14. Turbulent Kinetic Energy Comparison from the Mid Mesh (Table 1) to the Mid Mesh with Modified Aspect Ratio (AR)

It is evident that cell aspect ratio does have some impact on the turbulence kinetic energy. The mid mesh displays a change in slope in the turbulent kinetic energy in the near-wall regions. This is a numerical artifact associate with cell aspect ratio. As the aspect ratio is improved in the near-wall region, the curve becomes more continuous. However, it is evident that even a 10:1 cell aspect ratio in the boundary layer may still be somewhat large for turbulence quantities. Therefore, when using the v2-f turbulence model, it is recommended, when possible, that the cell aspect ratios within the near-wall region are better than 10:1. The turbulence quantities impact the mean flow quantities through the Reynolds stress and turbulent heat flux terms, however, because the turbulence quantities are not greatly affected, this requirement does not have a large overall impact on the mean flow quantities.

Nonlinear (Picard) Iterations and Buoyancy Driven Turbulence

In all of the v2-f turbulence results shown so far, a single non-linear iteration is taken per time step and the generation of turbulence due to buoyancy is neglected in each of the turbulence equations. Consider first the influence associated with the number of nonlinear (Picard) iterations taken per time step.

It is assumed that in marching towards a steady-state solution, a single nonlinear iteration (1 Picard loop) is adequate. However, to ensure that this simplification is indeed acceptable, a simulation with the mid mesh is performed using three nonlinear iterations (3 Picard loops) per time step. Temperature and heat flux are compared. From Figure 15 it is evident that for surface heat flux, performing a single nonlinear iteration is a reasonable simplification when marching towards a steady-state flow solution. Additionally, the average equivalent thermal conductivities are 7.64 and 7.54 for 1 Picard and 3 Picard loops, respectively. Subsequently, the average heat flux through the annulus is essentially unchanged. Figure 16 illustrates the nondimensional temperature distribution through the fluid in the annulus.

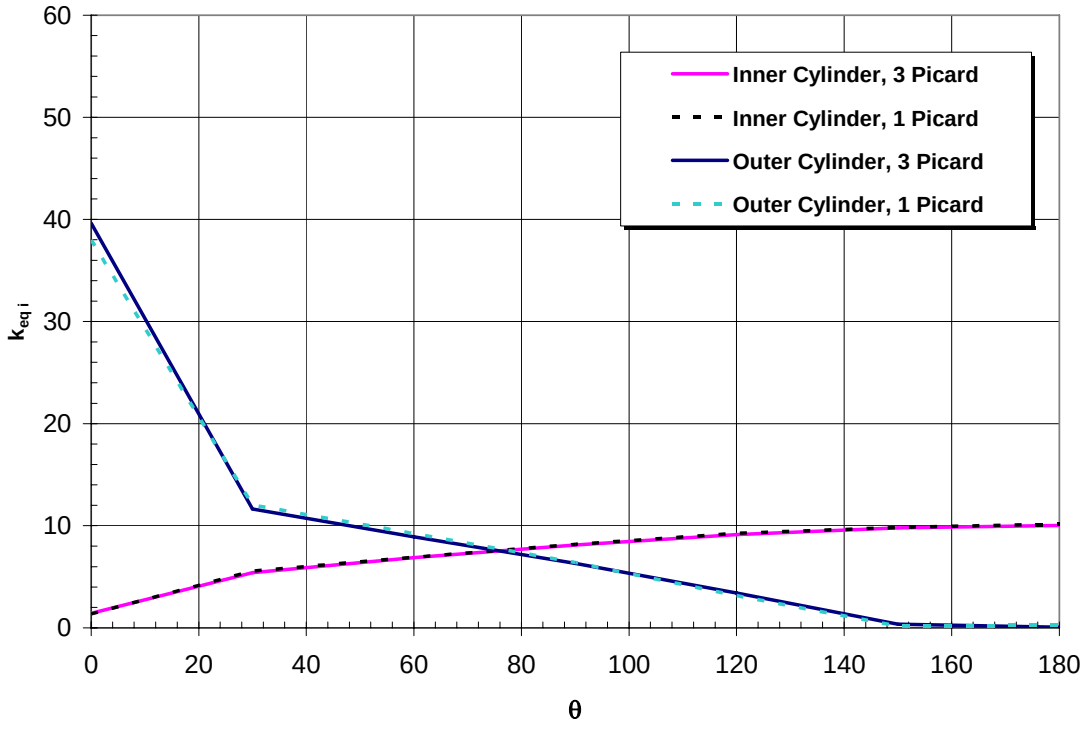

Figure 15. Heat Flux Comparison of a Single Nonlinear Iteration to Multiple Nonlinear Iterations using the Mid Mesh

The temperature distributions are also essentially identical. This is an important assessment. This provides a grounds for justification for one to take a single non-linear iteration when marching towards a steady-state solution. The simulation using multiple nonlinear iterations per time step required *less* mother-nature time but *more* compute time to reach a steady state solution.

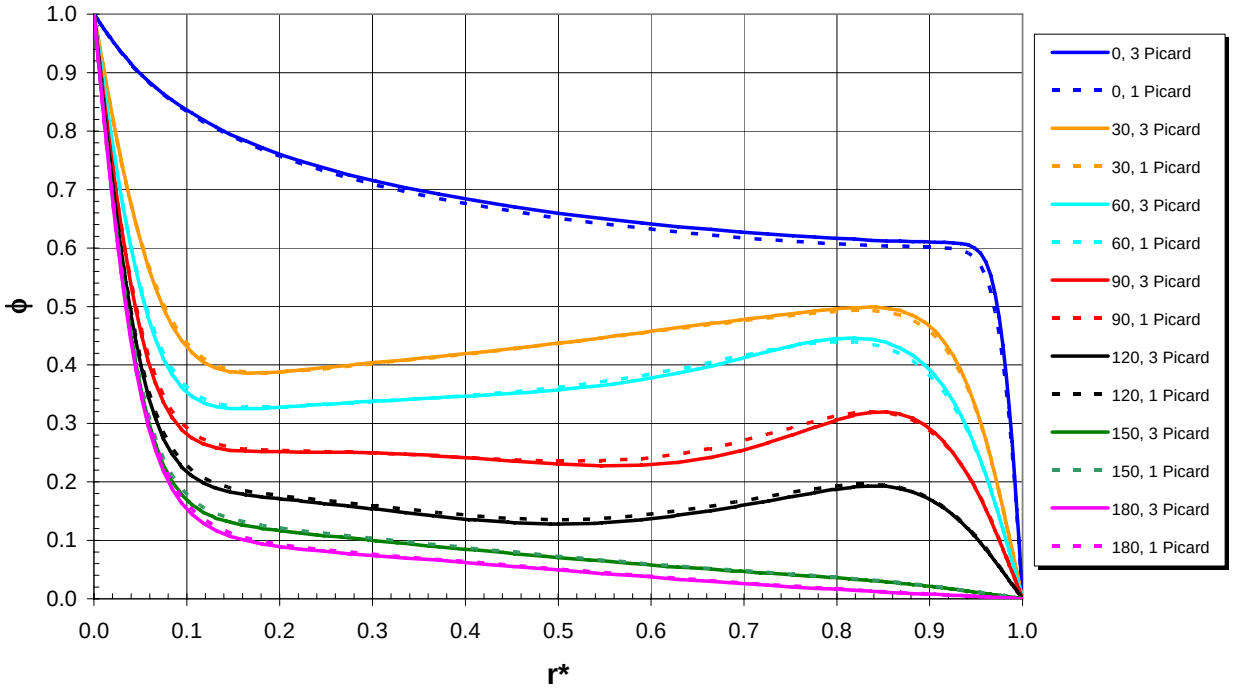

Figure 16. Annulus Temperature Comparison of a Single Nonlinear Iteration to Multiple Nonlinear Iterations using the Mid Mesh

The second simplification applied in each of the previous simulations using the v2-f turbulence model is related to the generation of turbulence resulting from buoyancy forces driving fluid motion. The Rodi buoyancy term,

$$G_b = \beta g_i \frac{\nu_t}{\mathrm{Pr}_t} \frac{\partial T}{\partial x_i} \qquad \text{(Eqn. 11)}$$

is neglected in both the *k*-equation and ε-equation. In order to further understand the influence of turbulence generated by a buoyancy driven flow, Equation (11) is now included on the right-hand side of the *k*-equation applied to the mid mesh with modified aspect ratio. Figure 17 illustrates the local heat flux around the circumference of the cylinders. The addition of the Rodi buoyancy term primarily affects the upward moving plume impacting the top of the outer cylinder. This is expected as the upper portion of the annulus is one of the locations in the flow field that exhibits turbulent flow. Overall, however, the impact of including the Rodi term is small as seen in the figure for local heat flux.

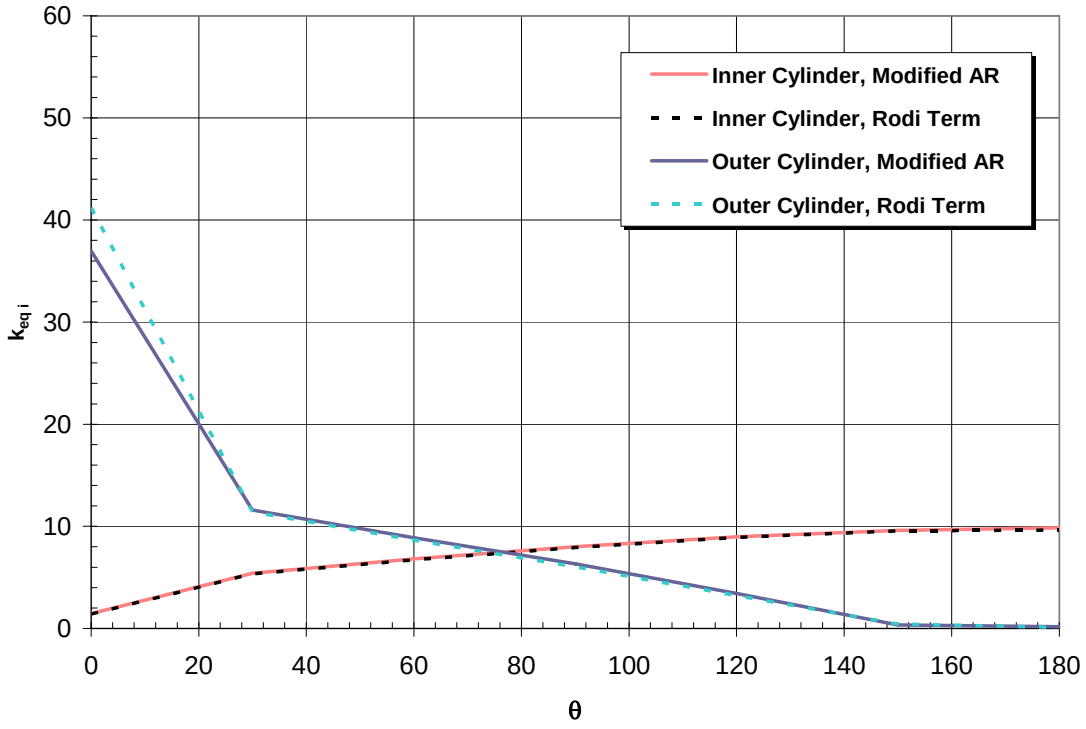

Figure 17. Heat Flux Comparison with and without the Rodi Buoyancy Term Included in the *k*-equation

The average equivalent thermal conductivity remains essentially unchanged when the Rodi buoyancy term is included in the *k*-equation (~ 1% change).

Figure 18 illustrates the annulus temperature distribution with and without the Rodi buoyancy term. It is evident that the addition of buoyancy driven turbulence has a slight impact on the temperature distribution in the fluid. The

inclusion of the Rodi buoyancy term in the *k*-equation increases the turbulent kinetic energy of the fluid. Subsequently, the turbulent viscosity increases and, as previously stated, this increases the leading coefficient of the energy diffusion term in the energy transport equation. Therefore, the temperature of the fluid in the upward moving plume is greater when the Rodi term is included. The fluid in the annulus below decreases in temperature as a result.

It is worth mentioning that including the Rodi buoyancy term resulted in a more unstable solution of the f-equation in the v2-f turbulence model. Just after a steady-state solution is essentially achieved, determined both by an overall energy balance and by noting that the flow field is essentially unchanging, the f-equation residual slowly diverges and the simulation stops. Without the Rodi term included, the simulation remains unchanging and stable with continued time stepping.

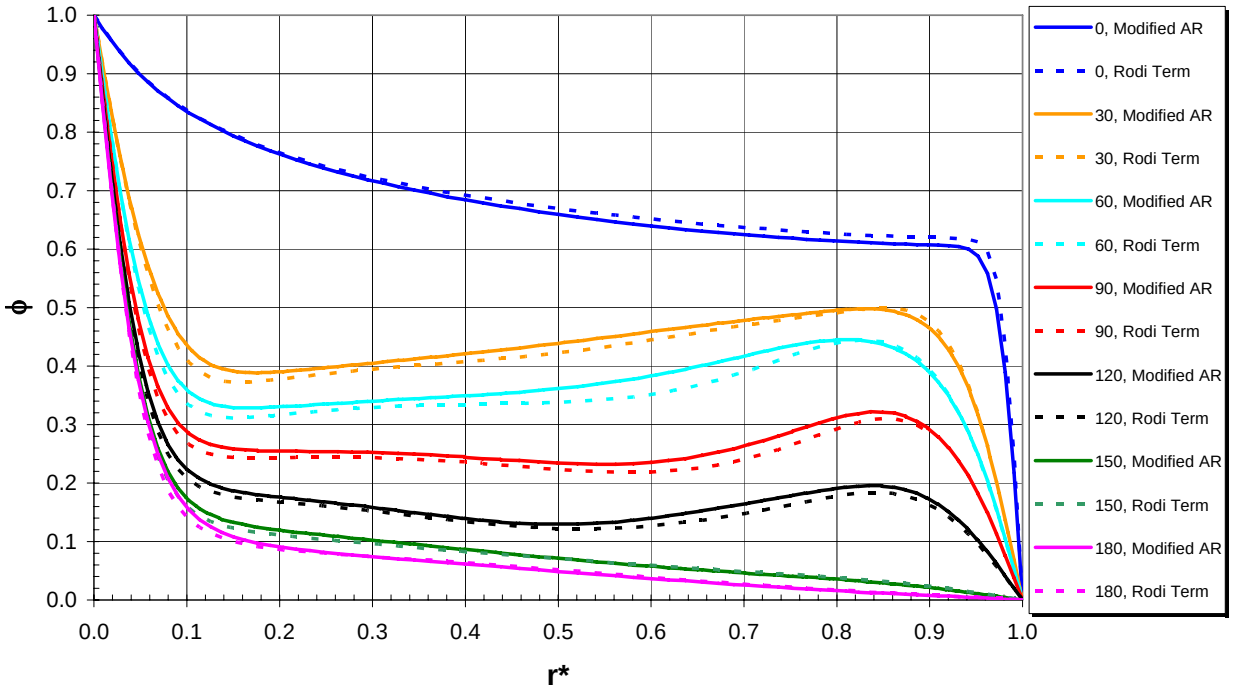

Figure 18. Annulus Temperature Comparison with and without the Rodi Buoyancy Term Included in the *k*-Equation

Up to this point in the analysis, not much has been said regarding the LRKE turbulence model in Fuego. It was found that the LRKE model displayed an inordinate amount of viscosity for this particular problem of turbulent natural

convection in the annulus between horizontal concentric cylinders. Some details associated with these findings are presented next.

CFD Simulation Specifications for Turbulent Flow Conditions: LRKE turbulence model

To attain a steady-state condition (if one is achievable) using the LRKE turbulence model, a CFL limit of 1.0 is chosen. This resulted in a time step on the order of 10^{-3} to 10^{-2}s during the early transient and about $7x10^{-2}$s later in the simulation. Under relaxation of pressure or momentum is not necessary because fourth order smoothing with time-step scaling is specified as the projection method. However, under relaxation is performed to various degrees for the other scalar equations and turbulence properties. The under relaxation parameters are given in Table 9. Typically, under relaxation parameters are specified so that runtime modifications are not required. A single nonlinear iteration is specified in the analysis. Overall, nonlinear equation residuals were reduced by between 3 to 7 orders of magnitude.

A turbulence dissipation source term is optional in the LRKE ε-equation. The dissipation source term (typically denoted by the symbol E, refer to [3]) is included in this LRKE simulation. How this selection impacts the turbulent kinetic energy, the dissipation rate of turbulence kinetic energy, and subsequently, the turbulent viscosity, will be discussed later.

The interpolation method for convection is a higher-order upwinding MUSCL approach with Fuego default values used for the upwind limiter (Superbee) and the hybrid upwind factor (1.0). Like the v2-f turbulence model, the first-order upwind factor is selected to be 0.5. (However, it is noted that artificial damping is probably not required to obtain a stable solution for this simulation.) Therefore, 50% of the convection operator is composed of pure first-order upwind convection. The remaining 50% is a higher-order upwind convection. The solution method for continuity and all scalar equations is Aztec GMRES. The preconditioning method is DD-ILUT for continuity and Symmetric-Gauss-Seidel for all other scalars.

The required initial conditions are identical to those specified in the v2-f model.

Table 9. Under Relaxation Parameters for LRKE Turbulence Model, Ra_L = $2.51x10^6$

Quantity	Value
Enthalpy	0.9
Turbulent viscosity	0.6
Turbulent kinetic energy	0.6
Turbulence dissipation	0.6

Using the coarse mesh, Figure 19 illustrates annulus temperature contours computed by both turbulence models. The v2-f model shows the expected result for the specified boundary conditions. It is interesting to note that the LRKE turbulence model *appears* to relaminarize flow conditions at low turbulence intensity as evidenced by the temperature contours computed for a Rayleigh number of $2.51x10^6$. In fact, the resultant flow field shown in (b) is more representative of a purely laminar flow solution somewhere in the Rayleigh number range of 10^3 to 10^4 (probably somewhat closer to 10^4).

This outcome could be that the onset of transition to turbulent flow in the upward moving plume and in the downward moving boundary layer flow along the top portion of the outer cylinder wall has not occurred (refer to [17] for details on relaminarization processes caused by low Reynolds number turbulence models). An observation associated with this turbulence model is just how "laminar" the flow field appears. This solution leads one to believe that the molecular viscosity of the fluid is nearly two orders-of-magnitude larger than it actually is. Interestingly, the average equivalent thermal conductivity computed from LRKE is 14.1. Therefore, the average heat transfer, which is *larger* than both the measured data and the other predicted results (refer to Table 8), is not consistent with an assertion that the flow has relaminarized. Something else must be happening. The inordinately large average equivalent thermal conductivity is a direct result of the large viscosity ratio computed from the LRKE model. The maximum viscosity ratio is on the order of 50, approximately ten times greater than the maximum viscosity ratio seen in the v2-f solution.

Evidently, the LRKE damping functions for the turbulent viscosity and the ε-equation are not appropriately tuned to this natural convection problem, which, for low-level turbulence, needs to account for (and cannot) the

anisotropic flow behavior near the wall. Therefore, strictly speaking, applying the Boussinesq hypothesis to relate the Reynolds stress terms to the mean velocity gradients cannot be performed simply with damping functions that do not account for the effects of anisotropic low-level turbulent behavior resulting from wall-bounded buoyancy driven flows. The v2-f model attempts to account for this behavior by including an elliptic equation thereby more accurately representing anisotropy than does LRKE. The LRKE turbulence model in its current form is not recommended for this problem. However, recommendations made in the next sections may enhance the ability of LRKE to model low-level turbulence intensity natural convection flows.

The turbulence dissipation source term, E, is included in this LRKE turbulence result. This dissipation source has the effect of reducing k and increasing ε, thus reducing the overall turbulent viscosity (a desired result). However, the term did not greatly influence the outcome of the solution.

Other models, such as those described in [9] and [11], incorporate the assumption of isotropic turbulence, but these models attain more success than LRKE with damping functions because of application of a two-layer approach in which the dissipation of turbulent kinetic energy is prescribed in terms of a length scale formulation rather than from the solution of an ε transport equation in the near-wall region. Additionally, the eddy viscosity in the near-wall region is similarly based on a length scale formulation.

In all of the turbulence simulations described above, the CFL limit is adopted as a somewhat conservative value of 1.0. For flow problems of the type described in this report, a reasonable value. However, for larger more complex problems, a CFL limit of 1.0 may be somewhat restrictive. In the description of the next geometry, this time stepping constraint will be investigated to determine if a larger CFL limit can be used when marching towards a steady-state solution

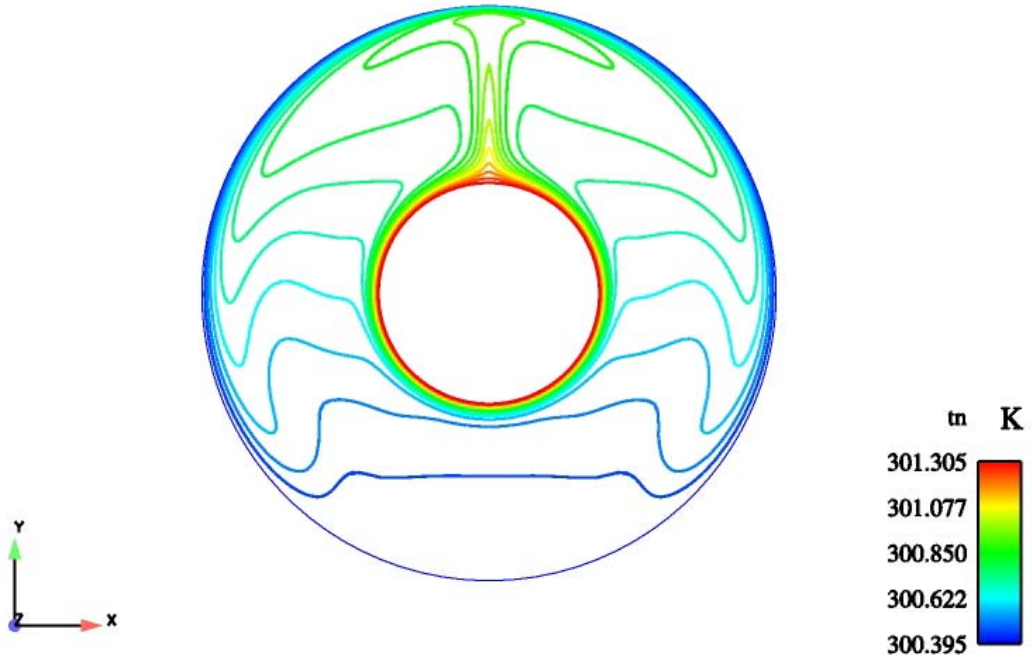

(a) v2-f Model

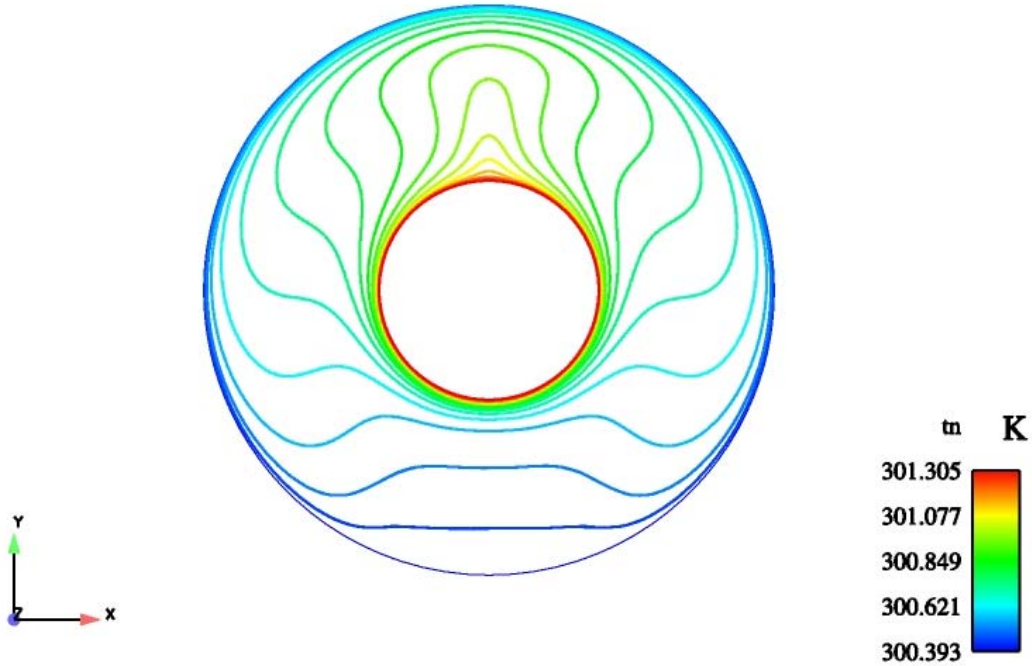

(b) LRKE Model

Figure 19. Predicted (a) v2-f, and (b) LRKE Temperature Contours in the Annulus between Two Horizontal Concentric Cylinders, $Ra_L = 2.51x10^6$

Square Enclosure

Natural convection heat transfer in an air-filled square cavity has been studied previously in the literature [11] – [15]. This too is a simple geometry, but still quite relevant to the more complex systems typical of weapons analysis. The boundary conditions applied in the Fuego fluids models are constant temperature active surfaces and variable temperature passive surfaces. The active surfaces are vertical: one hot surface, one cold surface. The passive surfaces are horizontal. The temperatures of the passive surfaces vary with position from hot to cold and are implemented with a user subroutine. The meshes are pseudo two-dimensional. That is, the mesh is one element thick in the z-direction (third dimension). Figure 20 illustrates a mesh applied in Fuego for this geometry. Both the v2-f and the LRKE turbulence models are applied. In order to get a sense of the grid independent nature of the CFD solutions presented in this report, two additional fluids grids are also considered. The numerical details of each mesh are given in Table 10.

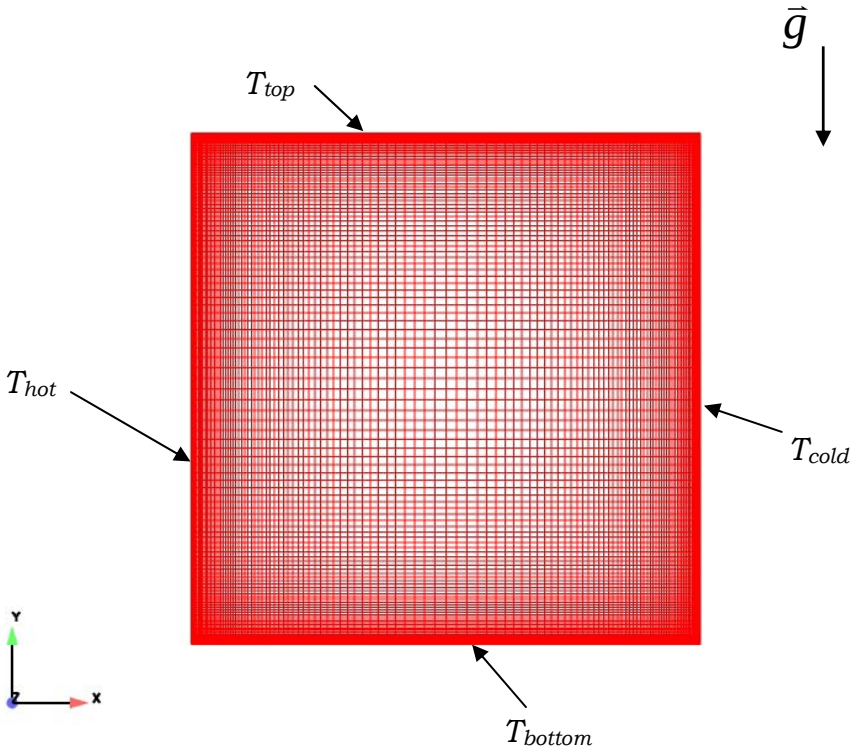

Figure 20. Fuego Mesh for an Air-Filled Square Cavity

Table 10. Three Square Cavity Meshes

Case	*x*	*y*	Description
Coarse Mesh	80	80	—
Mid Mesh	120	120	50% more than coarse
Fine Mesh	220	220	175% more than coarse

Note that the z-direction is one element thick.

The *x*-directed number of divisions represents the horizontal discretization within the cavity; the *y*-directed number of divisions represents the vertical discretization within the cavity. It is evident from the figure that cell-clustering occurs on each of the walls in which boundary layers form.

Both average and local heat transfer results acquired from the models are compared to measured data taken at a Rayleigh number of $1.58x10^9$. Average heat transfer data are compared in terms of an average Nusselt number computed at each wall. The average Nusselt number is given as the following:

$$\overline{Nu} = \frac{\bar{q}L}{\bar{k}\Delta T} \qquad \text{(Eqn. 12)}$$

where $\bar{q}$ is the integral average wall heat flux, L is the width of the cavity (=H, height), $\bar{k}$ is the average fluid thermal conductivity, and ΔT is the temperature difference, (= $T_{hot} - T_{cold}$). Local heat transfer data are compared in terms of a local Nusselt number. The local Nusselt number is given as the following:

$$Nu = \frac{q_i L}{\bar{k}\Delta T} \qquad \text{(Eqn. 13)}$$

where q_i is the local heat flux evaluated at each node along a given wall. To ensure the model has reached (an approximate) steady-state solution, the simulated energy balance between surfaces is required to approach zero. Additionally, the fluids solution is observed to be essentially unchanging.

Air as the Working Fluid, $Ra_H = 1.58x10^9$

This simulation is characterized by stable thermal stratification in the core fluid region and low-level turbulence in the near-wall region. The fluid circulates around the enclosure adjacent to the walls in a clockwise direction. Air is the working fluid in the square cavity [12]. The Rayleigh number, based on cavity height, *H*, is defined as

$$Ra_H = \frac{g\beta\Delta T H^3}{\nu\alpha} \qquad \text{(Eqn. 14)}$$

where the cavity height and width are equal to 0.75 m.

CFD Boundary Condition and Thermal Property Specifications

The active walls are constant temperature boundaries.

- T_{hot} = 323.15 K (50°C)
- T_{cold} = 283.15 K (10°C)
- ΔT = 40 K

The passive wall boundary conditions are specified with a user subroutine. The temperature data used in this analysis are taken directly as the top and bottom boundary conditions given in [11]. The temperature profiles are shown in Figure 21.

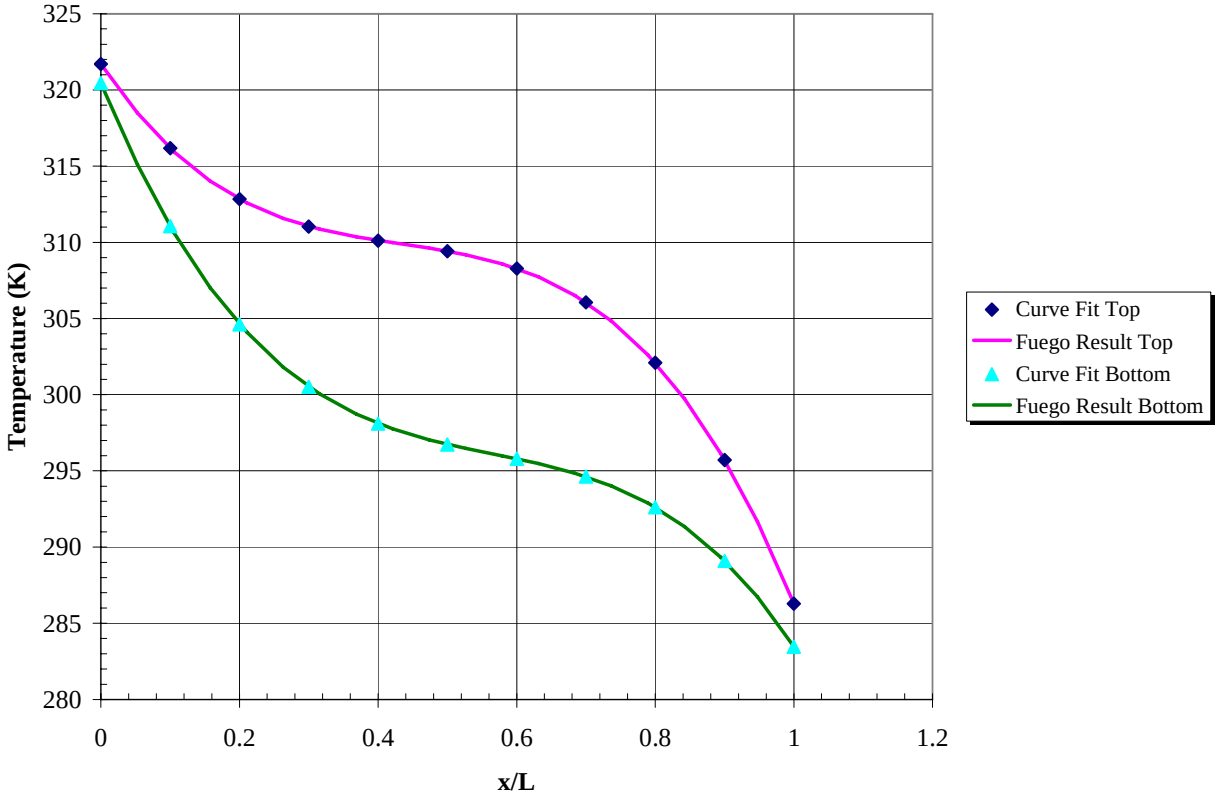

Figure 21. Passive Wall Temperature Distributions for T_{top} and T_{bottom}

The air thermal properties are all treated as functions of temperature. Each varies in a piecewise linear fashion. The variation in density drives the fluid motion. Table 11 provides the density, thermal conductivity, specific heat, and dynamic viscosity. Table 12 provides the required fluid enthalpy.

Table 11. Temperature Dependent Thermal Properties for Air, $Ra_H = 1.58x10^9$

Temperature (K)	ρ (kg/m³)	k (W/m-K)	c_p (J/kg-K)	μ (kg/m-s)
250	1.3947	$22.3x10^{-3}$	1006	$1.596x10^{-5}$
300	1.1614	$26.3x10^{-3}$	1007	$1.846x10^{-5}$
350	0.9950	$30.0x10^{-3}$	1009	$2.082x10^{-5}$

Table 12. Air Enthalpy, $Ra_H = 1.58x10^9$

Temperature (K)	h (J/kg)
240	$240.22x10^3$
260	$260.28x10^3$
280	$280.34x10^3$
300	$300.43x10^3$
320	$320.54x10^3$
340	$340.66x10^3$
360	$360.81x10^3$

Laminar Flow Solution in the Square Cavity

The mechanics associated with the fluid flow conditions in an air-filled square cavity at the prescribed thermal conditions are not overly turbulent. Turbulent kinetic energy contours from both turbulence models are illustrated in Figure 22. As expected, low-level turbulence is primarily restricted to the boundary layers adjacent to both active walls. Based on this result, it is instructive to consider this analysis using laminar flow equations as well.

It was found that a steady-state flow solution is unattainable with Fuego when five nonlinear iterations and a CFL limit of 1.0 are specified. The laminar flow equations are unsteady and predicted temperature contours shown in Figure 23 represent a transient flow response. Unsteady temperature contours are illustrated in the figure at two different times late in the simulation. The average laminar heat transfer rates are compared to measured data in Table 13. The Nusselt number data are obtained at the arbitrary end of the simulation. It is noted that the heat transfer data remain relatively constant throughout the simulation, even though the flow field displays unsteady behavior.

Table 13. Average Nusselt Numbers Obtained from Laminar Flow Equations

	Laminar	**Measured Data**
Hot wall	53.5	62.9
Cold wall	53.3	62.6
Top wall	13.9	13.9
Bottom wall	13.1	14.4

It is interesting to note that laminar flow heat transfer predictions are worse on the active (vertical) walls and better on the passive walls (when compared to the v2-f turbulence model results).

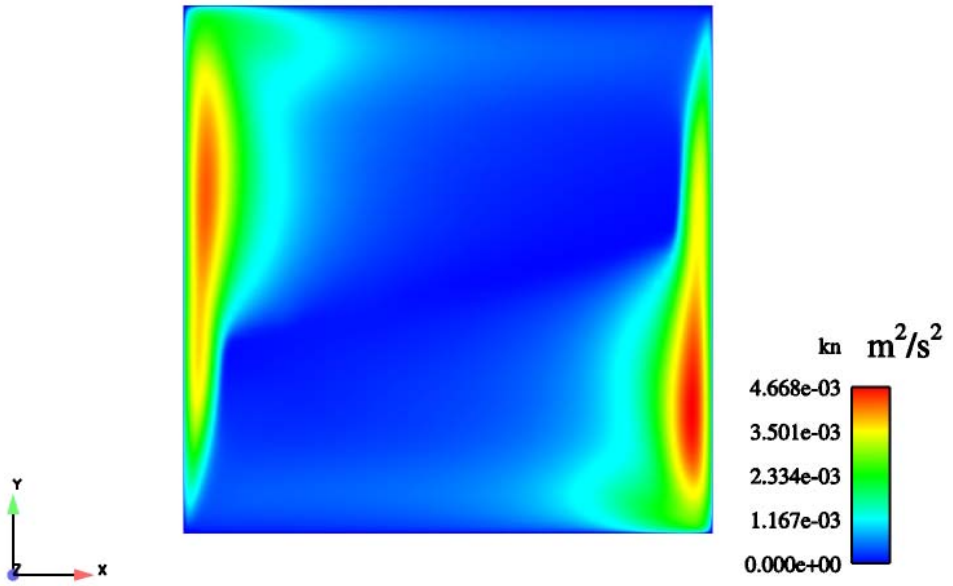

(a) LRKE Model

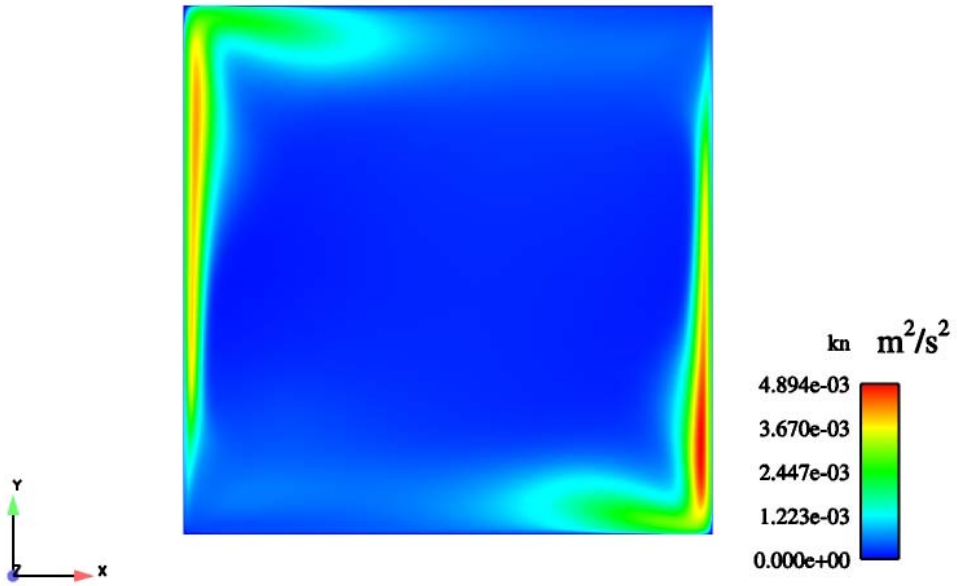

(b) v2-f Model

Figure 22. Turbulent Kinetic Energy Contours from (a) LRKE and (b) v2-f Turbulence Models

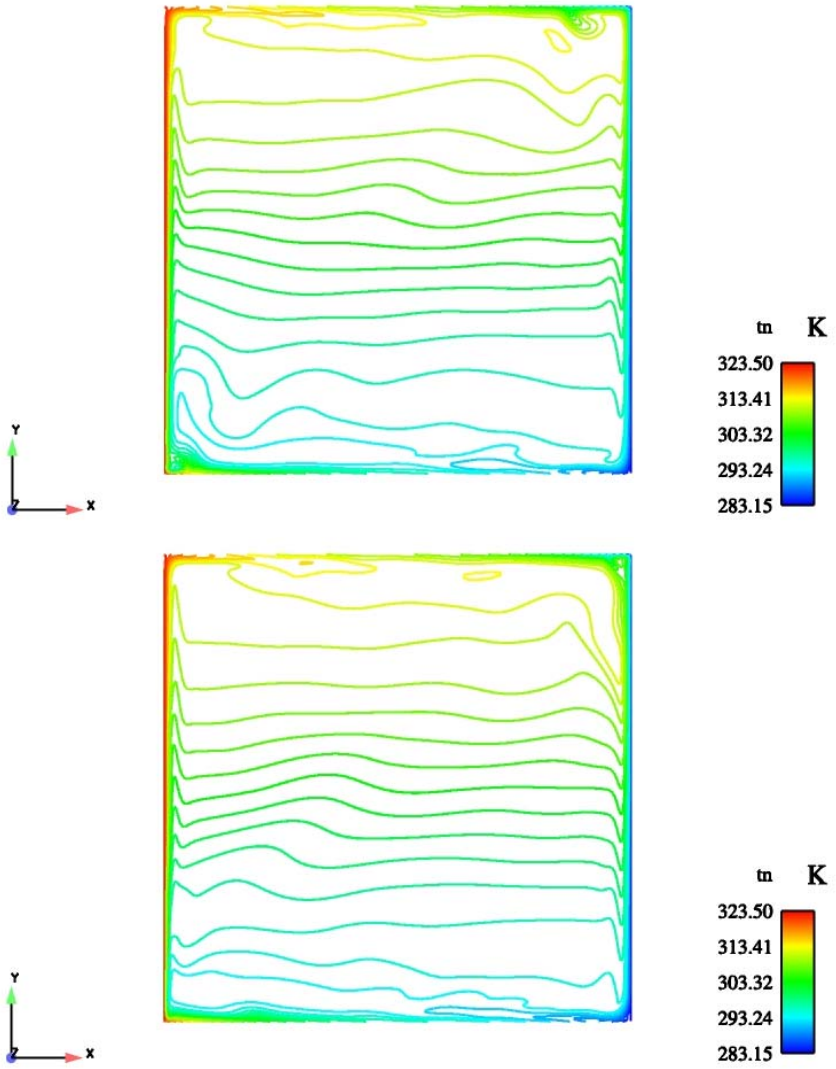

Figure 23. Unsteady Laminar Flow Response at Two Different Times

CFD Simulation Specifications for Turbulent Flow Conditions: v2-f turbulence model

To attain a steady-state condition (if one is achievable), a CFL limit of 1.0 is adopted. This resulted in a time step on the order of 10^{-3} to 10^{-2}s during the early transient and about $1.6x10^{-2}$s later in the simulation. A simulation described later in this section allows for an order-of-magnitude larger CFL. Indeed, the ability to increase the CFL limit may be necessary when considering more practical flow problems in the future. Under relaxation of pressure or momentum is not necessary when fourth order smoothing with

time-step scaling is specified as the projection method. However, under relaxation is performed to various degrees for the other scalar equations and turbulence properties. The under relaxation parameters are given in Table 14. Typically, under relaxation parameters are specified so that runtime modifications are not required. A single nonlinear iteration is specified in the analysis. Overall, nonlinear equation residuals were reduced by between 3 to 4 orders of magnitude. It is noted that the equation residuals from the f-equation had a tendency to wander; however, this equation too had low residuals, in the range of 10^{-4} to 10^{-8}.

The interpolation method for the convection operator is a combination of higher-order and first-order upwinding for continuity, momentum, and energy, and first-order upwinding for turbulence. The first-order upwind method (UPW) and a first-order upwind factor of 1.0 are applied to the four turbulence equations. The validity of this simplification is investigated by performing an additional simulation with higher-order upwinding specified for each of the turbulence equations. A higher-order upwind MUSCL with the default value used for the hybrid upwind factor (1.0) is applied to continuity, momentum, and energy equations. A Van Leer upwind limiter is used to prevent numerical oscillations of the equations. As in the previous geometry, it was found that the v2-f turbulence model *required an increase* in the first-order upwind factor from the default value of 0.01. Subsequently, in order to compute a stable solution with the v2-f turbulence model, one must allow for a portion of the convection operator to contain some pure first-order upwind convection. The first order upwind factor is selected to be 0.5. Therefore, 50% of the convection operator is composed of pure first-order upwind convection. The remaining 50% is higher-order upwind convection. The solution method for continuity and all scalar equations is Aztec GMRES. The preconditioning method is DD-ILUT for continuity and Symmetric-Gauss-Seidel for all other scalars. A single preconditioning step is applied.

Simulation initial conditions are the following:

- Pressure = 0 Pa
- Velocity (U, V, W) = 0 m/s
- Temperature = 303.15 K
- $k = 5x10^{-5}$ m^2/s^2
- $\overline{v^2} = 5x10^{-5}$ m^2/s^2
- $\varepsilon = 10^{-5}$ m^2/s^3
- f = 0

The velocity condition is specified everywhere as zero initially because much of the fluid domain is at or near no flow. That is, most of the flow occurs at the walls with the core fluid region essentially motionless.

Table 14. Under Relaxation Parameters for v2-f Turbulence Model, $Ra_H = 1.58x10^9$

Quantity	Value
Enthalpy	0.9
Turbulent viscosity	0.8
Turbulent kinetic energy	0.8
Turbulence dissipation	0.8
Turbulence Helmholtz f-function	0.8
Turbulent v2	0.8

CFD Simulation Specifications for Turbulent Flow Conditions: LRKE turbulence model

To attain a steady-state condition (if one is achievable) when solving the LRKE turbulent flow equations, a CFL limit of 1.0 is specified for time-stepping control. This resulted in a time step on the order of 10^{-3} to 10^{-2}s during the early transient and about $1.5x10^{-2}$s later in the simulation. Under relaxation for pressure or momentum is not necessary because fourth order smoothing with time-step scaling is specified as the projection method. However, under relaxation is performed to various degrees for the other scalar equations and turbulence properties. The under relaxation parameters are given in Table 15. Typically, under relaxation parameters are specified so that runtime modifications are not required. Multiple nonlinear iterations are specified in the analysis for the first 100 s of the simulation and a single nonlinear iteration is specified for the final 100 s. Overall, nonlinear equation residuals were reduced by between 1 to 4 orders of magnitude.

As described previously, a turbulence dissipation source term is optional in the LRKE ε-equation. The dissipation source term (typically denoted by the symbol E, refer to [3]) is omitted in this simulation. How this selection impacts the turbulent kinetic energy, the dissipation rate of turbulence kinetic energy, and subsequently, the eddy viscosity, will be discussed later.

The interpolation method for convection uses a higher-order upwinding MUSCL approach with Fuego default values used for both the upwind limiter (Superbee) and the hybrid upwind factor (1.0). Like the v2-f turbulence model, the first-order upwind factor was selected to be 0.5. Therefore, 50% of the convection operator is composed of first-order upwind convection. The remaining 50% is higher-order upwind convection. The solution method for continuity and all scalar equations is Aztec GMRES. The preconditioning method is DD-ILUT for continuity and Symmetric-Gauss-Seidel for all other scalars. A single preconditioning step is applied.

The required initial conditions are identical to those specified in the v2-f model.

Table 15. Under Relaxation Parameters for LRKE Turbulence Model, $Ra_H = 1.58x10^9$

Quantity	Value
Enthalpy	0.6
Turbulent viscosity	0.5
Turbulent kinetic energy	0.3
Turbulence dissipation	0.3

Both v2-f and LRKE turbulence model predictions are loosely compared to FLUENT predictions presented in [11] and directly compared to measured data presented in [12]. Both average and local heat transfer results are compared. Additionally, fluid and turbulence properties are compared at various locations in the cavity. The mid-mesh (120x120) described in Table 10 is used in the comparative analyses described below.

Figure 24 illustrates the local Nusselt number computed by Equation (13) for the active vertical walls (hot and cold walls). Figure 25 illustrates the local Nusselt number for the passive horizontal walls (top and bottom walls). The measured data taken from [12] are given by symbols in each of the figures. Table 16 shows the average heat transfer results, computed with Equation (12), from both turbulence models. Additionally, four other RANS turbulence formulations available in the commercial CFD code, FLUENT, are compared to Fuego predictions. Finally, measured data are also included in the table.

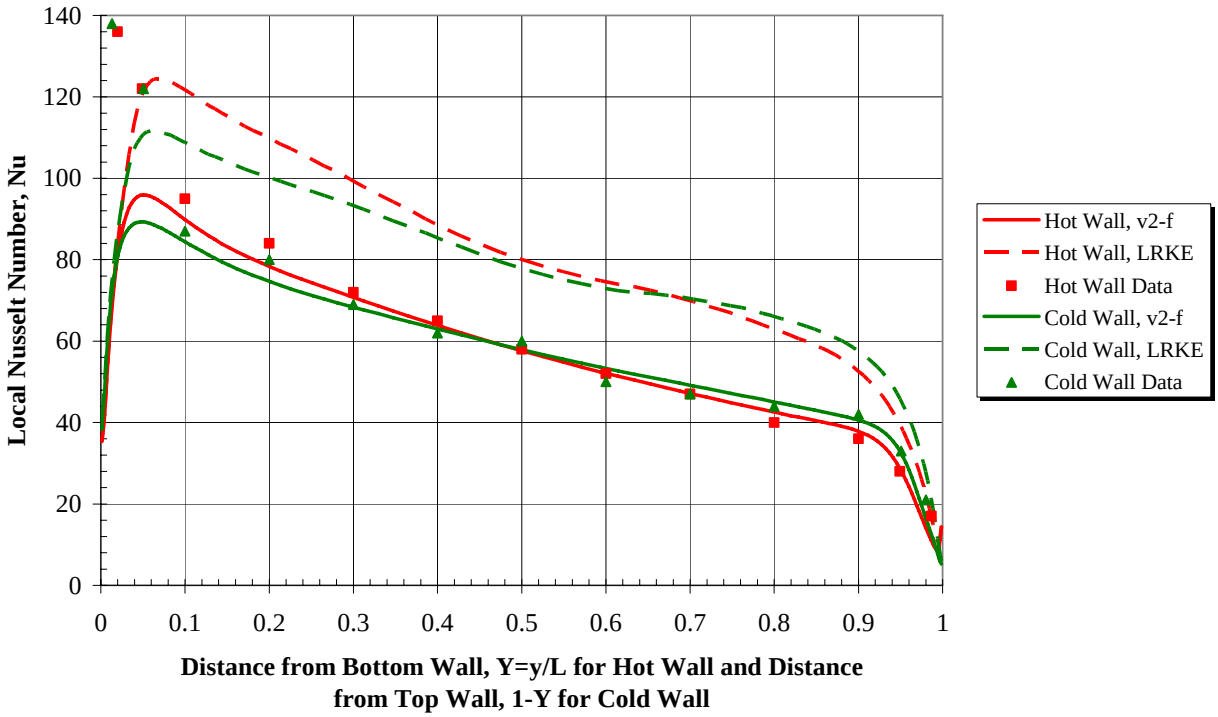

Figure 24. Local Nusselt Numbers for the Constant Temperature Hot and Cold Walls of the Square Enclosure, $Ra_H = 1.58x10^9$

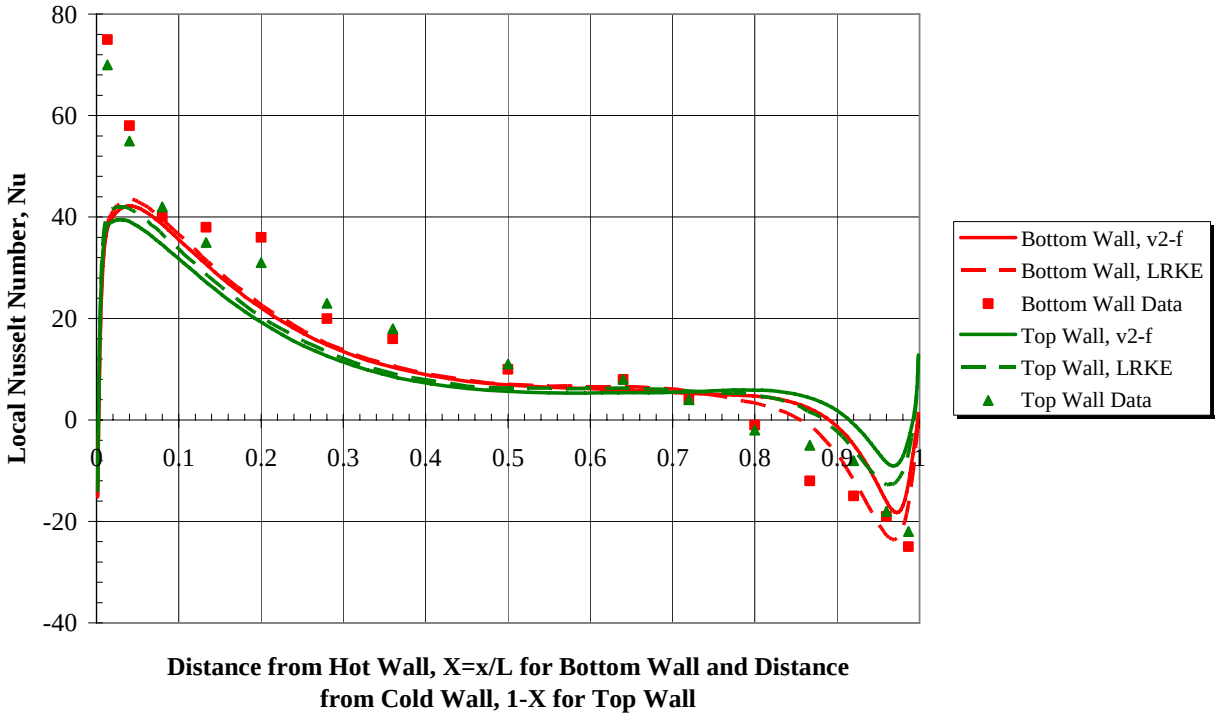

Figure 25. Local Nusselt Numbers for the Top and Bottom Walls of the Square Enclosure, $Ra_H = 1.58x10^9$

Table 16. Average Nusselt Numbers

	$k-\varepsilon$ **FLUENT***	**Realizable** $k-\varepsilon$ **FLUENT***	**RNG** $k-\varepsilon$ **FLUENT***	$k-\omega$ **FLUENT***	**v2-f Fuego**	**LRKE Fuego**	**Data**
Hot wall	76.1	76.1	76.8	78	58.7	81.4	62.9
Cold wall	76.5	76.5	77.6	78.3	58.4	79.0	62.6
Top wall	14.2	14.2	13.7	12.3	10.8	10.9	13.9
Bottom wall	14.7	14.7	14.2	12.6	11.2	10.7	14.4

* - Refer to [11] for details of the FLUENT simulations

The v2-f turbulence model reasonably predicts the local heat transfer on both active walls (refer to Figure 24). On average the v2-f Nusselt number predictions are about 6.5% low compared to measured data. Fuego LRKE and FLUENT predictions are similar. They both tend to over predict the heat transfer on the active walls, in some cases by as much as 20 – 30%. Passive wall Nusselt number predictions from Fuego tend to be too low. On average, both v2-f and LRKE under predict passive wall heat transfer by about 20 – 25%. FLUENT heat transfer predictions are much better on the passive walls, with about a 10% error or less.

In the near-wall region, the v2-f turbulence model exhibits less turbulent viscosity than the LRKE turbulence model. A lower turbulent viscosity decreases the overall heat transfer rate from the active surfaces. The FLUENT turbulence models appear to display slightly lower turbulent viscosities than v2-f (refer to Figure 27 below and figure 4 in [11]); however, the default turbulent Prandtl number in FLUENT is 0.85, compared to 1.0 used in the v2-f and LRKE turbulence models, thus resulting in a higher overall turbulent diffusion coefficient in the energy transport equation and a higher turbulent heat flux (thus FLUENT predicted higher heat transfer rates at each of the walls).

Horizontal and vertical fluid velocity and temperature are shown at mid-width and mid-height in Figure 26 and Figure 27, respectively.

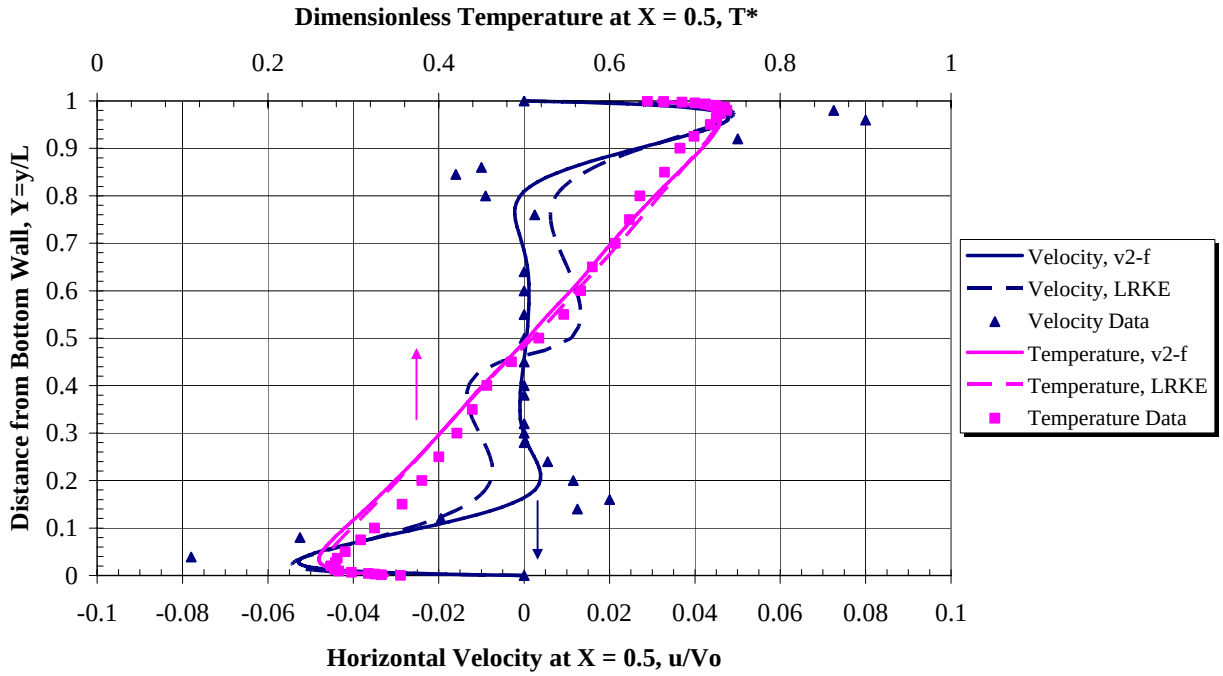

Figure 26. Mean Horizontal Velocity and Temperature Profiles as a Function of Height at Enclosure Mid-Width, X = x/L = 0.5, V_0 = 1 m/s, T* = $\frac{T - T_{cold}}{T_{hot} - T_{cold}}$

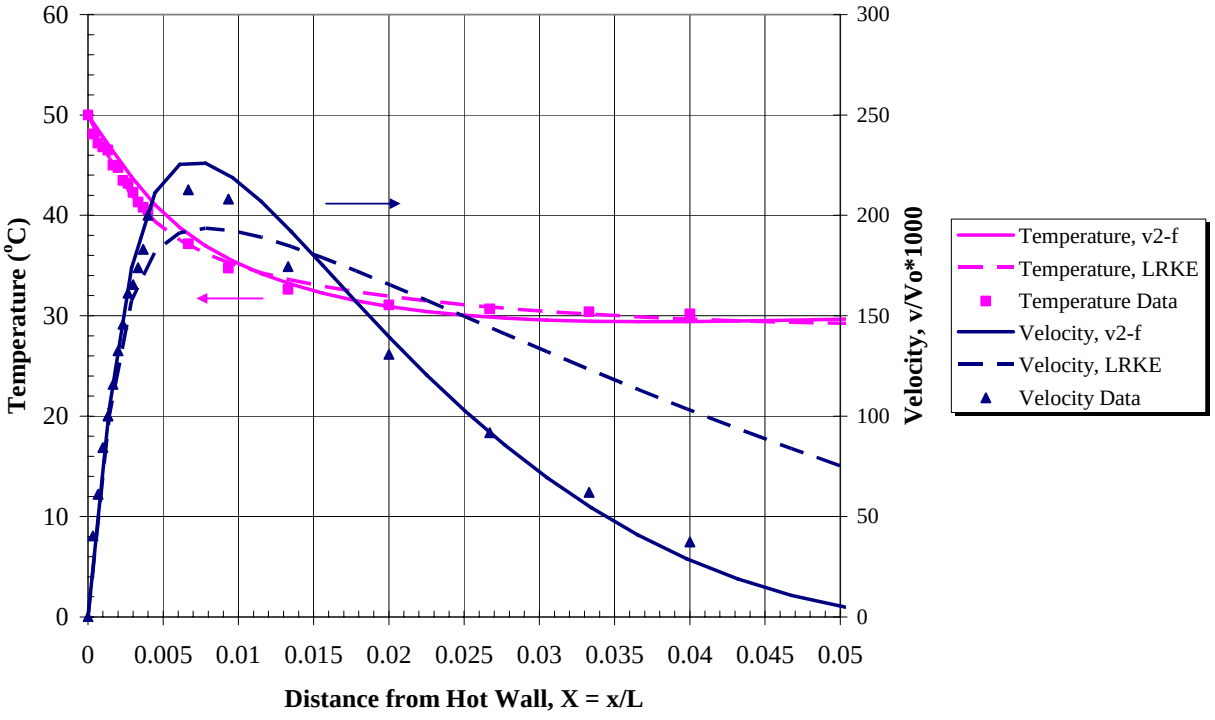

Figure 27. Mean Vertical Velocity and Temperature Profiles Near the Hot Wall at Mid-Height, Y = y/L = 0.5, V_0 = 1 m/s

Overall, the v2-f turbulence model compares reasonably well to measured velocity and temperature data. In Figure 26, the predicted mean fluid temperature adjacent to the passive walls at mid-width compares reasonably well to data; however, the horizontal fluid velocity, although essentially correct in trend, under predicts the maximum velocities in the respective boundary layers. In Figure 27, the predicted mean fluid temperature and vertical velocity adjacent to the hot wall at mid-height compare reasonably well to measured data. The v2-f model slightly over predicts the maximum velocity in the adjacent boundary layer. However, the model comparison to data at this location is excellent.

It is evident from each of the figures that the LRKE turbulence model predicts too much turbulent viscosity in the square cavity. The viscosity ratio in the boundary layers adjacent to the active walls is greater than v2-f by nearly an order of magnitude. Subsequently for a fixed turbulent Prandtl number, wall heat transfer rates are over predicted by LRKE. The exclusion of the dissipation source term, *E*, from the dissipation equation results directly in an (undesired) increase in the turbulent viscosity (i.e., ε decreases and k increases). However, this dissipation effect was found to be small in the previous geometry. Therefore, it is more likely that the model exhibits too much turbulence viscosity because the damping functions applied in LRKE are not appropriate for natural convection. (Refer to the description given for the previous geometry on page 45.) In particular, the turbulent viscosity damping function (f_μ) approaches unity too rapidly at small y^+ for wall-bounded buoyancy driven flow conditions, thus resulting in an inordinately large turbulent viscosity. This is one possibility; however, another possible dissipation mechanism may be worth discussion. Although not currently included in the equations for the LRKE turbulence model, it is also possible that a second (that is, in addition to *E*) dissipation source term is required in the modified ε-equation. The term is known as the Yap correction term [16]. It is given by the following:

$$S_\varepsilon = 0.83\left(\frac{k^{3/2}}{\varepsilon c_l y} - 1\right)\left(\frac{k^{3/2}}{\varepsilon c_l y}\right)^2 \frac{\tilde{\varepsilon}^2}{k} \qquad \text{(Eqn. 15)}$$

where the relationship between dissipation terms is $\varepsilon = \tilde{\varepsilon} + D$ and c_l (= 2.5) is the slope of the turbulent length scale in the near-wall region of a constant-stress shear flow. Equation (15) gets added to the right hand side of the modified ε-equation.

The Yap term increases ε thereby decreasing k in near-wall shear flow. It is a function of $\frac{k^{3/2}}{\varepsilon}$ and the normal distance from the wall, y, and has its primary impact in the viscosity affected near-wall region. This correction term has the effect of decreasing the overall turbulent viscosity. A second potentially useful modification to the LRKE turbulence model would be to include a streamwise heat flux using a generalized gradient diffusion hypothesis (GGDH). The turbulent heat flux is given by the following:

$$\overline{u_i'T'} = -c_T \frac{k}{\varepsilon} \overline{u_i'u_k'} \frac{\partial T}{\partial x_k} \qquad \text{(Eqn. 16)}$$

where $c_T = \frac{3}{2}\left(C_\mu / \mathrm{Pr}_t\right)$. Equation (16) would be incorporated in the energy transport equation and in the Rodi buoyancy term include in the k-equation. Therefore, the Rodi term previously given by Equation (11) now becomes the following in terms of the GGDH:

$$G_b = \beta g_i c_T \frac{k}{\varepsilon} \overline{u_i'u_k'} \frac{\partial T}{\partial x_k}. \qquad \text{(Eqn. 17)}$$

This representation is more complex than a simple gradient turbulent heat flux representation written solely in terms of a turbulent viscosity and a constant turbulent Prandtl number (e.g., $\beta g_i \frac{\nu_t}{\mathrm{Pr}_t} \frac{\partial T}{\partial x_i}$).

The GGDH includes a vertical turbulent heat flux driven by a horizontal temperature gradient in the presence of a turbulent shear layer (reference to table 1 in [16] illustrates the effects of these modifications, the Nusselt number predictions are more representative of measured data). The GGDH approach incorporates the Reynolds stress terms directly in its formulation of the turbulent heat flux.

Although these modifications (Yap and GGDH) have been judged by other researchers to improve predictions of wall heat transfer rates, it is also reasonable to question use of a linear profile to compute energy transport at the wall. The wall heat transfer rate is sensitive to the calculation of the enthalpy gradient in the fluid conductive layer. It is likely that a higher-order differencing scheme may influence the wall heat transfer rate (and Nusselt number) prediction. Furthermore, as indicated in the previous geometry, it may

also be useful to consider an alternative closure method for the turbulent thermal diffusivity and the turbulent Prandtl number.

Finally, the LRKE model predicts a weak circulation flow in the core fluid that the v2-f model does not (Figure 26). This too is a possible result of the inordinate turbulent viscosity. One final comparison between v2-f, LRKE, and measured data illustrates the turbulent kinetic energy adjacent to the hot wall at cavity mid-height. Figure 28 illustrates the same behavior by v2-f as seen in the horizontal concentric cylinder geometry. The discontinuous nature of the turbulent kinetic energy is a result of the large aspect ratios (about 17:1) associated with the computational cells in the boundary layer (typically found in an aligned flow problem). As seen previously, this numerical anomaly in a turbulence quantity had almost no impact on the mean flow quantities associated with the fluid region.

A comparison of mid-height and mid-width fluid velocity and temperature from the v2-f turbulence model and the turbulence models illustrated in [11] indicates that the FLUENT k-ω turbulence model comes closest to the v2-f turbulence results with regards to the vertical temperature and velocity profiles at midwidth.

Because the v2-f turbulence model more accurately depicts the measure data given in [12], the following sensitivity studies will be limited to the v2-f turbulence model.

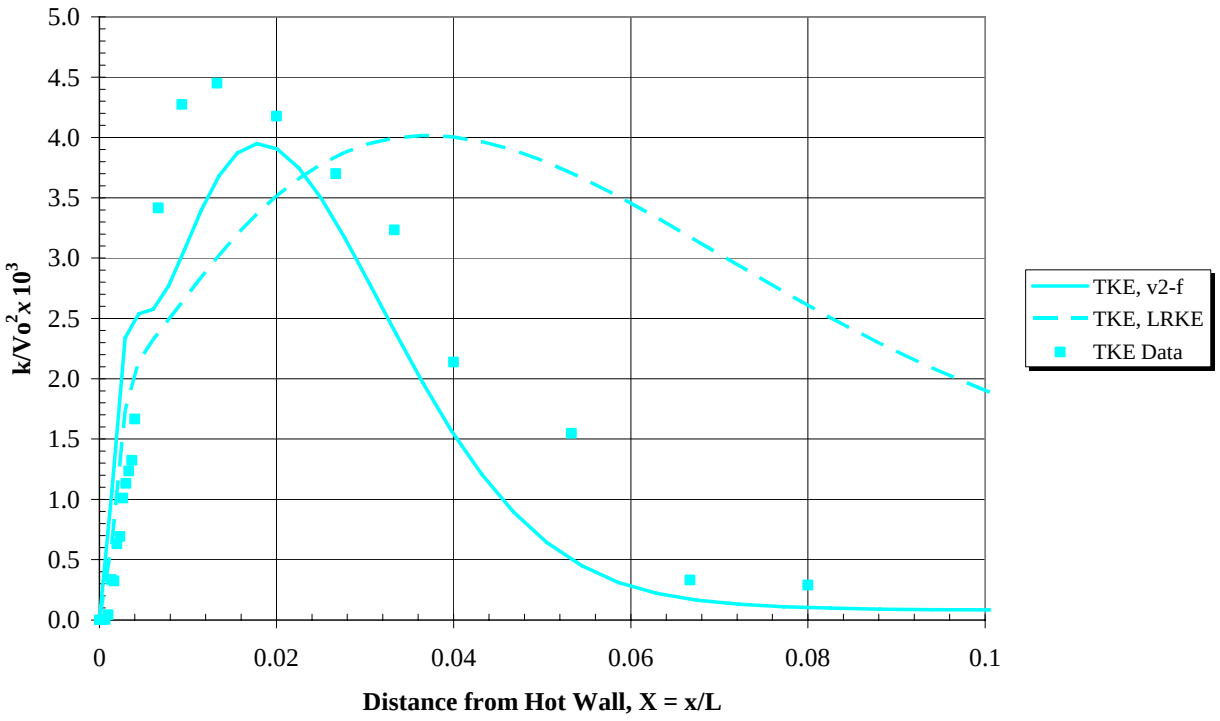

Figure 28. Turbulent Kinetic Energy (TKE) Profiles Near the Hot Wall at Mid-Height, Y = y/L = 0.5, V_0 = 1 m/s

CFL Limit Applied to the v2-f Turbulence Model

It is anticipated that a CFL limit less than or equal to 1.0 may be conservative for this flow problem. Additionally, future natural convection analyses applied to more practical V&V problems will require very detailed fluids regions that will no doubt necessitate the use of larger CFL limits. In this simulation, the CFL limit is increased by an order-of-magnitude and the solution marched to steady state. Figure 24 – Figure 28 are repeated in Figure 29 – Figure 33, without the measured data or the LRKE predictions, for the v2-f turbulence model using 1.0 or 10.0 as the CFL limit.

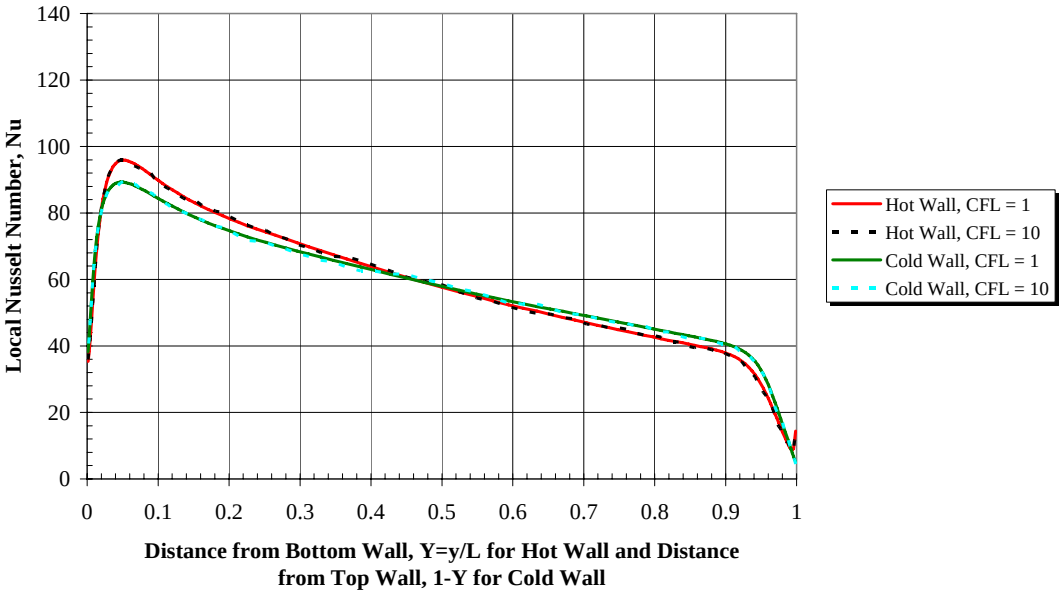

Figure 29. Local Nusselt Numbers at the Constant Temperature Hot and Cold Walls from the v2-f Turbulence Model with CFL Limits of 1 or 10, $Ra_H = 1.58x10^9$

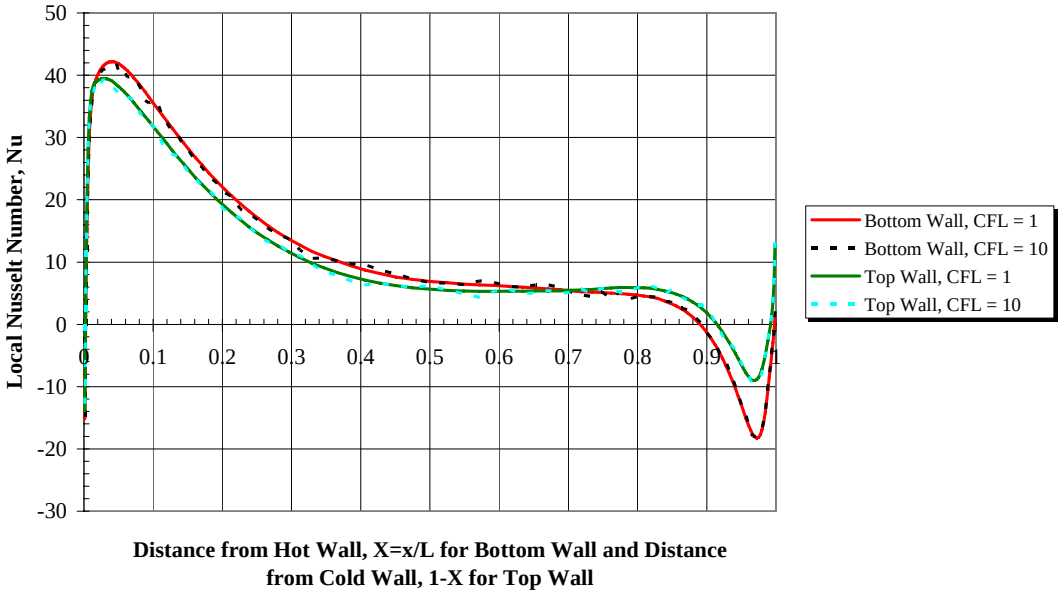

Figure 30. Local Nusselt Numbers at the Top and Bottom Walls from the v2-f Turbulence Model with CFL Limits of 1 or 10, $Ra_H = 1.58x10^9$

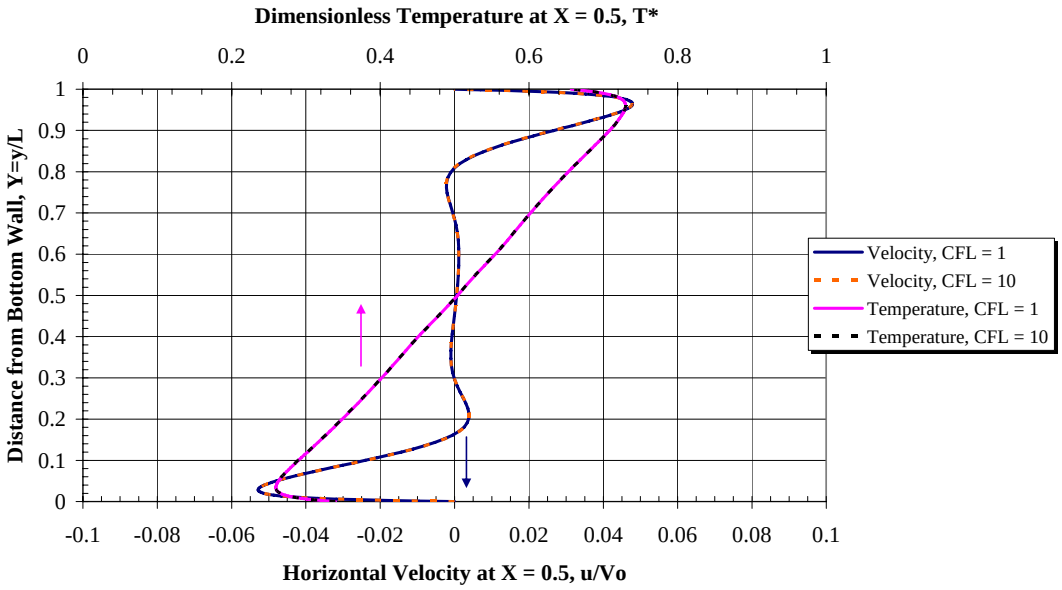

Figure 31. Mean Horizontal Velocity and Temperature Profiles as a Function of Height at Enclosure Mid-Width from the v2-f Turbulence Model with CFL Limits of 1 or 10, X = x/L = 0.5, V_0 = 1 m/s, T* = $\frac{T - T_{cold}}{T_{hot} - T_{cold}}$

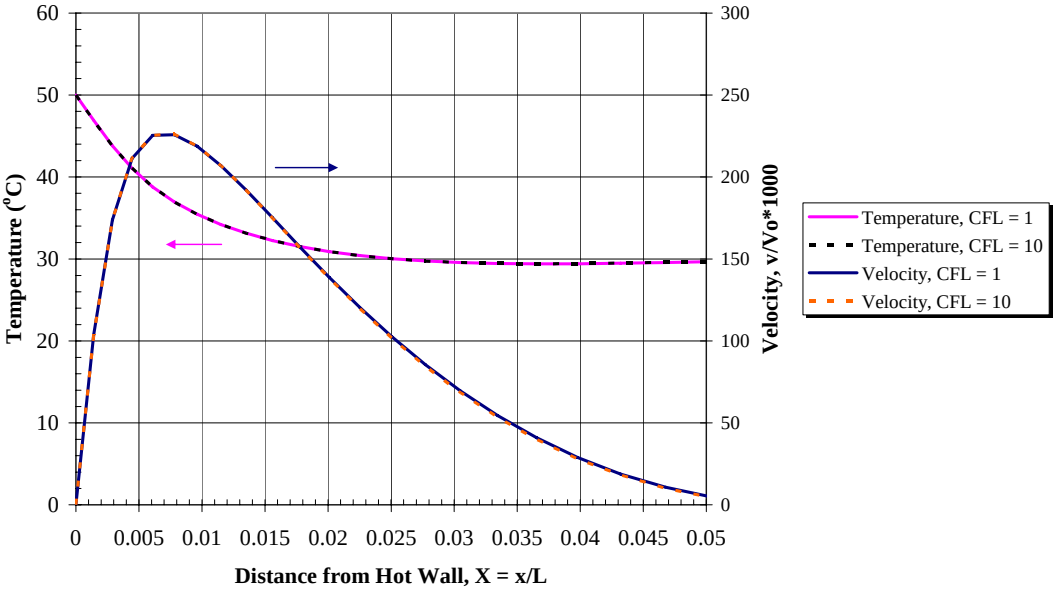

Figure 32. Mean Vertical Velocity and Temperature Profiles Near the Hot Wall at Mid-Height from the v2-f Turbulence Model with CFL Limits of 1 or 10, Y = y/L = 0.5, V_0 = 1 m/s

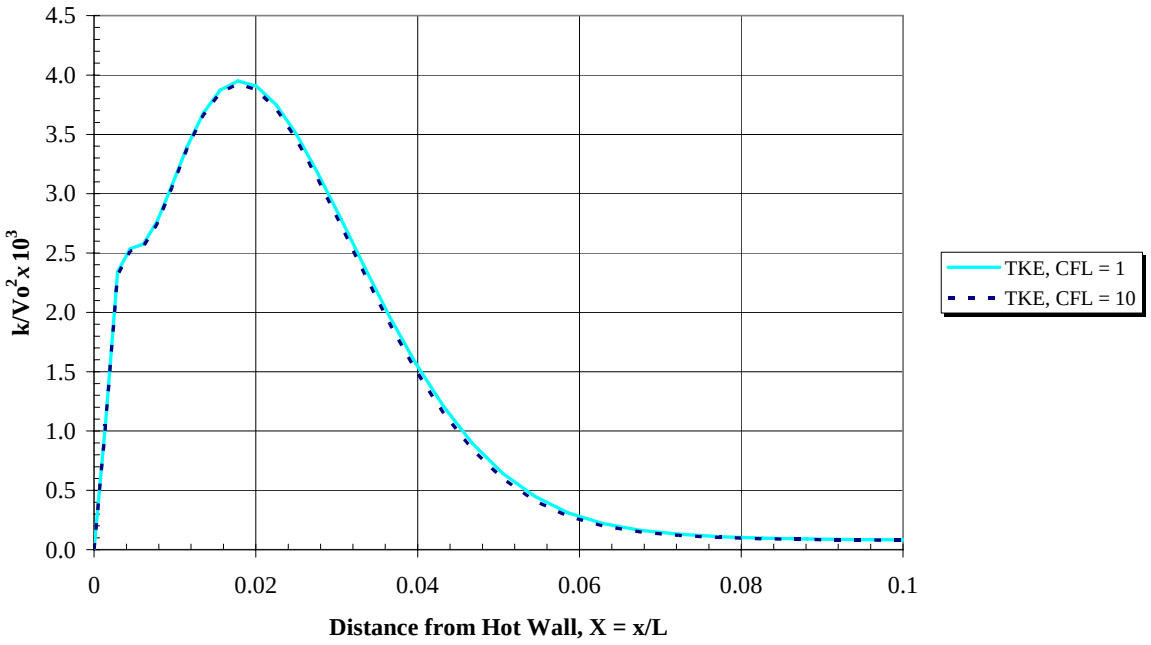

Figure 33. Turbulent Kinetic Energy Profiles Near the Hot Wall at Mid-Height from the v2-f Turbulence Model with CFL Limits of 1 or 10, Y = y/L = 0.5, V_0 = 1 m/s

From Figure 29 – Figure 33 it is evident that, for a square cavity with thermal conditions resulting in low-level turbulence near the walls, the larger CFL limit (10) produces the same steady-state flow solution as the conservative CFL limit (1). Additionally, the average Nusselt number on any wall changed by 1% or less. Subsequently, a higher CFL, in this case 10, provided the same fluids solution as a more conservative CFL limit of 1.0. One can continue to push the limit of the CFL specification to find a reasonable time-stepping expense.

First-Order Turbulence (FOT) Vs. Higher-Order Turbulence (HOT)

All of the Fuego predicted results from the square cavity use pure first-order upwinding in the convection operator associated with the four turbulence equations solved by the v2-f model. In some instances, in particular for a coarse fluids mesh, this can result in significant numerical diffusion. In order to determine the impact of using first-order turbulence (FOT) instead of higher-order turbulence (HOT), Figure 24 – Figure 28 are repeated in Figure 34 – Figure 38, without the measured data or the LRKE predictions, using the v2-f turbulence model with two different interpolation methods for the convection operator. HOT interpolation for each of the turbulence equations is consistent with the method described for the continuity, momentum, and energy equations on page 56.

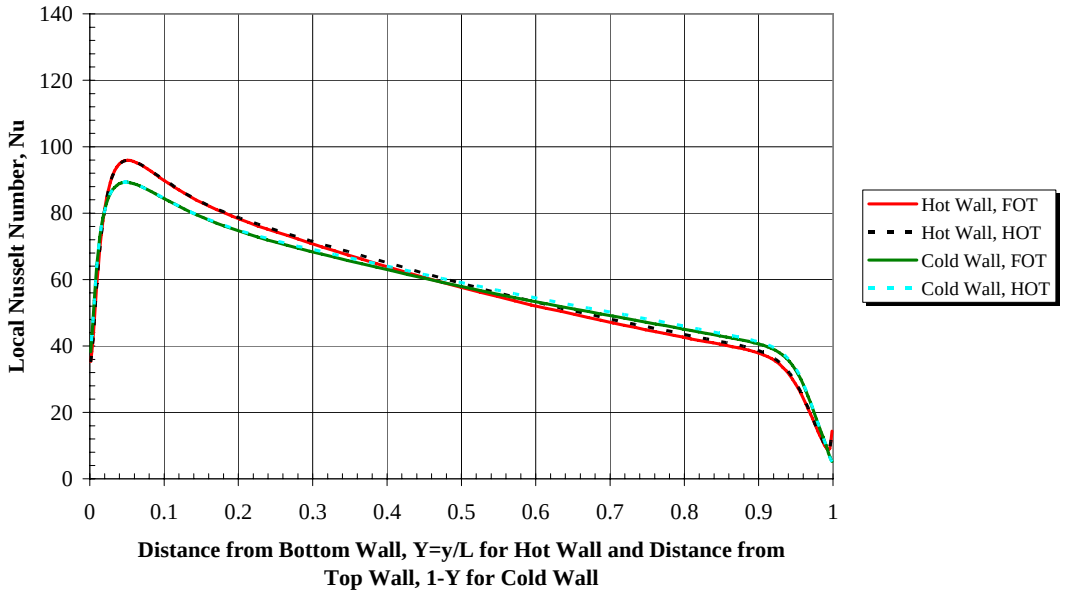

Figure 34. Local Nusselt Numbers at the Constant Temperature Hot and Cold Walls from the v2-f Turbulence Model using FOT or HOT, Ra_H = $1.58x10^9$

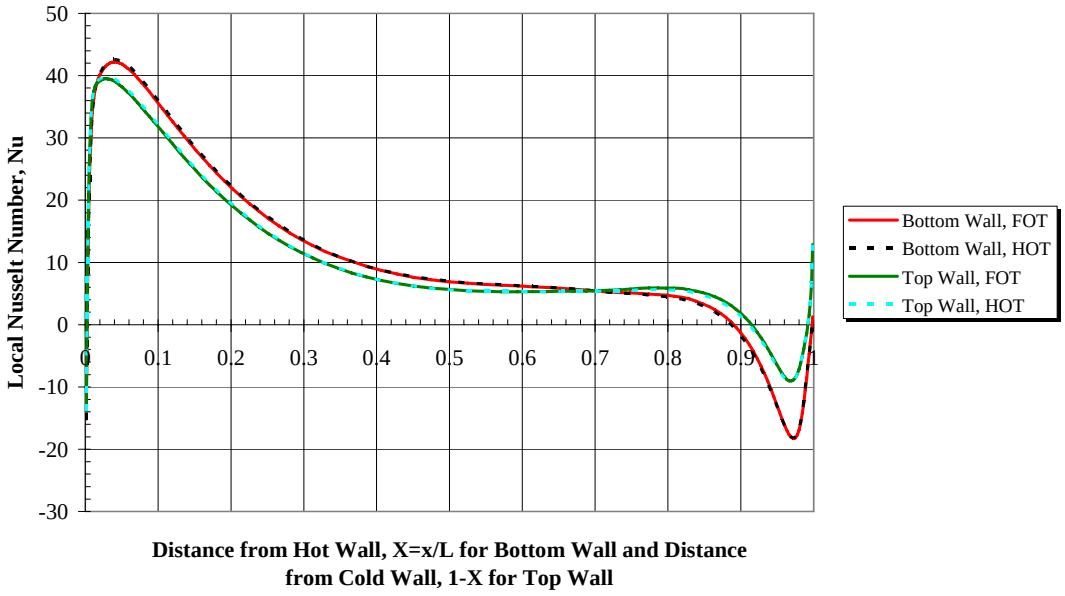

Figure 35. Local Nusselt Numbers at the Top and Bottom Walls from the v2-f Turbulence Model using FOT or HOT, Ra_H = $1.58x10^9$

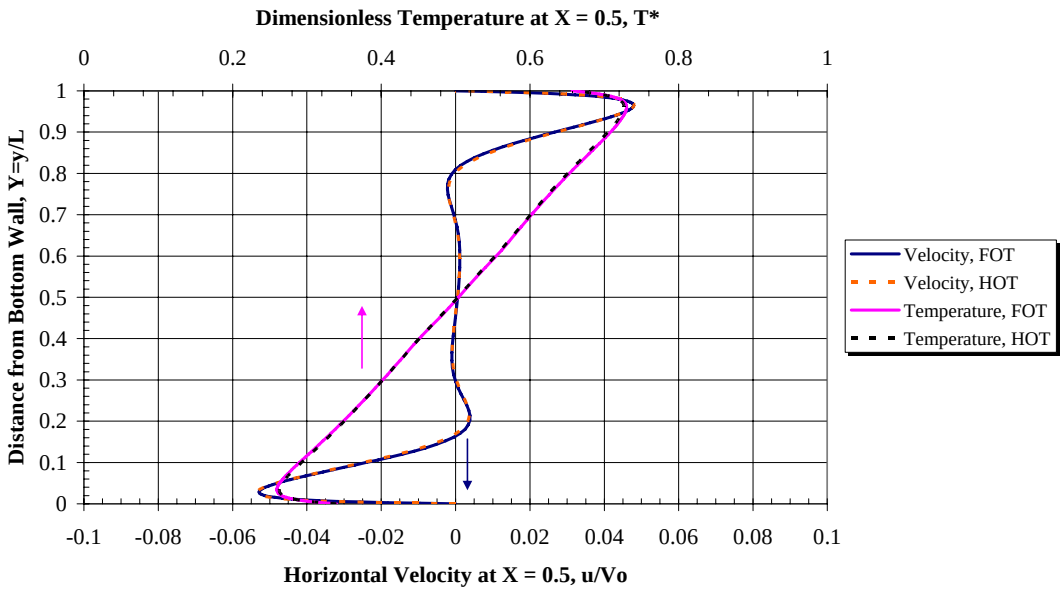

Figure 36. Mean Horizontal Velocity and Temperature Profiles as a Function of Height at Enclosure Mid-Width from the v2-f Turbulence Model using FOT or HOT, X = x/L = 0.5, V_0 = 1 m/s, T* = $\frac{T - T_{cold}}{T_{hot} - T_{cold}}$

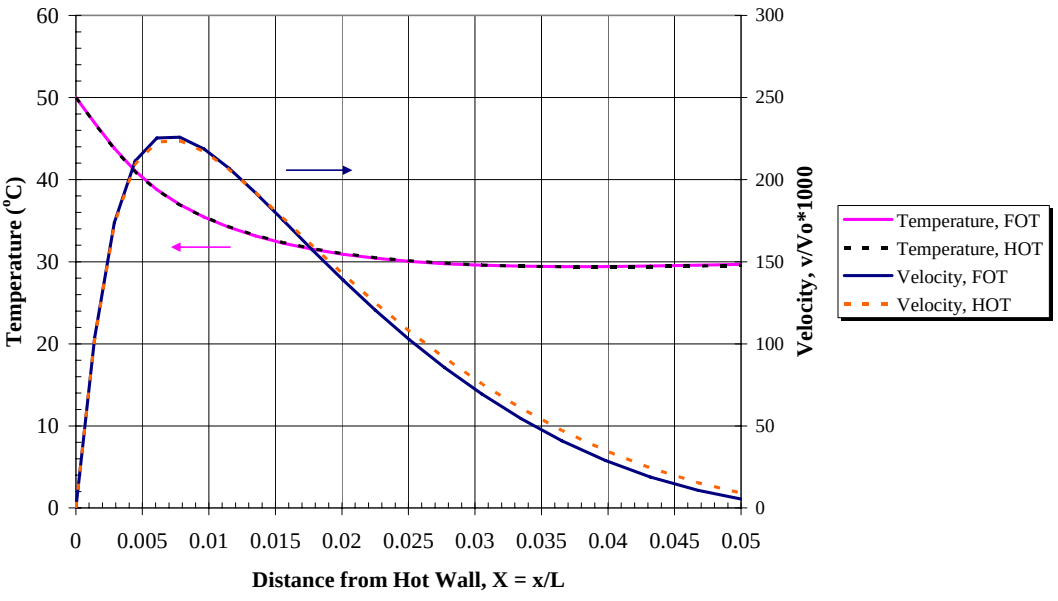

Figure 37. Mean Vertical Velocity and Temperature Profiles Near the Hot Wall at Mid-Height from the v2-f Turbulence Model using FOT or HOT, Y = y/L = 0.5, V_0 = 1 m/s

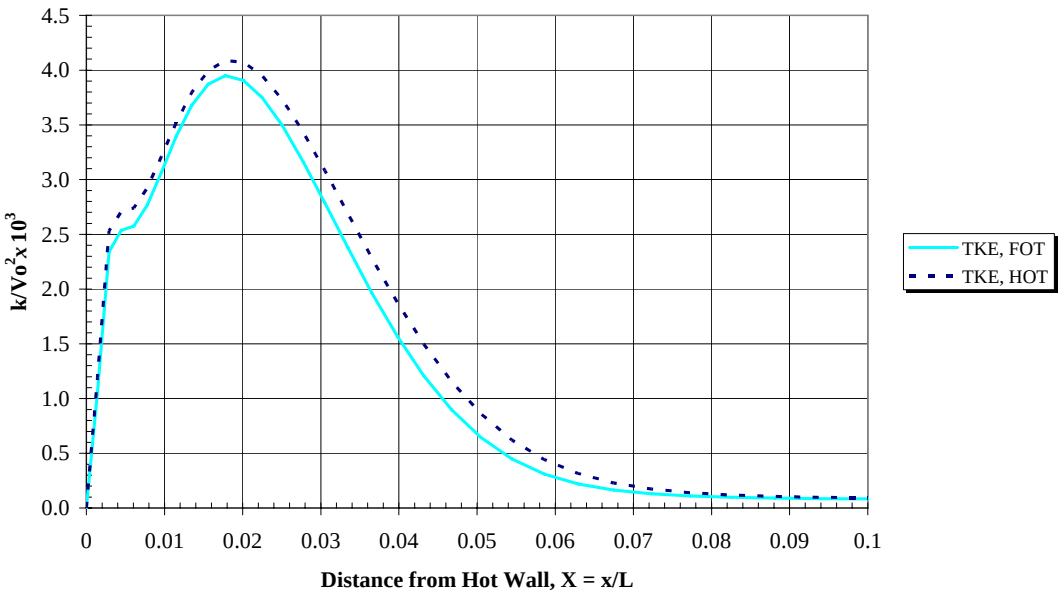

Figure 38. Turbulent Kinetic Energy Profiles Near the Hot Wall at Mid-Height from the v2-f Turbulence Model using FOT or HOT, Y = y/L = 0.5, V_0 = 1 m/s

As expected because the flow is largely aligned with the grid, the mean flow variables remain unchanged when allowing for a higher-order convection operator in the four turbulence equations in v2-f. A slight difference in the predicted turbulence kinetic energy is noted in the boundary layer adjacent to the hot wall at mid-height.

Grid Independence Study

Three square enclosure meshes are analyzed for grid independence. Flow solutions at steady state conditions are compared using the v2-f turbulence model. Additionally, the two most refined meshes in Table 10 are analyzed for grid independence using the LRKE turbulence model.

Figure 39 – Figure 43 illustrate the local heat transfer, fluids, and turbulence results of a grid independence study using the v2-f turbulence model applied to the 80*x*80, 120*x*120, and 220*x*220 fluids meshes. The process of computing a steady-state solution for the refined mesh (220*x*220) has been *exceedingly* difficult. This phenomenon has also been reported in the literature in which unsteadiness has been noted for higher-order discretization schemes and refined meshes [17]. The refined solution persistently displays a weak

circulation flow in a region that should essentially be stationary (the core fluid). Additionally, conditions in the corners where the boundary layers first begin to form appear to produce unsteady secondary flows. The less refined meshes (80*x*80, 120*x*120) seem to be able to reproduce the stationary flow behavior in the core fluid region (refer to Figure 26 for results from the 120*x*120 mesh) as expected. Additionally, flow in the corners is well-behaved. Various approaches have been considered to achieve a steady state response from the highly refined fluids mesh:

- Continued time-stepping at CFL limit of 1.0 (resulting in a time step on the order of 10^{-2} s),
- Use of a higher-order turbulence discretization scheme,
- Additional nonlinear iterations per time step, 5 iterations (which bogged the solution down considerably), and then 3 iterations.

The first two approaches did not influence the nature of the response. A weak circulation flow continued to plague the core fluid region. Additionally, the flow in the corners, where the vertical wall boundary layers form, continued to exhibit an unsteady response. Attention is subsequently focused on the last point, because of the potential for picking up transient mechanics of the flow with a finely resolved mesh. Because the flow in the core region and in the corners appears to be unsteady (but not nearly as extreme as the laminar flow result), additional nonlinear iterations per time step are specified in the simulation. Initially, 5 iterations are specified; however, this resulted in an inefficient solution. Ultimately, 3 nonlinear iterations are specified per time step. Similarly, the unsettled flow behavior did not change. Reference to Figure 39 – Figure 43 indicates that the refined mesh solution displays certain features in the flow field not evident in either of the coarser meshes. Two potential reasons why this is so, in particular for a refined mesh in which numerical error may be reduced when compared to the more coarse meshes, are the following.

It is somewhat uncertain how a standard turbulence model, and its associated model constants developed for situations without buoyancy effects, translates to flows in which buoyancy drives fluid motion. This, in a region in which buoyancy effects primarily occur in the near-wall region where viscous effects dominate.

It is also possible that the ergodic hypothesis may be violated for a transient flow in which the time averaging interval is not sufficiently small in comparison

with the period of *slow* variations of the averaged quantities of the flow field. That is, the time average and the ensemble average may no longer be identical for this flow field and the system is no longer quasi-steady. It was assumed that taking additional nonlinear iterations is the correct approach in handling this unsteady flow problem; however, it was found that this did not result in a steady state solution. It is evident from the figures that this flow solution begins to converge to the expected solution, but it does contain flow features that appear to be unsteady in nature.

Reference to Figure 44 – Figure 46 show the temperature contours for the square enclosure at steady state. Figure 46 indicates that the cavity temperature distribution is indeed not a steady state solution.

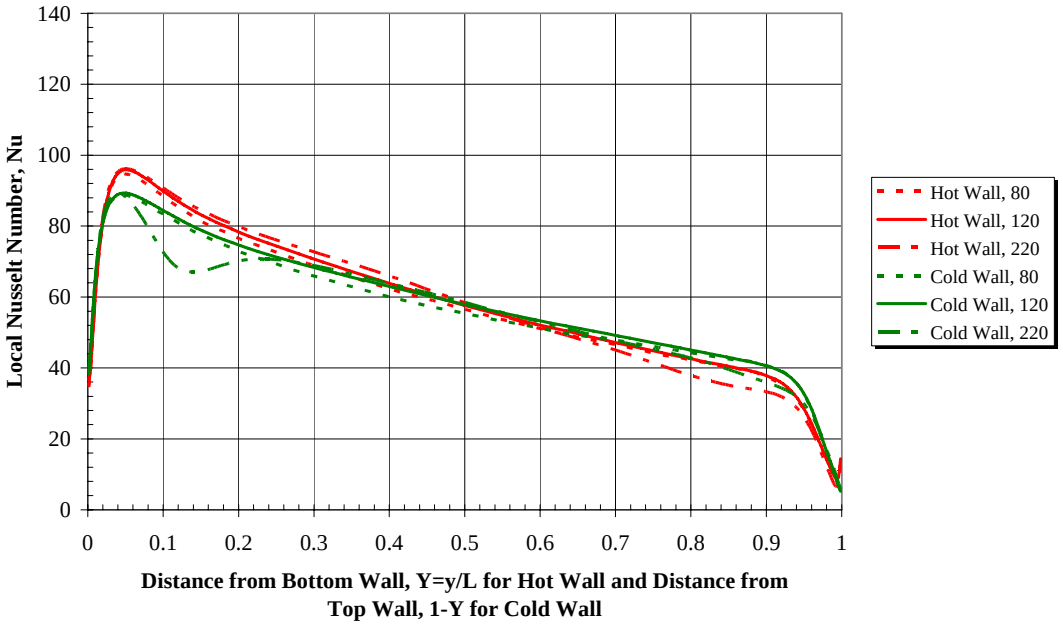

Figure 39. Local Nusselt Numbers at the Constant Temperature Hot and Cold Walls from Three Different Meshes Using the v2-f Turbulence Model, $Ra_H = 1.58x10^9$

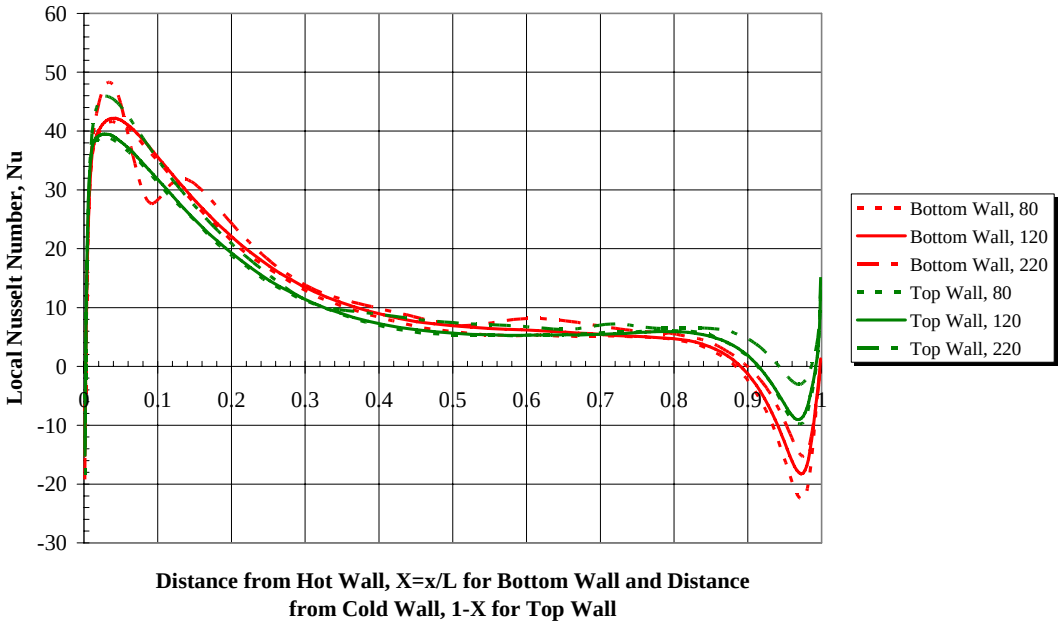

Figure 40. Local Nusselt Numbers at the Top and Bottom Walls from Three Different Meshes Using the v2-f Turbulence Model, $Ra_H = 1.58x10^9$

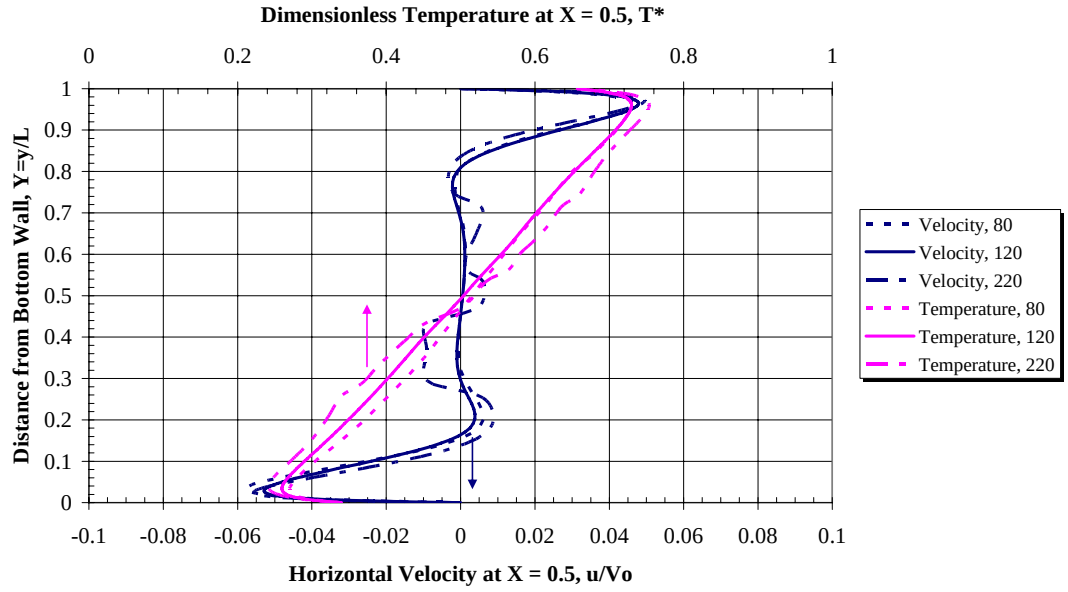

Figure 41. Mean Horizontal Velocity and Temperature Profiles as a Function of Height at Enclosure Mid-Width from Three Different Meshes Using the v2-f Turbulence Model, X = x/L = 0.5, V_0 = 1 m/s, T* = $\frac{T - T_{cold}}{T_{hot} - T_{cold}}$

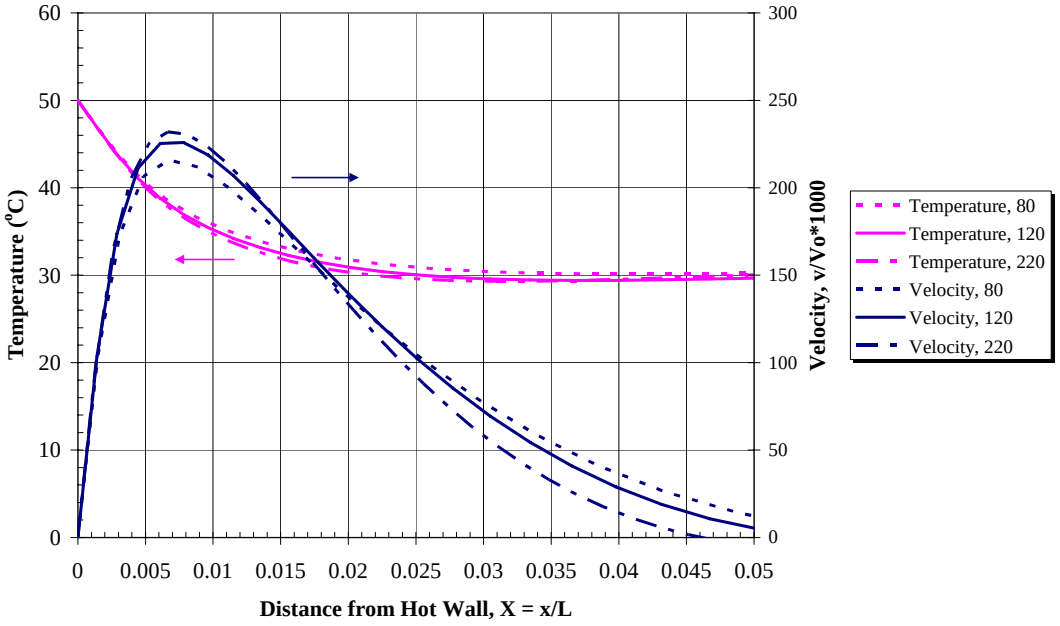

Figure 42. Mean Vertical Velocity and Temperature Profiles Near the Hot Wall at Mid-Height from Three Different Meshes Using the v2-f Turbulence Model, Y = y/L = 0.5, V_0 = 1 m/s

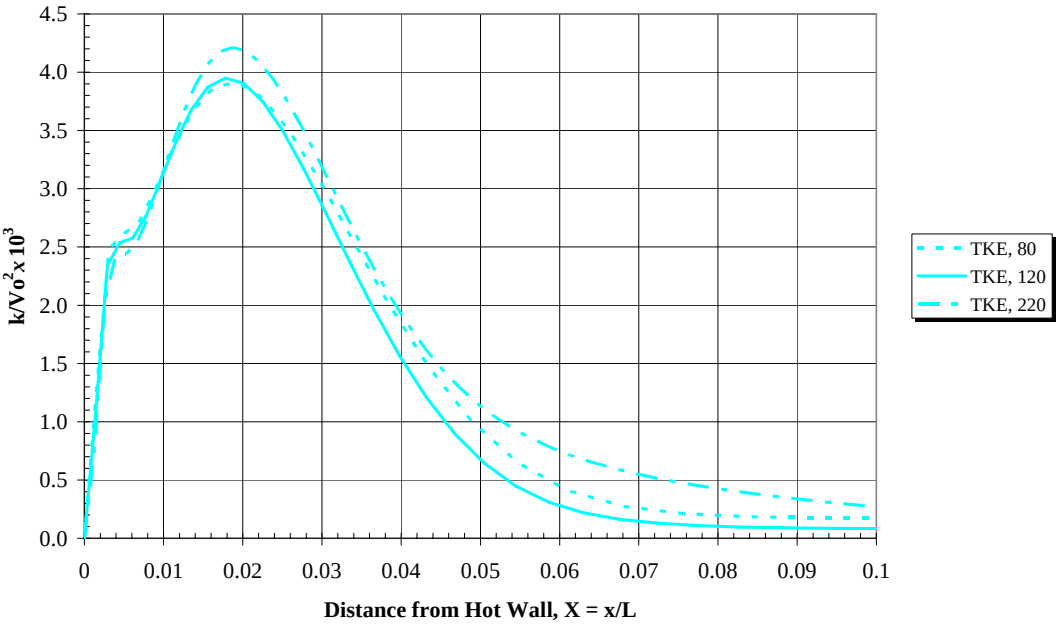

Figure 43. Turbulent Kinetic Energy Profiles Near the Hot Wall at Mid-Height from Three Different Meshes Using the v2-f Turbulence Model, Y = y/L = 0.5, V_0 = 1 m/s

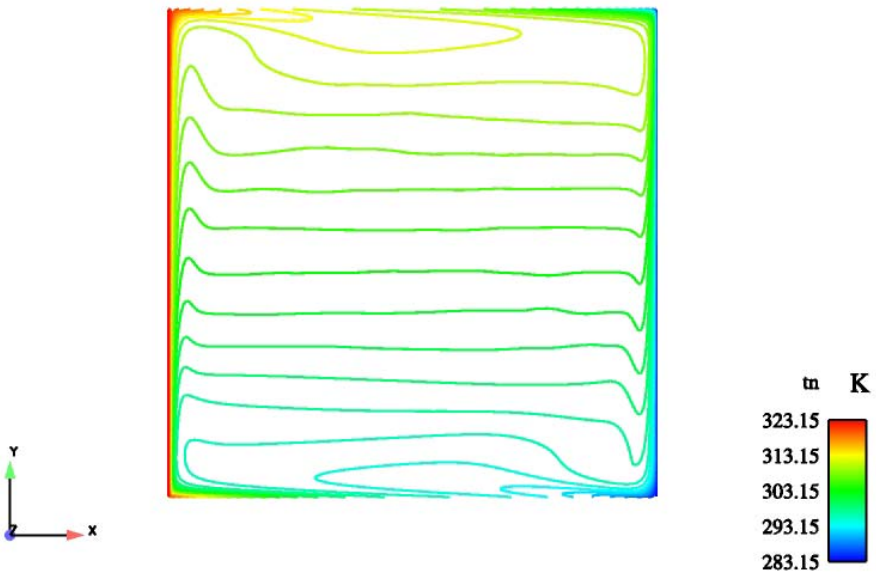

Figure 44. Temperature Contours from the 80*x*80 Mesh, v2-f Turbulence Model

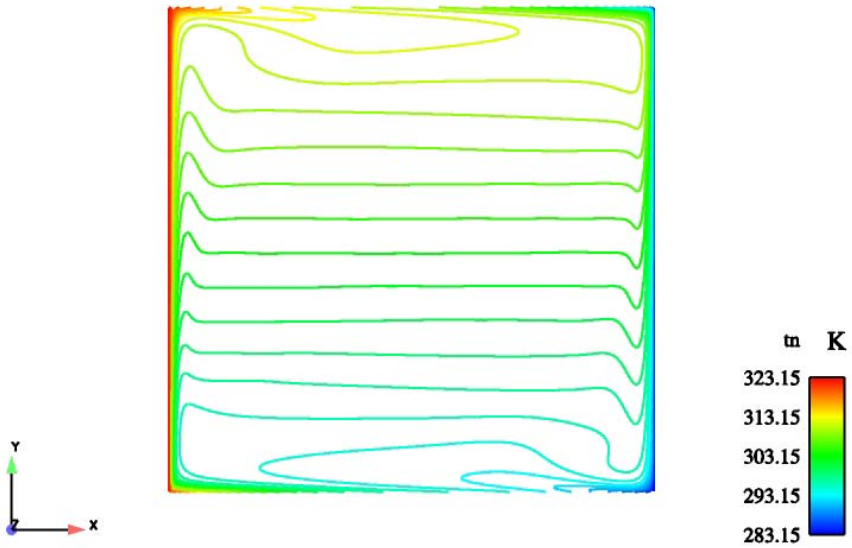

Figure 45. Temperature Contours from the 120*x*120 Mesh, v2-f Turbulence Model

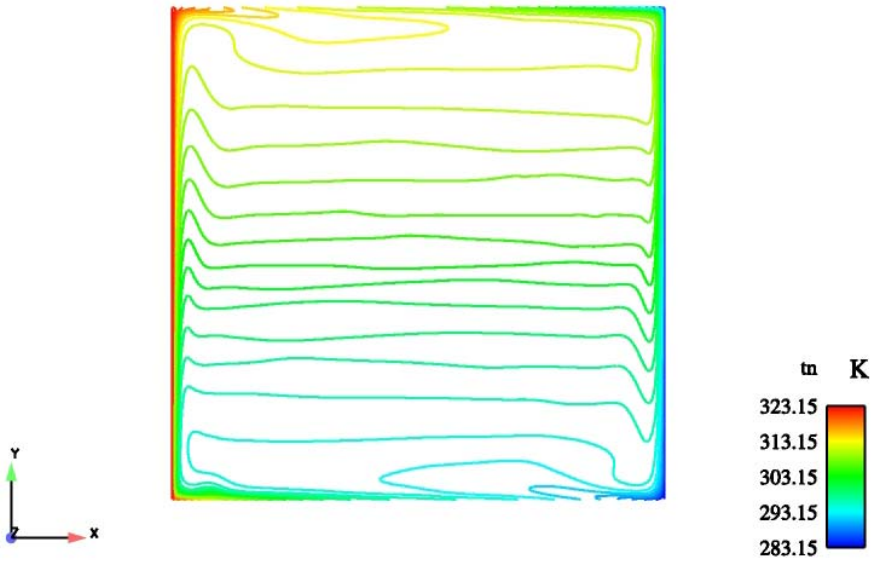

Figure 46. Temperature Contours from the 220*x*220 Mesh, v2-f Turbulence Model

Average heat transfer results for all three meshes are displayed in Table 17 at each wall in the modeled domain.

Table 17. Average Nusselt Numbers Obtained from the v2-f Grid Independence Study

	80*x*80	**120*x*120**	**220*x*220**	**Data**
Hot wall	57.7	58.7	58.2	62.9
Cold wall	56.9	58.4	56.3	62.6
Top wall	10.6	10.8	12.8	13.9
Bottom wall	10.4	11.2	12.1	14.4

It is important to consider the near-wall y^+ distribution on each of the walls in the mesh. This may be a clue as to the flow behavior in the refined cavity. Figure 47 – Figure 50 illustrate the non-dimensionalized normal distance from each wall in the square cavity.

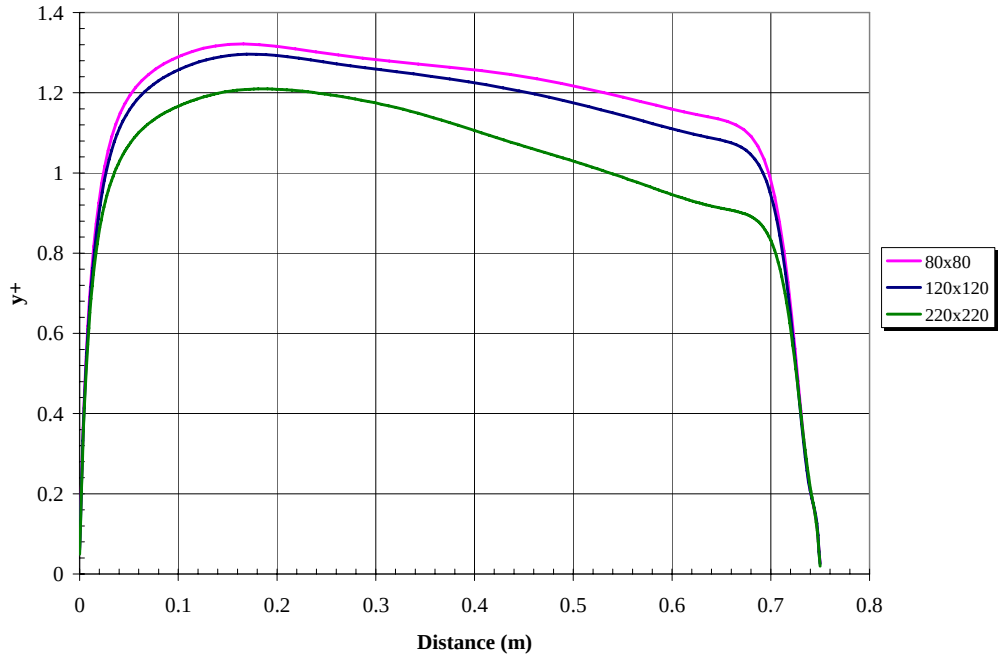

Figure 47. Non-Dimensional Normal Distance, Hot Wall, v2-f Turbulence Model

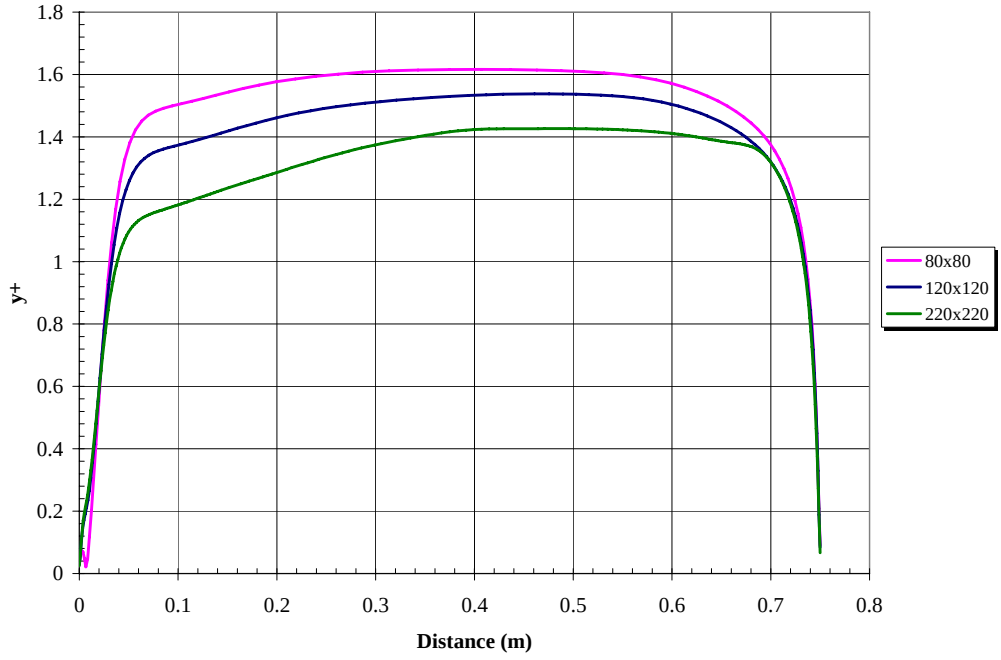

Figure 48. Non-Dimensional Normal Distance, Cold Wall, v2-f Turbulence Model

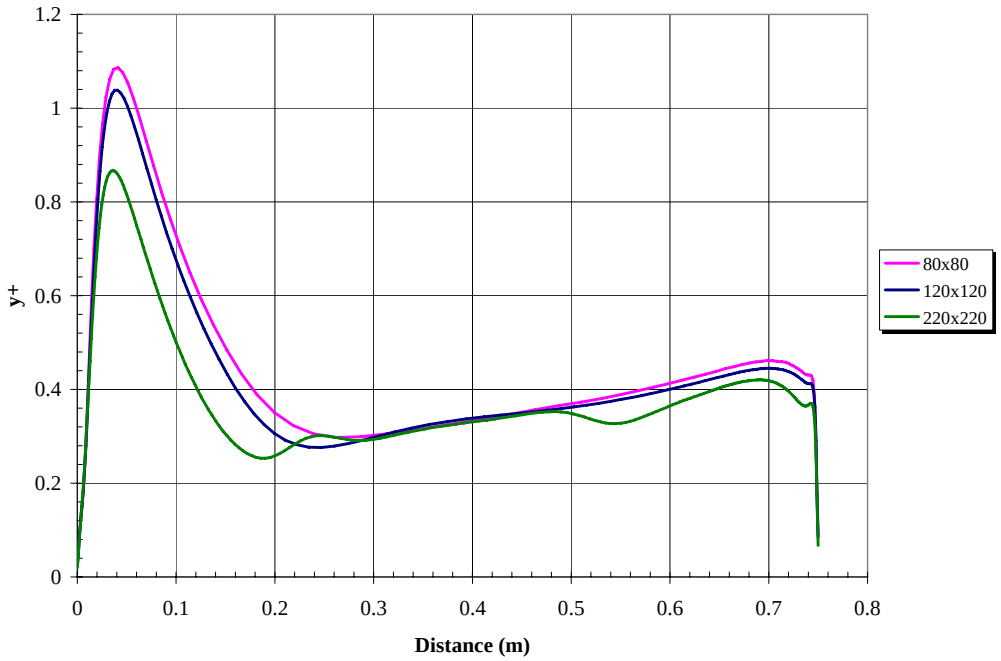

Figure 49. Non-Dimensional Normal Distance, Top Wall, v2-f Turbulence Model

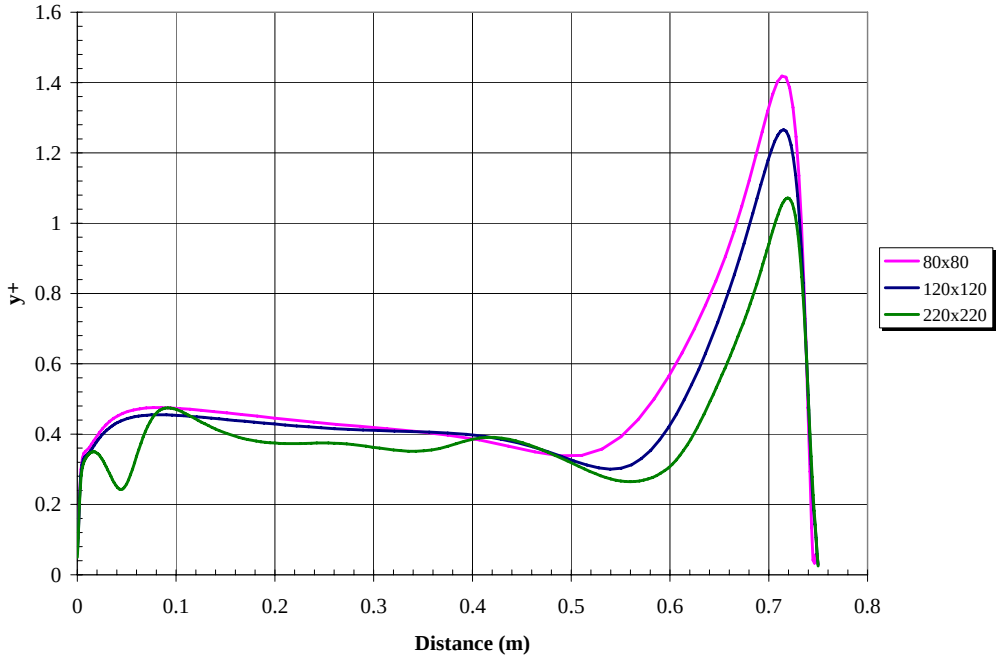

Figure 50. Non-Dimensional Normal Distance, Bottom Wall, v2-f Turbulence Model

With increasing mesh resolution, there are locations where the values of y^+ are higher. This suggests a rather different flow field is being predicted which supports increased scale capturing that is fundamental to the flow physics. It is evident that the wall y^+ values are acceptable for this application; each mesh displays a wall y^+ of about one. Subsequently, the first grid point resolution of the near-wall regions appears to be adequate for all three meshes. Therefore, it is unlikely that a y^+ meshing problem is to blame for this interesting behavior. Additionally, it is felt that adequate mesh density is specified to capture the physics occurring within the inner layer (which has been experimentally determined to be the first 5 mm from the wall as indicated in [12]). Each mesh has between about 5 and 6 nodes between the wall and the boundary of the inner layer. Based on these results, it is advisable to consider another turbulence model with the refined mesh. Therefore, the two most refined fluids meshes are also analyzed using the LRKE turbulence model.

Figure 51 – Figure 55 illustrate the local heat transfer, fluids, and turbulence results of a grid independence study using the LRKE turbulence model with the 120*x*120 and 220*x*220 fluids meshes. Producing a steady state fluid result for the refined mesh with the LRKE turbulence model has not been as problematic as v2-f. It is evident from the figures that some slight differences exist, possibly a result of marching towards a steady state solution; however, it is reasonable to declare that the solutions are fairly grid independent.

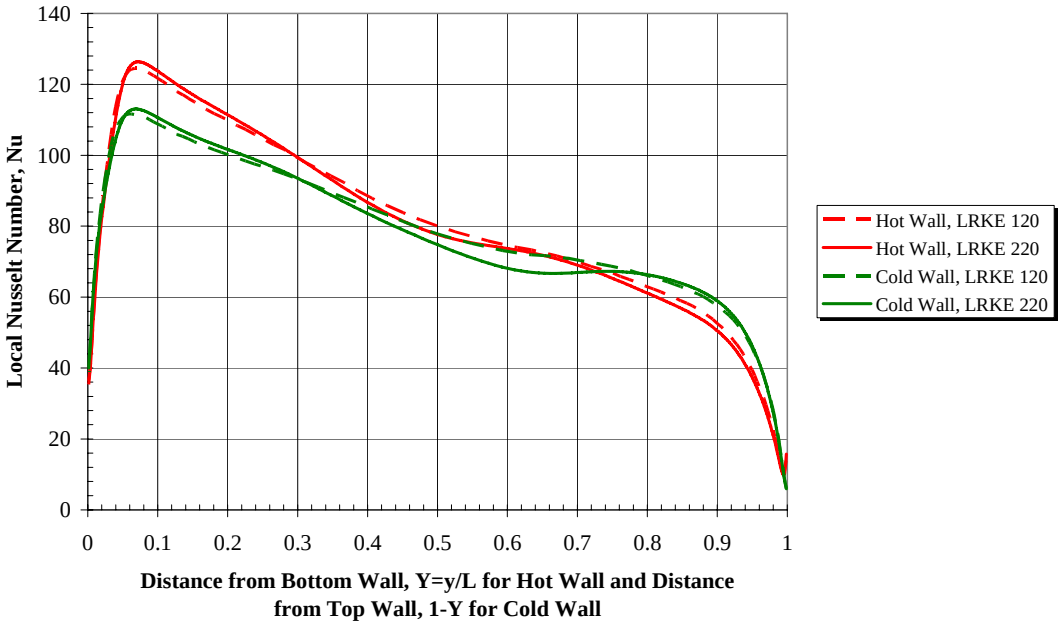

Figure 51. Local Nusselt Numbers at the Constant Temperature Hot and Cold Walls from Two Different Meshes Using the LRKE Turbulence Model, $Ra_H = 1.58x10^9$

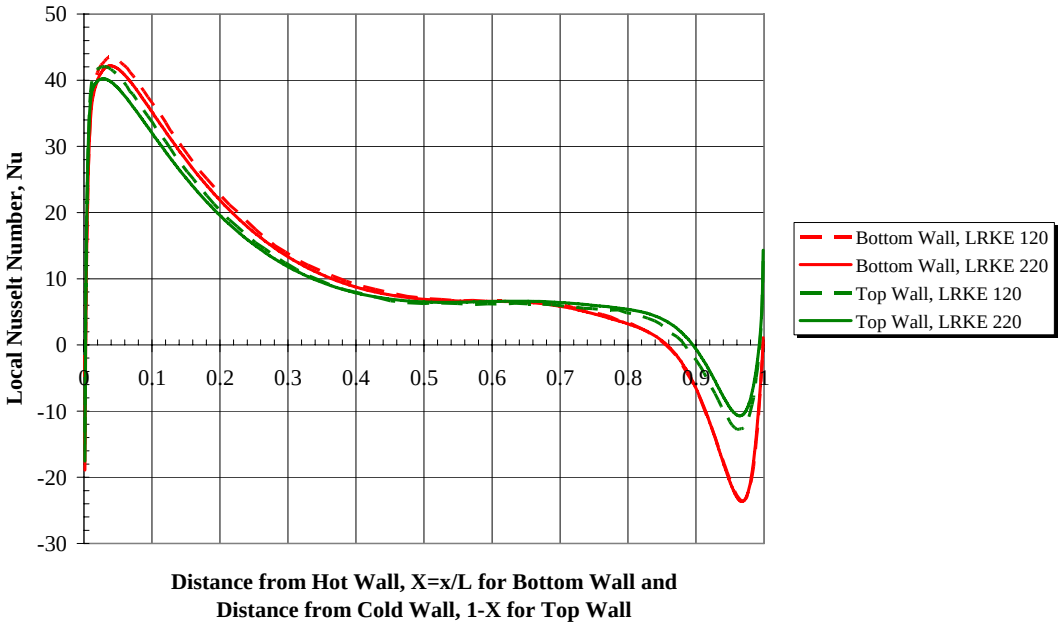

Figure 52. Local Nusselt Numbers at the Top and Bottom Walls from Two Different Meshes Using the LRKE Turbulence Model, $Ra_H = 1.58x10^9$

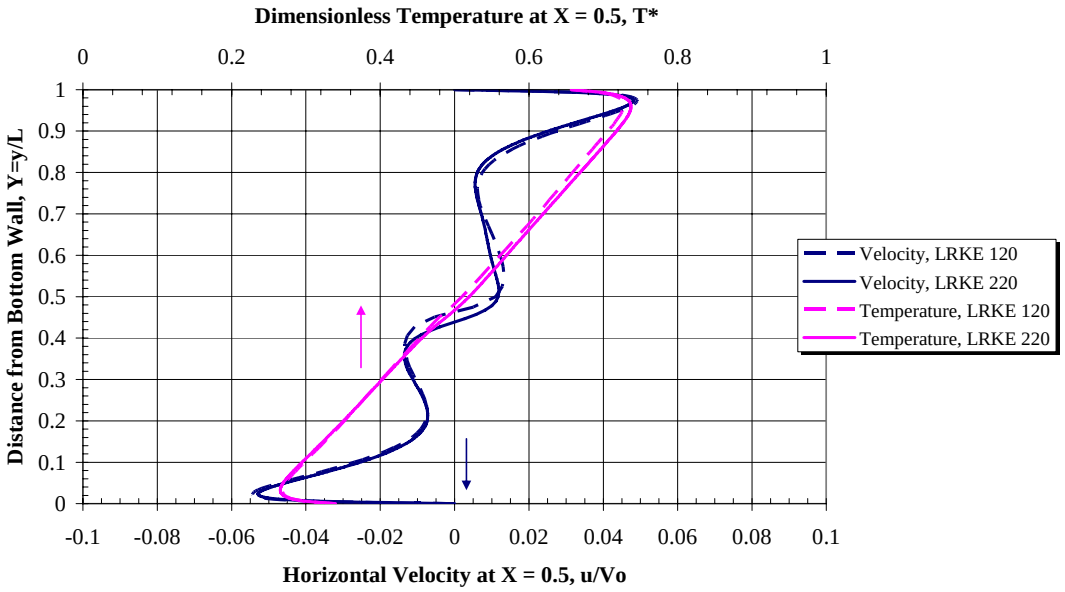

Figure 53. Mean Horizontal Velocity and Temperature Profiles as a Function of Height at Enclosure Mid-Width from Two Different Meshes Using the LRKE Turbulence Model, X = x/L = 0.5, V_0 = 1 m/s, T* = $\frac{T - T_{cold}}{T_{hot} - T_{cold}}$

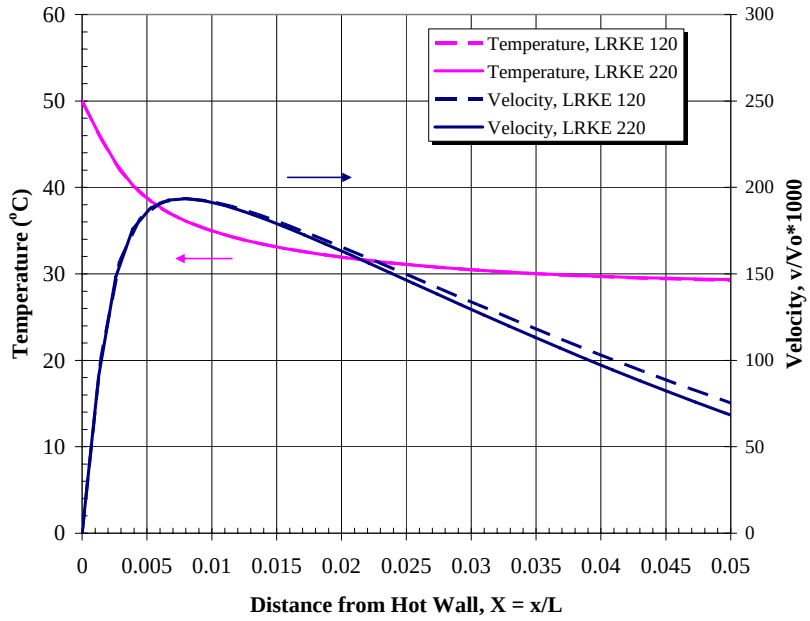

Figure 54. Mean Vertical Velocity and Temperature Profiles Near the Hot Wall at Mid-Height from Two Different Meshes Using the LRKE Turbulence Model, Y = y/L = 0.5, V_0 = 1 m/s

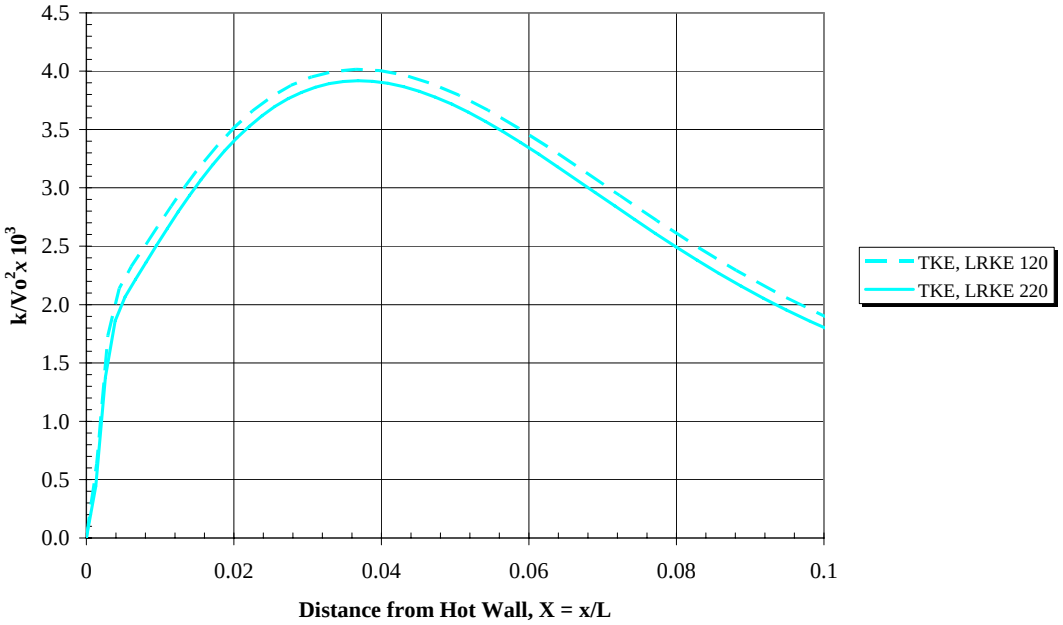

Figure 55. Turbulent Kinetic Energy Profiles Near the Hot Wall at Mid-Height from Two Different Meshes Using the LRKE Turbulence Model, Y = y/L = 0.5, V_0 = 1 m/s

On average, the Nusselt numbers varied by about 4% at worst on one passive wall and is within 1% on each of the active vertical walls.

Summary

This CFD analysis using the low Mach number code Fuego was limited to internal natural convection heat transfer. The flow conditions were either laminar, transitional, or low-intensity level turbulent flows. Two standard geometries were considered: the annulus formed between horizontal concentric cylinders and a square enclosure. Overall, the Fuego simulations for both laminar and turbulent flows compared very well to measured data, for both geometries under investigation, and to a widely accepted commercial CFD flow code (FLUENT).

For purely laminar flow in the annulus between horizontal concentric cylinders, Fuego predicted an average equivalent thermal conductivity about 3% lower than the measured data. Temperature contours and streamlines compared qualitatively to the measured data and other numerical predictions given in the literature. For transitional flows, Fuego v2-f turbulence predicted an average equivalent thermal conductivity that was about 3% lower than the measured data. FLUENT RNG k-ε predicted an average equivalent thermal conductivity

that was about 7% lower than the measured data. The local fluid temperature and equivalent thermal conductivity predicted by v2-f turbulence was similar to FLUENT predictions and reasonably well represented measured data. A grid independent solution was achieved with the v2-f turbulence model for this geometry and its prescribed thermal conditions. The v2-f model did a reasonably good job at predicting the flow conditions for this geometry and thermal conditions. In general, LRKE in its current formulation is not recommended for flow problems of this type (i.e., buoyantly driven low-level turbulence). However, improvements to this turbulence model may be possible; the Yap correction term in the ε-equation may be required (refer to Equation 15). Additionally, the turbulent heat flux may be better modeled using the GGDH to capture vertical heat flux in the presence of turbulent shear stress (refer to Equation 16). The modified turbulent heat flux is required in both the energy transport equation and in the Rodi buoyancy term optionally included in the k-equation (refer to Equation 17). Furthermore, it may be worthwhile to incorporate GGDH in the v2-f turbulence model as well (i.e., in the energy transport equation and in Rodi buoyancy). Finally, Fuego laminar flow equations predicted an unsteady, oscillating plume rising above the heated inner cylinder impacting on the outer cylinder. The average equivalent thermal conductivity was 6.5% below measured.

Sensitivity studies were performed with the concentric cylinder geometry to, 1.) determine the impacts of cell aspect ratio in the boundary layer of an aligned flow, 2.) determine the influence of multiple nonlinear iterations necessary in reaching a steady-state solution, and, 3.) determine the influence of buoyancy generated turbulence (i.e., Rodi buoyancy term included in the k-equation). Overall, none of these had a very large influence on the Fuego predicted results for natural convection heat transfer in the annulus formed by a concentric cylinder geometry.

A square cavity was also investigated with Fuego. Like the previous geometry, Fuego predictions of heat transfer and fluid flow in a square enclosure compared well to measured data. On average, Fuego v2-f Nusselt number predictions for the active walls were about 6.5% low when compared to the measured data. LRKE and FLUENT predictions were qualitatively similar on the active walls. They both tended to over predict the heat transfer, in some cases by as much as 20 – 30%. Passive wall Nusselt number predictions with Fuego tended to be too low. On average, both v2-f and LRKE under predicted passive wall heat transfer rates by about 20 – 25%. Comparison between v2-f turbulence and measured data locally shows that the v2-f turbulence model does a reasonably good job in predicting the fluid velocities and temperatures at both cavity mid-height and mid-width. Like the previous geometry, the LRKE turbulence model displayed too much viscosity. Previous recommendations regarding Yap and GGDH apply to this geometry as well. (Including GGDH may

improve the heat transfer and velocity predictions on the passive walls.) Grid independence was difficult to achieve for the highly refined mesh and the v2-f turbulence model. The flow response obtained from the 220*x*220 fluids mesh using the v2-f turbulence model exhibited an unsteady response both in the core fluid and in the corners of the near-wall regions. The LRKE turbulence model was shown to be nearly grid independent, even for the highly refined mesh. Finally, similar to the concentric cylinder geometry, the laminar flow equations applied to the square enclosure produced an unsteady result. On average, laminar heat transfer predictions were 15% low on the active walls and about 9% low on the passive walls.

Sensitivity studies were performed with Fuego and the square cavity geometry to, 1.) determine the influence of an order of magnitude increase in CFL limit applied to the v2-f turbulence model, and, 2.) determine the influence of interpolation scheme selected for the convection operator in the four turbulence transport equations in the v2-f formulation. Both of these were found not to have a profound impact on the Fuego predicted results. The Rodi buoyancy term (G_b) was not included in the square cavity results shown in this report. Because the fluid is primarily one of stable thermal stratification, this simplification is not expected to make a large difference. However, because buoyancy does drive the near-wall flow, this additional term will be investigated at a later date to assess it overall importance to near-wall behavior.

A final recommendation for potential improvement to both turbulence models may be to incorporate a two-equation heat flux model for closure of the turbulent Prandtl number (in lieu of assuming a constant value, the current approach). A turbulent thermal diffusivity can be written in a manner similar to the turbulent viscosity (refer to Equation 2) as the following [10]:

$$\alpha_t = C_\lambda \overline{v^2} \left(\frac{k}{\varepsilon}\right)^l \left(\frac{k_\theta}{\varepsilon_\theta}\right)^m \qquad \text{(Eqn. 18)}$$

where C_λ = 0.2, l = 1.5, and m = -0.5. Determination of Equation (18) typically involves the solution of a transport equation for the temperature variance (k_θ) and the dissipation rate of the temperature variance (ε_θ). However, this recommendation contains an obvious complexity as two additional transport equations require solution. Furthermore, production and dissipation source terms, in particular in the dissipation rate equation (ε_θ), are complex and not well understood.

References

[1] P. A. Durbin, "Near-Wall Turbulence Closure Modeling Without Damping Functions," Theoretical and Computational Fluid Dynamics, 3: pp. 1-13, 1991.

[2] SIERRA/Fuego Users Manual – 2.0 Draft. Sandia National Laboratories, February 15, 2005.

[3] V. C. Patel, W. Rodi, and G. Scheuerer, "Turbulence Models for Near-Wall and Low Reynolds Number Flows: A Review," AIAA Journal, Vol. 23, No. 9, pp. 1308-1319, 1985.

[4] H. Zhang, M. Faghri, and F. M. White, "A New Low-Reynolds-Number k-ε Model for Turbulent Flow Over Smooth and Rough Surfaces," Journal of Fluids Engineering, Vol. 118, pp. 255-259, 1996.

[5] FLUENT Incorporated. 2001. FLUENT 6 User's Guide. Volumes 1 – 5. Lebanon, New Hampshire.

[6] T. H. Kuehn, and R. J. Goldstein, "An Experimental and Theoretical Study of Natural Convection in the Annulus Between Horizontal Concentric Cylinders." Journal of Fluid Mechanics, 74, (part 4), pp. 695-719, 1976.

[7] T. H. Kuehn, and R. J. Goldstein, "Correlating Equations for Natural Convection Heat Transfer Between Horizontal Circular Cylinders." International Journal of Heat and Mass Transfer, 19, (10), pp. 1127-1134. 1976.

[8] T. H. Kuehn, and R. J. Goldstein, "An Experimental Study of Natural Convection Heat Transfer in Concentric and Eccentric Horizontal Cylindrical Annuli." Journal of Heat Transfer, Transactions of the ASME, 100, 635-640. 1978.

[9] N. D. Francis, M. T. Itamura, S. W. Webb, D. L. James, "CFD Calculation of Internal Natural Convection in the Annulus between Horizontal Concentric Cylinders," SAND2002-3132, 2002.

[10] M. Karcz, and J. Badur, "An Alternative Two-Equation Turbulent Heat Diffusivity Closure," International Journal of Heat and Mass Transfer, 48, pp. 2013 – 2022, 2005.

[11] D. L. James, and S. W. Webb, "Turbulent Natural Convection Heat Transfer in a Square Enclosure: Turbulence Model Comparisons," Proceedings of HT-FED2004, 2004 ASME Heat Transfer/Fluids Engineering Summer Conference, July 11-15, 2004.

[12] F. Ampofo, and T. G. Karayiannis, "Experimental Benchmark Data for Turbulent Natural Convection in an Air Filled Square Cavity," International Journal of Heat and Mass Transfer, 46, pp. 3551-3572, 2003.

[13] Y. S. Tian, and T. G. Karayiannis, "Low Turbulence Natural Convection in an Air Filled Square Cavity. Part I: The Thermal and Fluid Flow Fields," International Journal of Heat and Mass Transfer, 43, pp. 849-866, 2000.

[14] Y. S. Tian, and T. G. Karayiannis, "Low Turbulence Natural Convection in an Air Filled Square Cavity. Part II: The Turbulence Quantities," International Journal of Heat and Mass Transfer, 43, pp. 867-884, 2000.

[15] R. Henkes, and C. Hoogendoorn, Eds., "Turbulent Natural Convection in Enclosures: A Computational and Experimental Benchmark Study. Editions Europeenees Thermique et Industrie, 1993.

[16] N. Z. Ince and B. E. Launder, "On the computation of buoyancy-driven turbulent flows in rectangular enclosures," International Journal of Heat and Fluid Flow, Vol. 10, No. 2, 1989.

[17] K.J. Hsieh and F.S. Lien, "Numerical modeling of buoyancy-driven turbulent flows in enclosures," International Journal of Heat and Fluid Flow, 25, pp. 659-670, 2004.

Distribution: Internal

1	MS-0374	02991	J. W. Shelton
1	MS-0382	01541	S. W. Bova
1	MS-0382	01541	S. P. Domino
1	MS-0382	01541	S. E. Gianoulakis
1	MS-0382	01541	J. C. Sutherland
1	MS-0384	01540	H. S. Morgan
1	MS-0384	01500	A. C. Ratzel
1	MS-0481	02137	T. F. Hendrickson
1	MS-0481	02132	S. E. Slezak
1	MS-0719	06141	S. W. Webb
1	MS-0821	01532	L. A. Gritzo
1	MS-0824	01530	T.Y. Chu
1	MS-0825	01510	W. L. Hermina
1	MS-0828	01533	A. R. Black
1	MS-0828	01533	M. Pilch
1	MS-0828	01533	V. J. Romero
1	MS-0828	01533	M. P. Sherman
1	MS-0834	01512	J. E. Johannes
1	MS-0834	01514	M. J. Martinez
1	MS-0836	01516	B. D. Boughton
1	MS-0836	01516	D. Dobranich
1	MS-0836	01516	W. W. Erikson
5	MS-0836	01516	N. D. Francis
1	MS-0836	01516	E. S. Hertel
1	MS-0836	01516	M. L. Hobbs
1	MS-0836	01516	R. E. Hogan
1	MS-0836	01516	R. G. Schmitt
1	MS-0836	01532	W. Gill
1	MS-0836	01532	C. A. Romero
1	MS-1135	01532	A. L. Brown
1	MS-1135	01532	J. T. Nakos
1	MS-1135	01532	S. R. Tieszen
1	MS 9014	08242	A. R. Ortega
1	MS-9409	08775	G. H. Evans
1	MS-9409	08775	G. M. Laskowski
1	MS-9409	08775	C. D. Moen
1	MS-9409	08775	G. J. Wagner
1	MS-9018	08945-1	Central Technical Files
2	MS-0899	04616	Technical Library Files

Distribution: External

Darryl L. James, Ph. D.
Texas Tech University
Department of Mechanical Engineering
Box 41021
Lubbock, TX 79409-1021

Cuauhtemoc Aviles-Ramos, Ph.D.
ESA-Weapons Response Group MS P946
Los Alamos National Laboratory
P.O. Box 1663
Los Alamos NM, 87545